

EVALUATION OF 3D CONCRETE PRINTING  
IN THE UNITED ARAB EMIRATES

by

Aktham S. Alchaar

A Thesis presented to the Faculty of the  
American University of Sharjah  
College of Engineering  
In Partial Fulfillment  
of the Requirements  
for the Degree of  
Master of Science in  
Civil Engineering

Sharjah, United Arab Emirates

February 2020

## Declaration of Authorship

I declare that this (project/thesis/dissertation) is my own work and, to the best of my knowledge and belief, it does not contain material published or written by a third party, except where permission has been obtained and/or appropriately cited through full and accurate referencing.

Signature.....Aktham Alchaar.....

Date..... April 16<sup>th</sup>, 2020.....

The Author controls copyright for this report.  
Material should not be reused without the consent of the author. Due  
acknowledgement should be made where appropriate.

© Year 2020

Aktham S. Alchaar

ALL RIGHTS RESERVED

## **Approval Signatures**

We, the undersigned, approve the Master's Thesis of

Title:

Date of Defense:

**Name, Title and Affiliation**

**Signature**

---

---

---

---

---

---

---

---

---

---

Dr. Mohamed El-Tarhuni  
Vice Provost for Graduate Studies  
Office of Graduate Studies

## **Acknowledgment**

I herewith acknowledge my deep appreciation to my advisor, Dr. Adil Al-Tamimi, for his valuable guidance and continuous support throughout this study. I am very thankful to his great experience and useful critiques that have enriched the quality of this work. I would also like to thank Eng. Ansari, Civil Engineering lab technician at AUS, and my colleagues for their precious assistance in the lab. I would like to also acknowledge the help and cooperation from Eng. Roland at the manufacturing lab of AUS for making the nozzles and test fixture of the study. My special thanks are extended to Eng. Tarek Wahhab for his recommendations that were very helpful to the initiation of this research. As well, I wish to thank the examining committee members, Dr. Mohammad AlHamaydeh and Dr. Vian Ahmed, for their constructive suggestions at the time this research was proposed. Finally, I wish to express my gratitude to the American University of Sharjah for offering me a graduate teaching assistantship at the time this research was carried out.

## **Dedication**

*To God Almighty, my source of strength, understanding, and inspiration*  
*To my dear parents and my brother, for their upmost care and motivation*  
*To my friend Mahmoud, for his continuous encouragement*  
*Finally, to my beloved future wife, for her endless love and support*

## Abstract

3D concrete printing has been recently studied as a new scheme of construction. The automated nature of such technique allows for reductions in waste generation, less manpower requirements, and fabrication of complex geometries. However, the use of concrete for this application is challenging. The material shall be flowable for ease of extrusion. Printed layers shall preserve their shape and rapidly attain strength to bear their own weight and the subsequent layers. However, there is a lack of guidance on the design of 3D printing concrete mixes. In addition, the change in performance of 3D printing concrete under different environmental conditions is still generic. The aim of this research is to develop a concrete mix using local materials, and to evaluate it in two environmental conditions: ambient and site conditions. The experimental program addressed fresh state properties through flow table, open time, extrudability, and shape stability. Compressive strength, flexural strength, and interlayer bond shear strength have been evaluated as mechanical properties in this research by testing a total of 61 specimens. A novel test setup was designed for bond strength evaluation at different printing time intervals. 19 trial mixes were performed, and one mix was chosen as the optimum based on extrudability and shape stability/quality. It was observed that inclusion of fibers enhances shape stability, but higher dosages of superplasticizer become required. It was found that flow table and open time of site conditions decreased by 9% and 16% respectively, compared to ambient flow table (86%) and open time (7.2 minutes) on average. This was owing to accelerated loss of flowability. Shape retention index (ambient) was 0.94-0.96 for different lengths and number of layers, and dropped by 2-8.5% under site conditions. Compressive strength was evaluated to be 47 MPa in control cubes. Results from compression and bond tests indicated accelerated water evaporation and surface dehydration in site conditions, and that the presence of joints in printed parts is detrimental to such strength parameters. Finally, flexural strength was increased in site conditions compared to control and ambient specimens by 21% and 18% respectively. Flexural strength results demonstrated that fibers are better oriented through print process, and can be further improved in hot mixes due to lower viscosities.

**Keywords:** *3D Concrete Printing, Additive Manufacturing, Contour Crafting, Extrudability, Flow Table, Flexural Strength, Fibers, Bond Shear Strength.*

## Table of Contents

Abstract .....	6
List of Figures .....	10
List of Tables .....	13
Chapter 1 . Introduction .....	14
1.1    Background and Motivation.....	14
1.2    Research Significance .....	15
1.3    Research Objectives .....	16
1.4    Thesis Organization.....	16
Chapter 2 . Literature Review .....	17
2.1    Early 3D Printing Applications .....	17
2.2    Automation in Construction .....	20
2.2.1 Additive manufacturing by selective aggregation. ....	20
2.2.2 Contour crafting .....	21
2.2.3 D-Shape technique.....	28
2.2.4 Concrete printing. ....	31
2.3    Evaluation Criteria of 3DCP .....	31
2.3.1 Rheology evaluation. ....	31
2.3.2 Strength evaluation. ....	33
2.4    3D Concrete Printing in the United Arab Emirates.....	35
2.4.1 Vision.....	35
2.4.2 Recent achievements. ....	35
2.5    Summary .....	35
Chapter 3 . Methodology .....	38
3.1    Experimental Scenarios.....	38
3.2    Mix Design.....	38

3.3	Trial Batches and Extrusion .....	40
3.4	Methods for Testing and Evaluation .....	42
3.4.1	Flow table. ....	43
3.4.2	Open time.....	43
3.4.3	Extrudability. ....	44
3.4.4	Compressive strength.....	44
3.4.5	Flexural strength. ....	45
3.4.6	Bond shear strength. ....	45
3.4.7	Shape retention. ....	46
3.5	Test Specimens.....	47
3.5.1	Compressive strength specimens. ....	48
3.5.2	Flexural strength specimens. ....	48
3.5.3	Bond shear strength specimens.....	50
3.6	Materials.....	51
3.6.1	Aggregates. ....	52
3.6.2	Portland cement type 1. ....	52
3.6.3	Mineral fillers. ....	52
3.6.3.1	Ground granulated blast furnace slag (GGBS).....	52
3.6.3.2	Fly ash.....	52
3.6.3.3	Silica fume. ....	52
3.6.4	Water reducing admixtures.....	53
3.6.5	Set retarders. ....	53
3.6.6	Accelerators. ....	53
3.6.7	Micro fibers .....	53
3.6.8	Viscosity modifying admixtures (VMA).....	54
3.7	Experimental Program.....	54
Chapter 4 . Results and Discussions .....		57



4.1	Trial Batches .....	57
4.2	Flow Table.....	64
4.3	Open Time.....	65
4.4	Extrudability.....	68
4.5	Shape Retention.....	69
4.6	Compressive Strength .....	73
4.7	Flexural Strength.....	77
4.8	Bond Shear Strength.....	82
	4.8.1 Bond assessment.....	83
	4.8.2 Failure patterns.....	89
Chapter 5 . Conclusions and Recommendations.....		94
5.1	Conclusions .....	94
5.2	Recommendations .....	96
References .....		97
Vita .....		103

## List of Figures

Figure 1: Stereolithographic Apparatus and Process [7].	17
Figure 2: Selective Laser Sintering Process [8].	18
Figure 3: Simple Schematic of FDM Process [10].	19
Figure 4: Selective Aggregation Process [12].	21
Figure 5: Blow up of a printed sample using Selective Laser Sintering [14].	22
Figure 6: Schematic for the assembly in contour crafting [3].	23
Figure 7: Surface Finish of Products manufactured by Contour Crafting [16].	24
Figure 8: Wall manufactured by Contour Crafting [18].	25
Figure 9: Layer settlement without time gap (top) and with time gap (bottom) [20].	26
Figure 10: Elevation of Mortar Layers Printed for the Evaluation of Buildability [22].	27
Figure 11: Several printed objects with different number of strips in the horizontal plane [24].	28
Figure 12: D-shape Printer [29].	29
Figure 13: Single Room Printed using D-shape technique [29].	30
Figure 14: Top View of 2-m long printed mortar strip [22].	32
Figure 15: Bond Strength Test Setup and Sample Specimen [27].	34
Figure 16: (a) Office of the Future [44], (b) Sharjah 3D House [46], and (c) Warsan Buidling [45].	36
Figure 17: In-house Manufactured Nozzle (left) Top View and (right) Side View. ...	40
Figure 18: Manual Extrusion, (left) sample extruded concrete, (right) sample layered object.	41
Figure 19: Injection Tool and Fitted Nozzle for Extrusion.	41
Figure 20: Manual Extrusion using The Injection Tool.	42
Figure 21: Flow Table Apparatus.	43
Figure 22: Cubic Concrete Molds for Compression Test.	44
Figure 23: Concrete Prism Under ASTM C348 Flexural Strength Test [54].	45
Figure 24: Bond Shear Test Setup (a) Machine Configuration and (b) Details of Fixture.	46
Figure 25: (a) Load Mechanism on the Fixture, (b) Unloaded Specimen, and (c) Loaded Specimen.	47

Figure 26: Settlement of Concrete Layers while Additional Layers are Added.....	48
Figure 27: Specimens for Compressive Strength (a) Molded and (b) Printed.....	48
Figure 28: Molded Concrete Prism for Flexural Strength Test. ....	49
Figure 29: Printed Specimen for Flexural Strength Test (a) Designed and (b) Actual. .....	49
Figure 30: Printed Specimen for Bond Shear Test. ....	50
Figure 31: Control Specimen for Bond Shear Test (a) Geometry and (b) Load Configuration. ....	51
Figure 32: w/b, a/b, and s/b Variations Among Trial Mixes. ....	58
Figure 33: Printed Sample (Mix 1). ....	59
Figure 34: Mix 2 (a) Only Water is Added, (b) Admixtures are Added, and (c) Printed Specimen.....	60
Figure 35: Mix 3 (a) Surface Quality and (b) Printed Specimen. ....	61
Figure 36: (a) Mix 10 Surface Quality and (b) Mix 11 Bleeding. ....	61
Figure 37: Printed Specimen of (a) Mix 12 and (b) Mix 13. ....	62
Figure 38: Printed Specimen of Mix 19.....	62
Figure 39: Printed Specimen of (a) Mix 16, (b) Mix 17, and (c) Mix 18.....	63
Figure 40: Flow Table Test Configuration (a) Before Flow and (b) After Flow.....	64
Figure 41: Flow Table Test Results for Both Scenarios. ....	65
Figure 42: Stoppage in Extrusion Process. ....	66
Figure 43: Surface Quality of Open Time Specimens (a) Scenario 1 and (b) Scenario 2. .....	67
Figure 44: Continuously Printed Filaments for Extrudability Evaluation. ....	68
Figure 45: Shape Retention Index for Both Scenarios (SRI and HRI).....	70
Figure 46: Shape Retention and Surface Quality of Printed Parts (a) Mix with Fibers (b) Mix Without Fibers. ....	72
Figure 47: Compression Test Setup for Printed Specimens (a) Configuration and (b) Cardboard Pad for Load Distribution. ....	73
Figure 48: Summary of Compressive Strength Results of Control Cubes and Printed Cubes in both Scenarios.....	74
Figure 49: Printed Cube Specimens before and after Compression Test (Scenario 1). .....	75

Figure 50: Printed Cube Specimens before and after Compression Test (Scenario 2). .....	76
Figure 51: Flexural Test Setup for Printed Prisms.....	77
Figure 52: Flexural Strength Results of Molded and Printed Prisms. ....	78
Figure 53: Fractured Printed Prisms and Fiber Orientation (a) Side View and (b) Bottom View.....	79
Figure 54: Cross Section of a Fractured Printed Prism (a) Cross Section and (b) Side View.....	80
Figure 55: Bond Shear Test Setup for (a) Control and (b) Printed Specimens.....	82
Figure 56: Bond Shear Test Control Specimen (a) Mold and (b) Blow Up. ....	83
Figure 57: Summary of Bond Shear Strength Results in the Study.....	84
Figure 58: Bond Shear Strength of Printed Specimens versus Time Interval. ....	85
Figure 59: Fractured Bond Control Specimens (a) During Test and (b) Blow Up.....	89
Figure 60: Fractured Bond Printed Specimens (a) During Test, (b) Crack Initiation on The Left, and Separation of Interface on The Right. ....	90
Figure 61: Typical Fractured Interface of Printed Specimens (Left) $t = 2.5$ hrs and (Right) $t = 4$ hrs.....	91
Figure 62: Fractured Interface of Printed Specimens due to Setup Errors (a) During Test and (b) Blow Up at Interface. ....	92
Figure 63: Vertical Crack Along Layers of a Printed Specimen in Bond Test.....	92
Figure 64: Curvature in Specimen Due to Irregularity in Printing Path Under Bond Test. .....	93

## List of Tables

Table 1: Hollow-core Concrete Slab Mix Design [50].	39
Table 2: Bond Shear Test Categories.	51
Table 3: Properties of Polyethylene Fibers Used in the Study.	54
Table 4. Experimental Matrix of the Study.	55
Table 5: w/b, a/b, and s/b Ratios of Trial Mixes.	58
Table 6: Open Time Results for Both Scenarios.	66
Table 7: Percentage Reduction in BSS in Both Scenarios for Different Time Intervals.	84
Table 8: Percentage Reduction between Bond Strength Categories (Control, S1, and S2).	87

# Chapter 1. Introduction

## 1.1 Background and Motivation

Automation and digital fabrication have emerged in a variety of industries in the last decade. They have shown developments in many applications such as medicine, automobile, aerospace, electronics, and many more [1]. This represents a quantum leap in industrial disciplines by expediting productivities and limiting the need for massive workmanship requirements in many cases. Three-dimensional concrete printing (3DCP) is a developed automated manufacturing technique that has a potential convenience in construction applications. It is a promising future-generation of construction methods. However, the use of concrete material in automated construction is facing many challenges such as strength, workability, and durability.

An important advantage of concrete material is the ability to control its fresh state properties to suit construction needs and special situations. Researches continue to investigate all possible ways of controlling fresh properties such as rheology, setting time, slump, thixotropy, flowability, fluidity, and many more. The incorporation of different materials such as short fibers and fine minerals, have shown enhanced strength and resistance not only under compression, but under tension as well. However, durability is always a matter of concern. A properly designed concrete can be durable enough to significantly extend service life of structures.

Developments were not only focused in the material field, but it was also approached in terms of construction and manufacturing methods. At the very beginning, concrete material used to be prepared by hand mixing at construction sites, then automated mixers were developed to speed up the work and lower labor requirements. After some time, ready mix concrete was incorporated in construction projects where concrete is being mixed at a factory, then transported to site in specialized trucks. Precast concrete came later to be a competitive choice for stakeholders, allowing speed in construction and higher quality control. Nevertheless, it had some limitations that made it not recommended in some structurally complex applications. The most practiced construction methods using concrete are categorized into cast in situ and pre-cast construction. Each category has its own advantages over the other one.

Concrete construction projects are well known to be involving labor-intensive works, and labor effectiveness and skilled manpower has been declining over the years. In addition, exposure to dust and operation of heavy equipment especially for higher structures make such construction schemes hazardous and affecting health and safety of construction crews. It was observed also that there is no enough control on construction projects usually, which in turn influences achieving the targeted quality within the specified project period [2]. Additionally, after the burning of fossil fuels, production of Portland cement comes as the second most industry that contributes to the greenhouse gases effect on the globe. On average, for each ton of cement produced, there is almost 1 ton of Carbon dioxide released. Furthermore, the waste produced through using conventional construction methods with concrete is considered very high, hence, there will be always a need to reduce the generated waste through higher quality control. This will decrease the amount of concrete used in construction which in return will limit CO<sub>2</sub> emissions to the environment [3].

The ability to enhance both the fresh and hardened state properties of concrete along with the need to achieving more efficient construction schemes, has brought the idea of concrete extrusion and digital fabrication to mind. Major construction projects are being architecturally complex and based on fast track contracts, and this is exactly where automation in construction will fit the most. By this means, research is being intensively emerged in this area. The first practical large-scale application of additive manufacturing was developed by Dr. Behrokh Khoshnevis, named Contour Crafting (CC). Such technique is able to produce dwellings that are ready for architectural finishing and installation of MEP services [4].

## **1.2 Research Significance**

Although several developments were made on 3D concrete printing (3DCP), there is still a lack of standards and guidance on mix design and performance evaluation of 3D printed structural elements. Concrete mixtures that can be used in such technologies shall have unique characteristics. Furthermore, the material is required to have reduced setting time, defect-free surface finish, and well-controlled shrinkage of the material. In addition, mechanical performance is a key for success of this application as the printed parts are intended to be structural elements. This is primarily related to strength, stability, durability, and bond between the 3D-printed layers. Additionally, the

applicability of such technique in a harsh environment as in the United Arab Emirates remains questioned. Such challenges are limiting the integration of such technologies into large-scale construction applications.

### **1.3 Research Objectives**

The overall purpose of this study is to investigate properties of 3D-printed concrete parts while taking into consideration the effect of harsh environmental conditions at fresh and hardened state of the material. Objectives of the study are summarized as follows:

1. To design a concrete mixture that is suitable for the 3D printing applications.
2. To evaluate rheological and hardened state properties of the developed mixture.
3. To investigate bond shear strength of the interface between layers.
4. To study the effects of the UAE's harsh environmental conditions on the material properties.

### **1.4 Thesis Organization**

The remaining part of this thesis is organized such that chapter 2 discusses relevant research and previous studies that were performed on 3D concrete printing along with the related regional experience, chapter 3 illustrates the way objectives are to be achieved and methods of evaluation in this study, chapter 4 interprets the results of the study and its analysis, and chapter 5 lastly concludes the study with the major findings and recommendations for future work within the same field.



## Chapter 2. Literature Review

In the sections of this chapter, the early developments of 3D printing will be discussed, in addition, large-scale applications of the same technique will be discussed, mainly contour crafting and D-shape technique. Findings of some researchers in this field of study will be shown at the end of the chapter. Following the latter, the proposed research will be demonstrated and illustrated.

### 2.1 Early 3D Printing Applications

The scale-based first 3D printing application was named stereolithography; a process patented by Charles Hull in 1984 [5]. The term lithography is meant to indicate precise printing where ink is adhered to greasy image area on a platform, and repelled from other areas on that platform, to produce a unique lithographic image [6]. Stereolithography was the first to be referred as an additive manufacturing process, by means of its way of operation. It is based on placing thin layers of liquid polymers depending on a specific cross section, and the plastic polymer is solidified using ultra violet (UV) radiation directed towards the printed polymer, and once the whole layer becomes solid, the platform lowers down and a new layer laying on top of the previous one starts to be processed in the same manner depending on another specific cross section. The final product is a 3D printed object, and the layer-based process is referred to as additive manufacturing [5]. The system used in stereolithographic printing is called SLA (Stereolithographic Apparatus), and it is consisted mainly of three parts. As shown in Figure 1, the first part is the polymer container that is filled with a resin

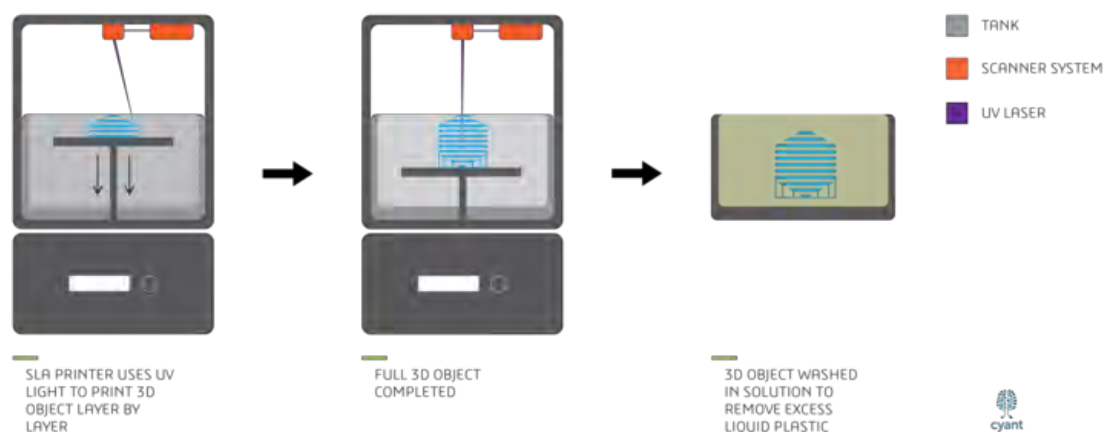
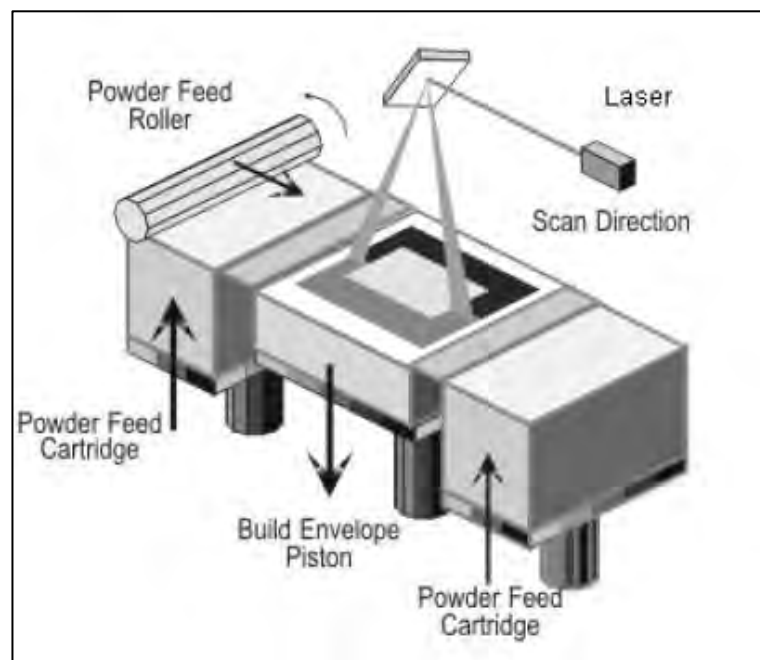


Figure 1: Stereolithographic Apparatus and Process [7].

that is sensitive to UV radiation. The second part is the movable platform where UV laser is solidifying layers, and the third part is the scanner system that reflects UV radiation to form the layer on the platform based on a specific cross-sectional detail [7].

Another additive manufacturing technology was invented in 1989, called selective laser sintering, by Carl Deckard. This patent was dependent on forming solid porous particles from powdered materials using heating laser from a certain laser source. This process happens by means of vacancy diffusion whereby powder particle motion is thermally activated through laser, leading to sintering of those particles and forming a solid object. Figure 2 illustrates the operation of selective laser sintering



**Figure 2: Selective Laser Sintering Process [8].**

process. On the sides of the shown printer, powder containers are placed to supply powder to the printing bed. The bed is placed in the middle with an ability to move up and down. The roller has a role of distributing powder particles on the bed surface, and the laser beam is pointed toward specific points on the bed based on a CAD file. Furthermore, the CAD file is where the object shape is designed and the geometry is defined, then it is sliced into two-dimensional layer sketches through conversion to standard tessellated language (STL) format. The printer directs the laser by following the STL layer-based drawings on the printing bed. Once the first layer is shaped, the bed is moved down by the layer thickness, and the process is repeated layer by layer to

form the final product. In this heat-dependent process, the diffusion of powder happens without reaching the melting point, which is the reason behind the “sintering” label [8].

Fused Deposition Modeling (FDM) was the next additive manufacturing technology which was invented by Scott Crump in Stratasys and got patented in 1992 [9]. Similar to SLA, FDM printers are composed of beds or platforms that can be made of plastic or ceramics. This bed is where the layers are being built simultaneously with lowering down that bed upon getting each single layer printed until getting the final product. In contrast with SLA, FDM employs a printing nozzle that is motorized by a mechanical and geometrical system that is linked to computer aided design files (CAD). The nozzle is able to move in all directions (x, y, and z) and a thermoplastic filament is being fed to the nozzle during the printing process. Thermoplastics are known to have a glass transition temperature which is a limit between the liquid and solid state of the thermoplastic material. Nozzles are heated continuously to maintain a temperature above the glass transition value, so that the filament remains not solidified until it gets out of the nozzle to shape the desired cross section. Once the nozzle prints a layer using the filament, it solidifies to create a solid layer, and the solidification is induced by the medium temperature that is below the glass transition temperature of the filament. The dimension stability of the object is highly dependent on the heating temperature of the nozzle, the closer it is to the glass transition value, the faster the material solidifies after being printed as it takes less time to fall below the transition value. As shown in Figure 3, the nozzle keeps extruding the material in layers where each layer gets fused with the layer below, and the process is repeated for subsequent layers until the final 3D

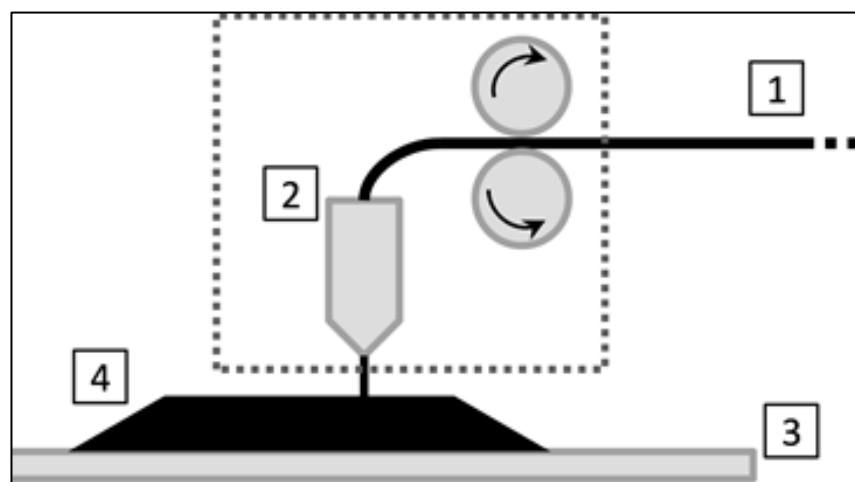


Figure 3: Simple Schematic of FDM Process [10].

printed product is achieved. This method sometimes needs to print support objects to prevent damage or overhanging to the main object that is to be achieved, these supports can be melted again and reused as they are commonly of the same material of the object. This technique is known to be much slower than its counterparts [11]. Figure 3 simply illustrates the FDM process, where 1 indicates filament feeding into the nozzle, 2 is where the filament material gets heated above its glass transition temperature, and the end is the nozzle that extrudes the heated filament, 3 is the object being printed, and 4 is the movable printing bed or platform that is changing position on Z-Axis (lowered) while layers are being printed.

## **2.2 Automation in Construction**

Along the fast track developments that were achieved in automation technologies within different industrial fields, large-scale construction remained out of these fields for so long. As opposed to the norm in construction using cementitious materials like concrete, construction automation started to be researched and has shown a great potential in many terms.

**2.2.1 Additive manufacturing by selective aggregation.** Selective Aggregation was the first researched application of AM in large-scale construction in 1997 by Joseph Pegna. Two distinct dimensions for classifying additive fabrication processes were identified by Pegna, geometry of the final product presented the first dimension as the process involves incremental construction of multiple layers to achieve the desired shape. In addition, transportation of materials to the output was the second dimension where it could be delivered in different phases [12]. As illustrated in Figure 4, in selective aggregation, a layer of sand is placed uniformly on the building bed (A), and with the layer geometry scanned in the CAD file, the cement powder is non-uniformly plotted on the specified geometric surface (B), then the binder agent is impregnated (water in this case) by spraying it on the bed (C). The process is repeated with elevating placement of sand and cement corresponding to the geometry of every single layer. Fabricated samples were observed to be brittle and cracked due to surface tension effect of sprayed water on cement particles, hence, steam was used as an activation binder along with application of water vapor at layers' interface instead of spraying water particles on fabricated sand/cement layers. After testing hardened

fabricated specimens, the concrete was found not to be isotropic, and interestingly the compressive strength of samples was on average twice the tensile strength [12].

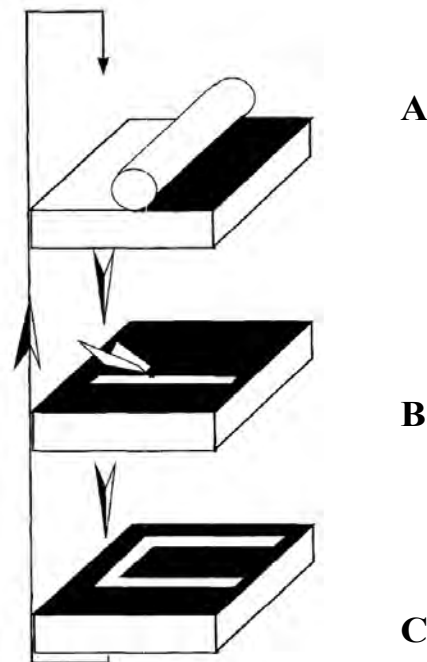


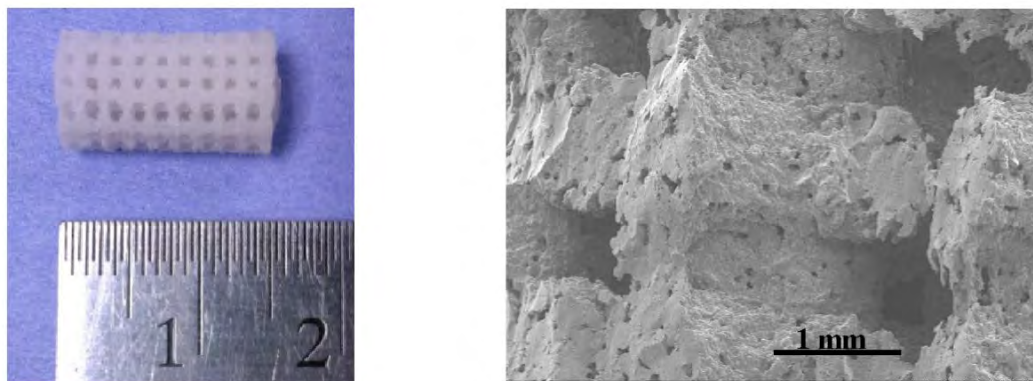
Figure 4: Selective Aggregation Process [12].

In the study performed by Pegna, it was concluded that there is a high potential of using concrete material in automated construction applications. The material shape was uniform, but it was observed to be not isotropic. By using high cement-to-water ratio, Pegna achieved a tensile strength that is approximately half of the compressive one in his developed mixture, while the usual ratio between these two strengths (tensile/compressive) is around 8% [12].

**2.2.2 Contour crafting.** Contrary to the method researched by Pegna in [12], Dr. Behrokh Koshnevis thought of additive fabrication of large-scale building elements in a different way. Instead of fabricating assemblies by selective deposition of the construction material, Koshnevis focused on applying the technique through depositing a fluid pre-mixed material that is able to harden after it gets laid on the building bed, generally speaking. He claimed highly reasonable advantages for the application of rapid prototyping in construction. This technique relies mainly on automated operations, which will require less monitoring and avoid human errors. Furthermore, automation would reduce the time needed for design and execution by conventional

methods, and this will significantly satisfy the global market. In addition, the computer-based nature of this technology will allow designers to involve more complex concepts in the geometry of built products. Moreover, environmental pollution is increasingly being of concern, and the use of automated building processes will reduce construction waste up to 0% of the total used construction materials [13].

The incentive for developing the additive manufacturing process was mainly the drawbacks of the previously discussed processes that were dependent on the use of photopolymers (resin materials that solidify when exposed to light at a specific wavelength). The speed of those techniques was not satisfactory and slow especially when considering that the first interest behind automation is reducing manufacturing time. In addition, shape and surface of finished products was not fine by means of quality which would impose heavier finishing works especially when used on a large-scale basis. As shown in Figure 5 , the surface of a small product manufactured using

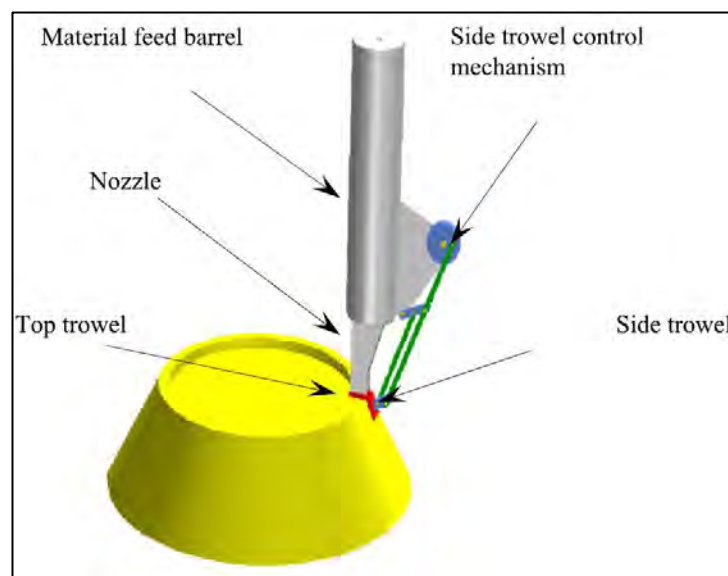


**Figure 5: Blow up of a printed sample using Selective Laser Sintering [14].**

selective laser sintering technique has small fractures on its surface. Furthermore, products made with such processes were breakable and fails in a brittle manner, and this is considered a deficiency when considering large-scale applications. The previously developed techniques are constrained to the use of certain materials, and polymers in particular, where the problem here becomes the relatively high cost of such materials specifically when large quantities will be consumed to produce large assemblies. The size of the products manufactured with those techniques are relatively small and limited by 1-meter measure. Lastly, the cost of apparatuses that operate by those techniques are as high as \$300,000 on average, and this cost is subjected to

increase proportionally with the desired quality and size of the final product [13]. As a result, all of the discussed disadvantages represented a necessity to develop and enhance a technology that overcomes the drawbacks of earlier advances and provide the needed possibility of being used in large-scale construction automation applications.

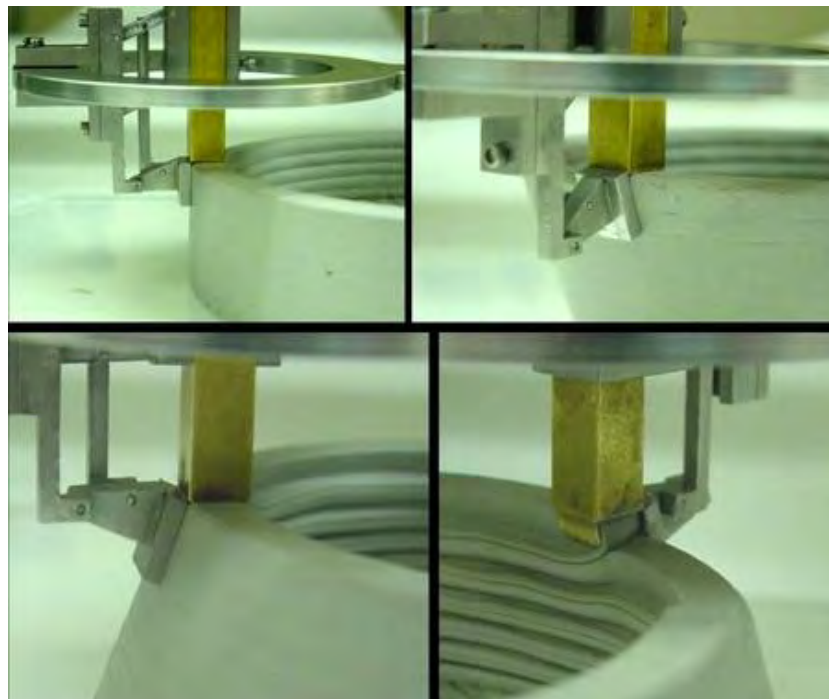
This invention is in fact a layering-based additive fabrication process that employs a flowing construction material to build the final product. The flowable material shall have the ability to solidify after being poured in the designated positions. The technique involves three main aspects that are necessary for successful operation. Furthermore, this technique uses a nozzle, and it is a part fixed at an arm that receives the delivered fluid material and extrudes it in layer-by-layer basis while moving on a prearranged path. It also adopts product surface finishing via a trowel that moves in correspondence to the movements of the nozzle, and preferably two trowels are being used for side and top surfaces. One more major aspect in this technique, is the control that specifies the movement of the material extrusion and finishing part, which can be done through different mechanisms [13]. Figure 6 illustrates the process main aspects briefly, the fluid material is pumped through a barrel to the nozzle, the nozzle then extrudes the material on the specified path with a computer-controlled movement velocity, and the trowels are placed at the top and exterior side of the nozzle assembly for directly finishing the extruded material, whereas these trowels are controlled as well by a certain mechanism.



**Figure 6: Schematic for the assembly in contour crafting [3].**

Later advances in contour crafting at the beginning of 21<sup>st</sup> century has shown a great potential in construction application when compared to similar techniques such as stereolithography and laminated object manufacturing, especially when considering that it is controlled by computer aided design (CAD). Furthermore, the unique thing about contour crafting is the ability to get a nice surface finish of final products due to the inclusion of trowels in its extrusion operation. This makes the technique featured and preferable on other potential counterparts, because it reduces the time and cost needed to perform traditional finishing works and offers the possibility of fabricating shapes that are geometrically complex as well [15]. Figure 7 shows how the side and top trowels of contour crafting machine works leading to have a nice surface finish of the final product that is viewed from all corners and at different angles of extrusion, and it is worth-telling that this can be achieved only when proper control is applied.

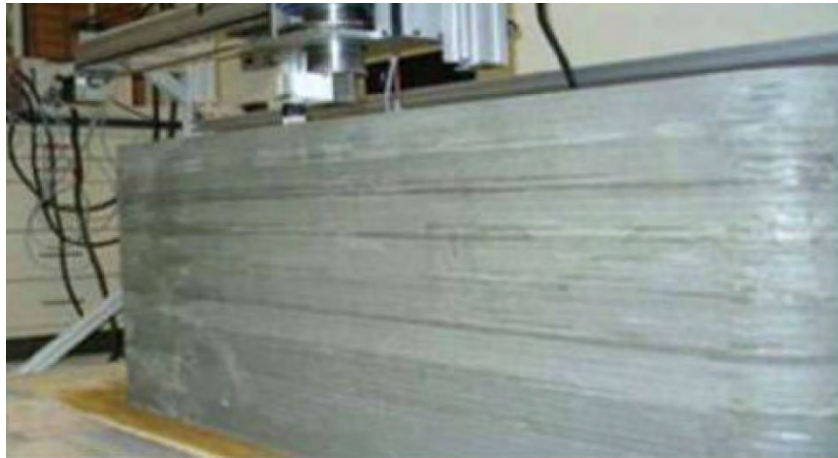
Contour Crafting was able to prove its capability of being used in construction-scale applications. As a special case for manufacturing large-scale building components, this technique is considered a 2.5-dimensional process. It extrudes products vertically with a constant section, and it is unable to manufacture unsupported or irregular parts as it builds a layer upon another one on the same predetermined path. This could be a disadvantage of this technique. Nevertheless, it still has the capability



**Figure 7: Surface Finish of Products manufactured by Contour Crafting [16].**



in a wide range of construction applications [17]. Figure 8 illustrates how the product is extruded in exactly a vertical direction.

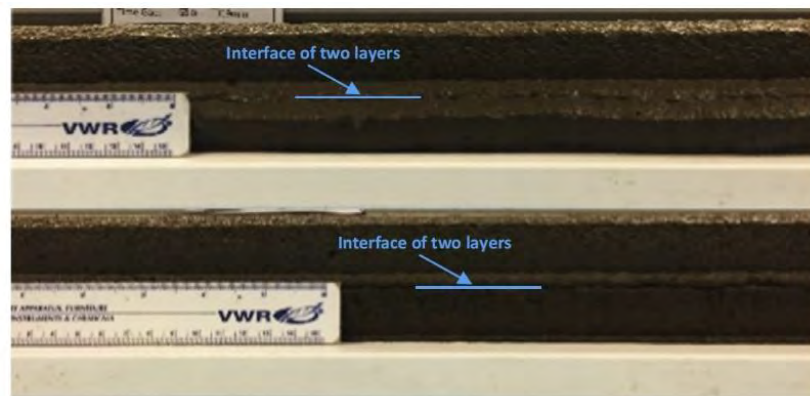


**Figure 8: Wall manufactured by Contour Crafting [18].**

Experimental work in [19] had investigated the main parameters concerning flowability of the printing material, and shown that using squared nozzles provide better outcomes than other shapes. In addition, the pressure of the pump needs to be at an optimum point where it is high enough to ensure smooth and homogeneous extrusion, and low enough to avoid internal bleeding and clogging of the material in delivery pumps. Khoshnevis has figured out that the use of such a rapid prototyping technique (contour crafting) as a new construction scheme is advantageous in many terms. As a result of the speedy nature of this building technique, it can provide a superior solution when building emergent accommodations like shelters in damaged cities encountering extreme events such as floods or wars [3]. Since automation in construction is a computer-based/controlled process, it allows complex design concepts to be implemented, and it will produce almost zero waste while being operated, making it a green construction choice compared to conventional methods [3]. Furthermore, the high control-ability on construction using this technique, and the less equipment needed compared to conventional casting methods, makes rapid manufacturing techniques potentially capable for being used in building on other planets in [21]. Kazemian, Yuan, Cochran, and Khoshnevis in [20] investigated three major flowability parameters of printed concrete. The first target was print quality, which was evaluated by observation of discontinuities, and it was figured out that the variance of printed layer width from the designed width is acceptable up to a value of 10%. The second parameter was the

shape stability. However, it was experimented by printing two layers that are 40 mm thick with and without a time gap between extruding them, and the presence of time gap reduced the layer settlement from 2.9mm to 0mm in one of the targeted mixtures as shown in Figure 9. The third parameter was printability, and it was evaluated by the printability limit measure, which was the time until the material quality starts to decline and show defects while being printed in [20]. Printability limits of values up to 55 minutes were achieved with a certain mixture [20].

Ma, Li, and Wang in [22] investigated a crucial property of construction materials that can be used in 3D printing applications, which is buildability. Lim, Buswell, Le, Austin, Gibb, and Thorpe defined buildability as “the resistance of deposited wet material to deformation under load” [23]. It can be also recognized such that the more buildable a material is, the more layers can be manufactured above each



**Figure 9: Layer settlement without time gap (top) and with time gap (bottom) [20].**

other without visible and significant deformations occurring in the printed layers [24]. This parameter is a strong indicator of the shape stability [22] of the printed mortar strips, and hence very crucial for ensuring good structural uniformity of the printed layers and avoiding differential variation in layers' thicknesses that could happen due to loading each layer strip by the weight of the overlaying layers. As illustrated in Figure 10, they printed several stacking layers with a rest time between extruding each and other layer, and then the vertical deformation and strain  $\epsilon$  were measured to indicate how capable the material is to preserve the shape of the printed layers, and it characterizes the buildability of the material. In addition, the ratio between the width of



**Figure 10: Elevation of Mortar Layers Printed for the Evaluation of Buildability [22].**

the layers and their height was obtained and compared to design values in order to indicate the stability of the overall extruded object [22]. They concluded that increasing the rest time between extrusion of layers will end up in greater buildability of the final object, and the height to width ratio in one of the trial mixtures was as high as 4.55 when relatively compared to the design value of 5.33. Additionally, Panda, Lim, and Tan reported that buildability can be enhanced by incorporating nano clay to the cementitious material that is used in printing, and found out that buildability is not only dependent on strength of the printing material, but is also based on the overall structural stability (structural global geometry) of the final printed object [25].

A major issue in calibrating cementitious materials to suit the need of 3D printing processes is the workability parameter. In such construction processes, this term identifies a proper and homogeneous flow of the material through the machine pipes until reaching the extrusion nozzle [22]. Researchers pointed out that shear vane test would give more suitable results in comparison with conventional methods of evaluating workability of concrete [24]. Shear vane mainly employs a rotating arm that has blades at the ends of it, and this arm is put in a container which has the targeted material and apply torque on it [26]. Therefore, the measured torque will be converted to shear strength, and will vary depending on the flowability of the material. It was reported by [24] that a shear strength of 0.55 KPa was good enough to print 15 stacking layers each composed of a single strip (not a group of adjacent strips that support each other) without collapsing. Figure 11 exhibits, with the same shear strength, the ability

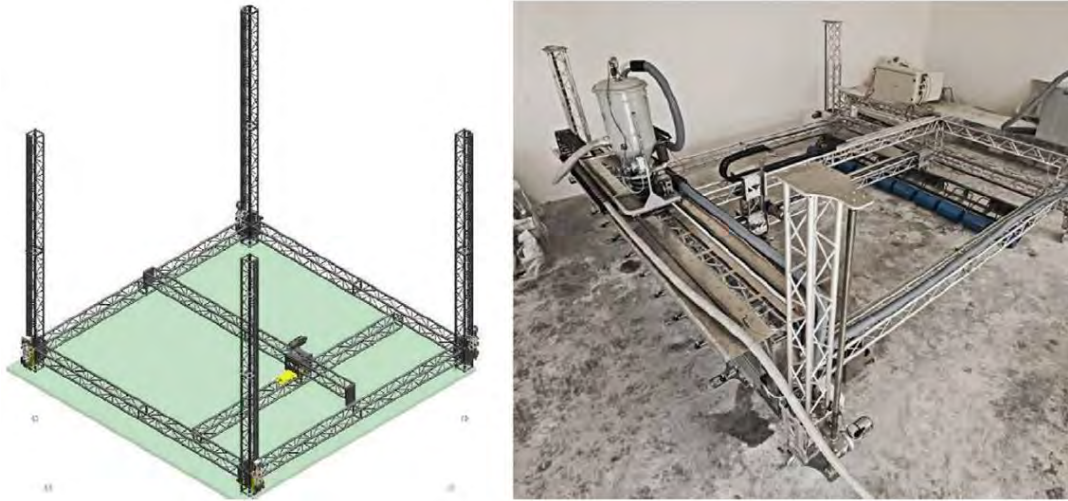


**Figure 11: Several printed objects with different number of strips in the horizontal plane [24].**

of having a greater number of layers printed vertically by having more strips in each layer, where these strips help each other not to fall down.

Panda, Paul, Mohamed, Tay, and Tan in [27] have investigated the factors affecting the tensile bond strength between printed layers of geopolymer mortar. They found out that the bond strength could reach up to 1.1 MPa along with decreasing the time gap between printing each and other layer to 5 minutes [27]. Moreover, they have shown that the bond strength increases with decreasing nozzle standoff distance and printing speed [27].

**2.2.3 D-Shape technique.** In 2008, Enrico Dini patented the D-Shape technique and got filed and identified as another rapid prototyping process [28]. It was specially intended for the purpose of manufacturing building components at construction-scale. This technique operates in a fully 3-dimensional way allowing it to produce shapes with irregular cross sections, and that was the discriminant between this method and contour crafting which extrudes constant cross sections. Figure 12 shows a schematic of the manufacturing machine on the left, and a real large-scale D-shape 3D printer on the right. This technique works by having a frame that defines a plane for which each horizontal layer of the final object is constructed, and represents the enclosure of the printing area along with the existence of circumference walls. This frame is able to



**Figure 12: D-shape Printer [29].**

move vertically on the z-axis from its four corners at the same time. A crane is connected to the mentioned frame, where it is capable of moving in the direction of x-axis or y-axis simultaneously, and it elevates by the effect of the frame movement. The printing head is fixed at the movable crane and moves in the direction perpendicular to the crane's motion. Since this technique is based on a layer-by-layer based fabrication, it depends on a computer-aided design model that defines the geometry of each layer as a surface. The CAD model is sliced into several number of layers that conform to the thickness of each layer, and the printing process starts by scanning the sliced CAD surfaces from bottom to top of model. The printing head builds each layer by deposition of grainy material at the specific locations that were determined by the computer model, followed by sprinkling liquid polymers that bind the deposited powders to create a solid object. The process is repeated for each layer in compliance with the CAD sliced models. In the printing area, the granular material accumulates, and as binding occurs to specific path and locations, remaining areas are having unbonded material. Those unbonded grains is not only cleaned away to be used again in another manufacturing process, but also acts as a supportive structure to the overhangs in printed layers especially when building irregular shapes [28]. The right part of Figure 12 exhibits the way objects are shaped using D-shape technology, and this technique was discriminated from contour crafting by binding the material after depositing it into place, while the other technique pre-binds the material before extruding it, which makes it similar to the use of conventional concrete in construction. The post-binding-based operation in D-

shape technique allows building a full large-sized object at one phase of the process, as illustrated in Figure 13.

It is important to consider that the printing head operation is well controlled in terms of volumetric flow, and this is to ensure that the amount of deposited material complies with the designed layer width and thickness, in addition to being suitable with the speed of deposition [28].

For the purpose of good-appearing finish of the final product's surface, a blade is attached to the printing head, which ensures the uniformity of the deposited layers of the grainy material such that when binding occurs, the thickness of each layer is constant [28].

In the first filed patent of Dini, the liquid binders were polymer resins including epoxy and Polyurethane. Binding action of granular materials happened by spraying the resin in its fluid state so that it ensured to penetrate the voids in the grains of the pre-deposited layer until reaching the previously solidified layer below. The reason behind requiring this depth of penetration is that the major intention is not only solidifying the last printed layer of grainy material, but also to make sure the bond at interlayer surface is strong enough [28].



**Figure 13: Single Room Printed using D-shape technique [29].**

The use of polymer resins has led to problems as they adhere to whatever they touch, and the major problem was the significant cost for the maintenance of the fabricating machines. In addition, polymers are poisonous and easily set afire. Hence, Dini has improved the patent in 2009 to involve the use of inorganic binders to avoid the previously faced issues and make the patent more efficient in all terms of applicability and cost [17].

**2.2.4 Concrete printing.** Concrete printing technique is very similar in principle and application to contour crafting. Minor differences can be found, such as the surface finish not being smoothed by a trowel attached to the printing nozzle, and that the size of the final object is limited to the size of the printing frame where the final object is contained within that frame [23][29].

### **2.3 Evaluation Criteria of 3DCP**

Two major aspects of the material used in 3DCP are crucial for evaluation, which are fresh-state properties representing the workability and constructability of the material, and mechanical properties reflecting how strong the material is when loaded in different directions. In addition, it is worth noting that such technology is yet not mature enough to have evaluation standards. Hence, some of the standard tests were used as is, others were manipulated to be used in testing printed concrete, whereas some new testing methods and criteria were newly developed by researchers to investigate specific parameters of the material.

**2.3.1 Rheology evaluation.** 3DCP technology is a totally different construction scheme when compared to the normal concrete construction practices. All of these technologies like concrete printing and contour crafting share the same construction method that is based on robotic extrusion of the material to obtain the final object [23]. Hence, this implies the need to focus on rheological parameters of the material used in 3DCP technology as this is one of the key factors in assuring the success of the procedure and the success of getting an acceptable quality of the final printed object. Rheology is crucial not only for maintaining quality of the process, but also for the integrity of the robot and the attached delivery system like pipes, tubes, or conduits, which are responsible of the extruding the material on the bed through the end nozzle. In other words, the material shall be rheologically capable of being pumped through the

delivery system without any stoppage, clogage, or hardening while being pumped because maintenance costs are significantly high [31], which in return has a counter-effect on the potential economic efficiency of the technology. This has pushed researchers to investigate the rheology of 3DCP materials in both standard methods and newly developed methods as can be seen in [22–24] and [30–32]. Standard tests to evaluate rheology are mainly slump, flow table, an V-funnel, and they represent how workable the material is. New rheological parameters along with methods for evaluating them, solely designated for 3D printing techniques, were developed and experimented such as buildability, workability that were discussed in section 2.2.2, open time, and extrudability that will be illustrated in the upcoming paragraphs.

Extrudability is a very important parameter in the evaluation of mortar mixtures for 3D printing, it describes the capability of the material to be ejected in a continuous manner to form homogenous printed strings without the flow being stopped or the delivery system being clogged during the printing process. Furthermore, the better the extrudability of a material, the longer strips can be made without being separated or fractured during the extrusion [22],[24]. The method to evaluate extrudability as per [22] is to extrude a 2000 mm long continuous strip that returns 8 times every 250 mm, creating 8 subsegments as illustrated in Figure 14. The conclusion of this test is based on observation of continuity and separation-less of the print process, which is either a YES or NO result, and the experiment was conducted by [24] in a similar way, but the length of the printed strip was 4500 mm.



**Figure 14: Top View of 2-m long printed mortar strip [22].**

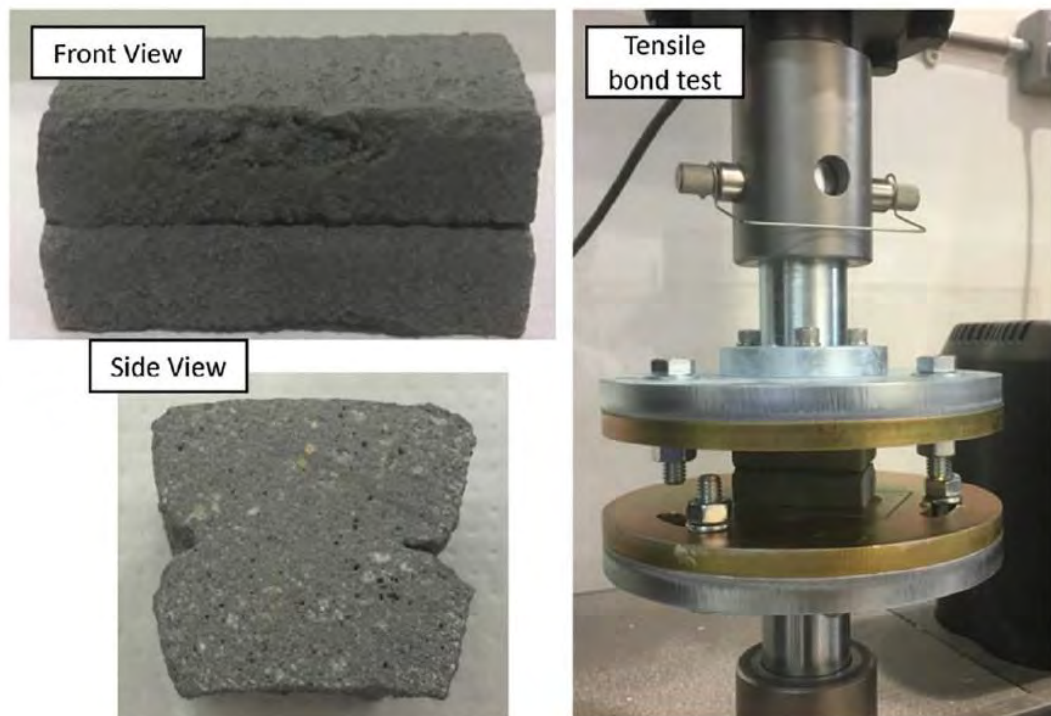


Open time is the period for which the printing material can still be extruded continuously without separation, and it is related to the setting time of the material [22]. Conventionally, this parameter is obtained by Vicat apparatus or slump tests, but it is not useful when considering printing of the material as such methods target initial and final setting time only, hence, it helps evaluating overall workability rather than specifying a specific flow parameter that varies over time (that is critical in extrusion process). Alternatively, vane shear test was employed [24]. Vane shear test applies torque to a mortar mix in a certain container at different time intervals and then shear stress is calculated, and this stress characterizes the workability and pumpability of the material and the variations of these properties with time [35]. The open time then is specified as the time until reaching a certain shear stress that corresponds to a level where workability loss exceeds the limit of acceptable printability. To simplify the method as in [22], the open time is measured by extruding mortar strips with equal dimensions at consequent time intervals (e.g. 10 minutes), and the open time will be the time until the first separation or blockage happens during the print process.

**2.3.2 Strength evaluation.** Although rheology is the major focus in experimenting materials for 3DCP, mechanical properties of materials remain of high importance. This is to achieve a certain level of integrity for the final output in terms of durability and strength, that mainly defines the structural behavior, capacity to different types of loading, and service life of 3D structures. Standard tests were used to investigate compressive strength, tensile strength by splitting, and flexural strength of the material. Another parameter is interlayer axial bond strength, discussed in the next paragraph, which was considered by some researchers such as in [27], [36], [37], and [38].

3D printing processes is based on additive manufacturing and on extrusion of stacking layers that are standing upon each other. Hence, the strength of the interface bond between stacking layers is a crucial factor that has a major role in the overall stability of the printed structure. Although the nature of 3D printing processes is based on layering and the multiple stacking layers that form the final object are printed at different times, the presence of interface between these layers is an advantage for the stability of digitally fabricated objects as it prevents crack growth and propagation between layers [39] if it happens in one or more of the layers during early and/or service

life. Bond strength was found to be dependent mainly on the printing material properties, speed of printing, vertical nozzle offset, and the time period between printing each and another layer [27]. A useful method for testing the bond strength of printed concrete layers was explored by [27], that is preparing specimens composed of two layers of a certain dimension, and investigating the failure of these specimens in INSTRON universal testing machine for axial tensile strength. As shown in Figure 15, two steel plates are attached to the top of upper layer and the bottom of lower layer, respectively. Accordingly, a suitable test setup is prepared to fix the plates in the machine, and then the test is conducted. To measure the bond strength as a stress value in MPa, failure load is recorded, and the interface area is measured [27]. Uniaxial compression test and splitting tensile test were also used to identify the bond strength of interfaces between layers of contour crafted specimens, and the results of these two tests could vary in terms of mode of failure and its regions [40], [41]. However, all of such testing methods can provide helpful results to measure the strength of the bond between printed concrete layers. Placing a cementitious colored paste on each layer before printing the upper one was found beneficial to the interlayer axial bond strength, as stated by Taylor, Jay, and Ming in [42].



**Figure 15: Bond Strength Test Setup and Sample Specimen [27].**

## 2.4 3D Concrete Printing in the United Arab Emirates

**2.4.1 Vision.** According to Dubai Future Foundation, by the year 2030, Dubai municipality is willing to have a regulation that requires 25% of every new building in Dubai to be 3D-printed [43].

**2.4.2 Recent achievements.** The first 3D fully functional building in the world was constructed in Dubai in 2016 and named the office of the future, and it is clearly shown in Figure 16a. However, this 250 m<sup>2</sup> building was printed off-site in a precast concrete factory, where it took 17 days to be printed, 2 days to be erected in the site, and 3 months for mechanical, electrical, and finishing works. It was evident that a 50% cut in labour cost is achieved through the use of printing technology [44]. In 2019, Warsan building was revealed in Dubai as the largest two-storey printed building in the world, that has a 640 m<sup>2</sup> area and is 9.5 m high. This building is considered more advanced than the printed office since it was printed on-site using locally available materials [45]. Figure 16c shows Warsan building after completion of construction. In the same year, the first 3D printed heritage house was printed in Sharjah using a giant printer that is operated by CyBe construction company [46]. This house combines the use of recent technologies in construction and the cultural fingerprint of UAE's houses in its architectural design, as can be seen in Figure 16b.

## 2.5 Summary

As seen in the previous sections, few researches are being done to investigate the large-scale application of 3D printing using cementitious materials e.g. concrete. Several material parameters are being continuously studied to characterize the behavior of the material at both fresh state and hardened state.

Since this process is based on additive placement of layers, the bond shear strength is an important parameter affecting the structural behavior and stability of printed members where they are not monolithically casted as one unit. On the structure level, the action can be considered composite due to the existence of contact regions between printed layers. For instance, in the case of a 3D-printed wall, the interface shear strength will have a major contribution to resist lateral forces such as wind and seismic forces. Bond axial strength was addressed in some previous researches by applying axial tension to two stacking layers as in [27], [36], and [38]. Additionally, Marchment,

Sanjayan, and Xia enhanced bond axial strength using glue [42], where Hosseini, Zakertabrizi, Habibnejad, Korayem, and Xu have used sulphur and black carbon polymer instead, and they achieved more than a 100% enhancement in the tensile axial strength at interfaces between printed layers [47]. On the other hand, bond shear strength was experimented indirectly by conducting splitting tests (force applied at layer interfaces) on printed specimens with different orientations as in [41] and [48]. Direct bond shear test was carried out on extracted specimens from large-scale printed objects by Rahul, Santhanam, Meena, and Ghani in [49]. However, their bond test setup was deemed complicated. It is believed that interface shear fracture represents a more convenient failure mode than interface axial separation, which is an additional reason to target the bond shear strength between concrete layers in this study.

The properties required for having a material suitable for being printed are all challenging to get in one mix. For instance, getting the material to be more flowable, could lead to sacrificing some of the mechanical and strength-related properties, and vice versa. Furthermore, there is a significant lack of guidance on mix design and evaluation, and the majority of related works that were discussed in the literature are



(a)

(b)



(c)

**Figure 16: (a) Office of the Future [44], (b) Sharjah 3D House [46], and (c) Warsan Building [45].**

either veiling their ways of proportioning concrete mixtures, or still experimenting the suitability of different material compositions in this application. Moreover, the previously explored researches were implementing their works in laboratory-controlled environments. The aim of this study is to achieve a proper concrete mixture that suits the application of 3D concrete printing or contour crafting using local materials, and to investigate the effects of exposure to the harsh climatic conditions of the United Arab Emirates on extrusion process and mechanical properties of extruded objects.

## **Chapter 3. Methodology**

The main aim of this study, is to achieve a concrete mixture for the use in 3D printing operations, and evaluate its properties at different environmental conditions. The material shall be having adequate flowability, extrudability, buildability, strength, and setting time in order to suit the printing processes [24]. All of the mentioned characteristics are primarily related to the design of mix and the choice of mix ingredients and proportions. Hence the first focus in this study is to design a mixture that fits as many requirements as possible. Trial mixtures will be worked out, and their investigation will depend on the success of the printing operation. Thereafter, the fresh and mechanical properties will be observed through standard and non-standard testing methods, which will be discussed further in this chapter. In addition, this study will focus on investigating the effect of harsh climatic conditions of the UAE on the process of 3D concrete printing by simulating its effect on the material level and how its fresh and hardened state properties might be impacted as a result to that simulation.

### **3.1 Experimental Scenarios**

In order to achieve a comparable outcome that indicates how environmental conditions affect the process, two different mixing and exposure scenarios are considered in this research for the same concrete mix.

The first scenario represents ambient laboratory environment, where the water used in mixing will have a temperature that is same as the cool laboratory temperature, and all of the specimens will be kept uncured inside the laboratory for 7 days before being tested.

The second scenario represents the outside hot temperature, where the same mixture is prepared using heated water that has a temperature equal to 50° C. This was found acceptable to simulate the effect of on-site material mixing. All of the specimens will be kept uncured outside the laboratory and exposed to high temperature and sun radiation for 7 days before being tested.

### **3.2 Mix Design**

Since 3D concrete printing processes are based on extrusion techniques to construct the final object, hence, it is very similar to the way of producing precast

hollow core slabs through extrusion machines. The similarity between these two applications can be very beneficial when considering mix design and requirements for 3D printing of cementitious materials. It can be good as a starting point in developing a proper concrete mixture for use in 3D printing applications.

According to PCI hollow core slab design manual, the mixture for hollow core slab extrusion shall be dry enough with a low slump and flowable to be suitable for the extrusion machine and preserve the shape of section after being extruded. Such concrete mixtures are well known with their low water-to-cement ratio that is very close to the minimum needed for cement hydration. Water reducing admixtures are involved for the purpose of attaining a proper workability for extrusion despite the reduction of water and cement requirements [50].

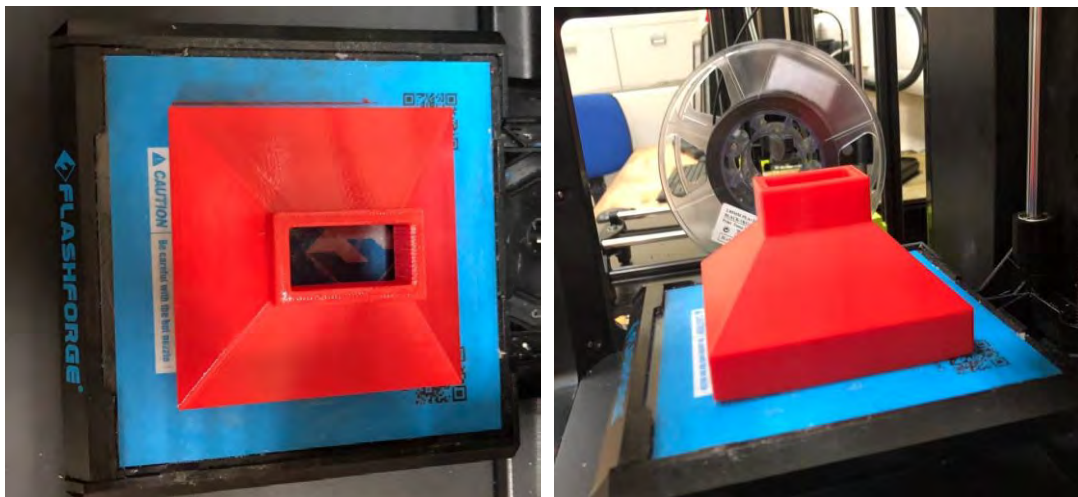
The development of mix proportions for 3D printing in this study will be based on a starting point that is represented by a hollow core slab mix design that is of Elematic type, which suits production by extrusion techniques. This mix was designed based on Standard Practice for Selecting Proportions for Normal, Heavyweight, and Mass Concrete, ACI 211, and approved for use in construction by local building officials (Dubai Municipality) in Dubai, United Arab Emirates. The start-up mix will be composed of locally provided materials that are proportioned as shown in Table 1. Since this study is incorporating the effects of harsh climatic conditions in the United Arab Emirates in terms of high temperature, it is worth noting that the air content of the targeted mixture shall be low to provide better durability and service life [51]. In addition, since the mix has a low water to cement ratio, dispersion of air in the mix is difficult which is another reason behind the low air content [50].

**Table 1: Hollow-core Concrete Slab Mix Design [50].**

<b>Ingredient</b>	<b>Corrected Batch Weight (kg/m<sup>3</sup>)</b>
Cement	288
GGBS	162
Water	130
10 mm Aggregate	1073
0-5 mm Aggregate	558
Dune Sand	224
Water Reducing Admixture	4

### 3.3 Trial Batches and Extrusion

The start-up mixture that was shown in Table 1 contains coarse aggregates with diameter exceeding 5 mm. This presents a major problem when thinking of 3D printing due to the difficulty of passing coarse aggregates through printing nozzles. To account for that, major modification is done to that mixture before proceeding with trial mixing stage. This modification will be discussed in the next chapter. The modified mixture will be used as the actual starting mix. Based on the latter mix, several trial batches will be worked out and experimented by manual extrusion through an in-house manufactured nozzle. Figure 17 shows the nozzle that was created using a 3D printer. The nozzle outlet is 40 mm wide and 20 mm high which was seen acceptable to represent a cross section for 3D printed filaments in this study. The nozzle is used by filling the cementitious material in its inlet squared area, then applying pressure manually on the filled area. This leads the material to pass through the outlet and shape concrete layers. This is better explored in Figure 18, where the left part shows how the extrusion takes place manually, and the right part shows a sample layered object from the extrusion process. All mixes of the study are batched in volumes of 1 liter using Hobart mixers.



**Figure 17: In-house Manufactured Nozzle (left) Top View and (right) Side View.**

A sample layered specimen is made out of every trial mix for evaluation purposes. Each specimen is composed of 2 layers, or more in some cases. The evaluation criterion for trial mixes will be based on observation of both shape retention





**Figure 18: Manual Extrusion, (left) sample extruded concrete, (right) sample layered object.**

and surface quality of the extruded objects. Based on that evaluation, one trial mix will be chosen as the optimum, being the most suitable for extrusion and printing.

The chosen mix will be used to cast all of the specimens in both scenarios for the main experimentation of this research, that is illustrated in the upcoming section. However, extrusion of main specimens of the study is done using an adhesives' injection tool and an in-house 3D-printed nozzle that fits the injection tool. The nozzle and the tool are illustrated in Figure 19. Nozzle output is still 40 mm wide and 20 mm high, and the injection tool is cylindrical in shape, 60 mm in diameter, and 500 mm



**Figure 19: Injection Tool and Fitted Nozzle for Extrusion.**

long. This was seen better simulating the actual extrusion that happens through giant concrete printers as can be observed in Figure 20. It was considered as the main extrusion method in this study after the trial mixing evaluation stage.

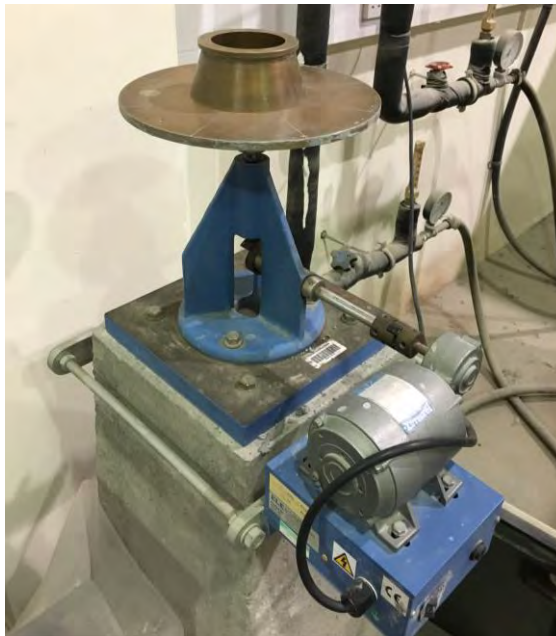


**Figure 20: Manual Extrusion using The Injection Tool.**

### **3.4 Methods for Testing and Evaluation**

In this study, material testing and investigation will be divided into two main phases, the first phase is testing at fresh state of the cementitious material, and the second phase happens at the material's hardened state. The first phase of testing is concerned with workability, through the use of flow table test, open time, and extrudability. The second phase of testing focuses on the mechanical properties and strength related parameters. Stiffness and Strength of Cementitious materials that are designed to be used for 3D printing processes are crucial at both early and mature ages of the material. Each layer of printed mortar is responsible for carrying the above layers without having significant deformations. In addition, the printed layers shall be consistent, free of defects, and featuring dimension conformity in order to operate a successful print process that ends up in a final product that complies well to the predetermined design [20]. The targeted strength parameters in this study will be mainly compressive, flexural, and shear bond strengths.

**3.4.1 Flow table.** Standard Specification for flow table for use in tests of hydraulic cement, ASTM C230, was used to evaluate the rheology of the mortar mix developed in this research. Figure 21 shows the apparatus used for this test, and it is composed of a rigid circular platform that is 225 mm in diameter, and connected to an electrical engine that causes rotation to the platform and lifts it up on a cyclic basis. In each cycle, the platform is lifted up slightly and left to drop back to the same initial level by its own weight. The mold is open from top and bottom, where concrete is placed at its fresh state in two layers, and each layer shall be compacted 10 times by a standard hammer for this test. After the concrete is placed and mold is filled, the mold is removed slowly, then the engine is turned on until 15 drops happen to the platform. Afterward, two orthogonal diameter measurements are taken from the sample, and



**Figure 21: Flow Table Apparatus.**

averaged as the flow table diameter for that specific mortar mixture. After concrete has flowed, the difference in the diameter of the sample from the original base diameter of the cone (100 mm) is calculated as a percentage of that original base diameter [52].

**3.4.2 Open time.** As discussed in the previous chapter, 3D concrete printing is in need for newly developed tests that account for parameters that highly affect the success of the process, and open time is a critical parameter that is important to identify a concrete mixture for use in extrusion processes. In this study, open time is measured

while printing as the time from when mixing has finished until the extruded filaments start to show stoppage, blockage, or discontinuities.

**3.4.3 Extrudability.** Extrusion in this study is subjective, such that it tells whether the concrete mix has the possibility to be extruded smoothly without stoppage while the shape of the printed filament is relatively preserved with a good surface finish. This is evaluated through observing the extrusion and the shape of the layer after being extruded.

**3.4.4 Compressive strength.** Compressive strength of concrete is a crucial performance indicator, and the design of all structural elements is dependent on it. According to the standard specifications ASTM C109, the molds for this test are steel cubes 50 mm in width, length, and height. Figure 22 shows the mold for concrete specimens in this test. The specimens shall be removed out of the molds after 16-72 hours from pouring, and then cured for 28 days, but 7 days curing is still accepted with the application of some modification factor [53]. Both molded and printed cubes are considered for this test. The printed specimens will be composed of 2 stacking layers



**Figure 22: Cubic Concrete Molds for Compression Test.**

40 mm on each side that could vary in height due to post-printing settlements. The size of printed samples followed previous research work by Wolfs, Bos, and Salet [48]. Both molded and printed specimens will be tested under compression in the same manner to obtain the compressive strength in MPa. Thereby, the failure force is divided by the

pressured surface area for control cubes, and by the average surface area between top and bottom layers for printed cubes.

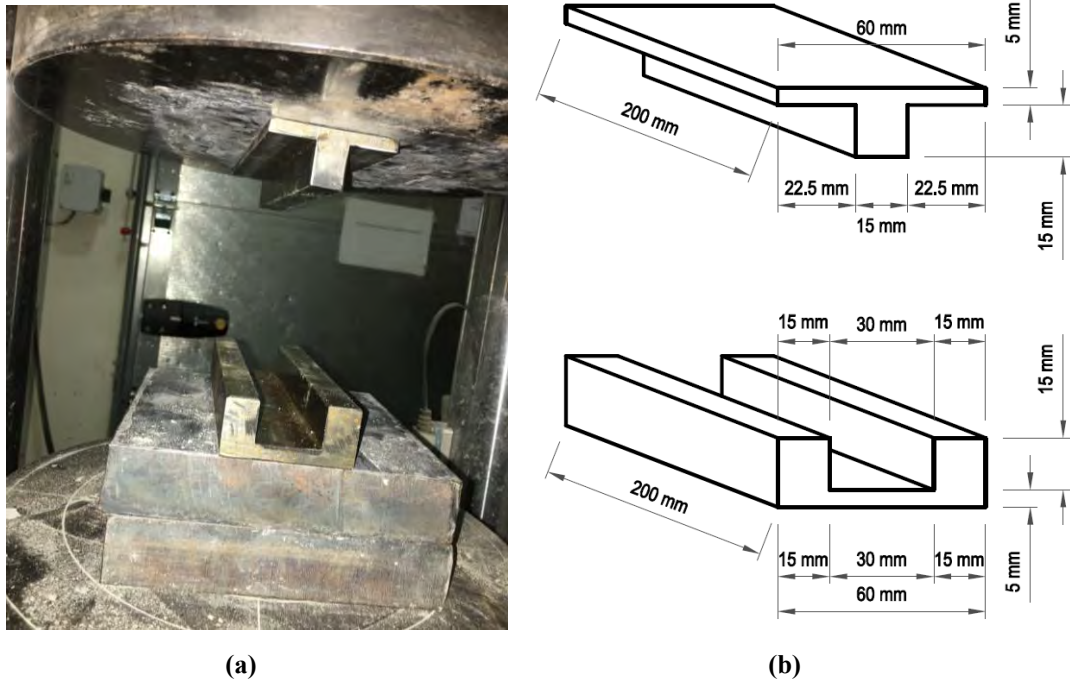
**3.4.5 Flexural strength.** Flexural Strength test is another measure of performance of concrete, and the results are named moduli of rupture of the concrete specimens. According to ASTM standards C348, this test is based on applying a point load on a simply supported concrete prism that is 50 mm in length and width, and 200 mm in length. As shown in Figure 23, flexural test setup and calculation equation, the load is centered at the middle of the specimen.  $F$  is the failure force,  $L$  is the span between supports,  $b$  and  $d$  are the width and depth respectively. The mold is a beam-shaped steel mold, the dimensions of the mold can be chosen such that the depth of the beam is 1/3 the clear spacing between the 2 simple supports. The beam is loaded until fracture, and the modulus of rupture can be measured from the fracture force [55].



$$\text{Flexural Strength (MPa)} = \frac{3FL}{2bd^2}$$

**Figure 23: Concrete Prism Under ASTM C348 Flexural Strength Test [54].**

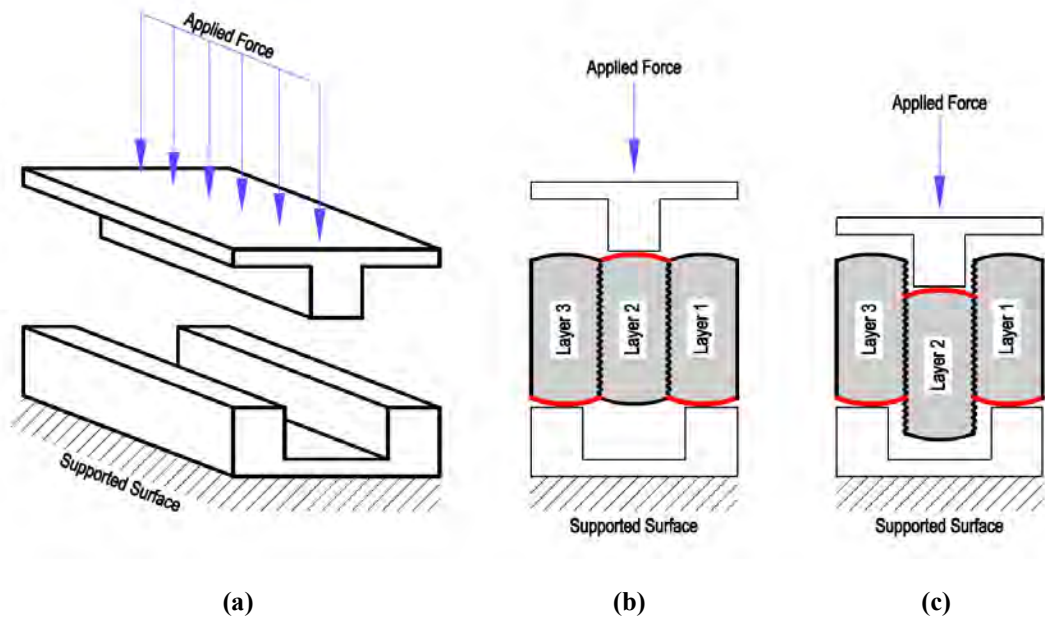
**3.4.6 Bond shear strength.** Evaluating bond strength of 3DCP specimens is difficult when INSTRON universal axial tension machine is used. This can be due to gripping problems, complexity of fixture, and force alignment issues. In order to streamline the mechanism of evaluating shear strength of the bond between concrete layers, a simplified novel setup was designed in this study such that it can be used in the compression testing machine as shown in Figure 24a. The fixture for this test is basically composed of two in-house manufactured steel objects. Figure 24b shows the bond shear test fixture used in this study. The upper part of fixture is a T-shape section



**Figure 24: Bond Shear Test Setup (a) Machine Configuration and (b) Details of Fixture.**

that is responsible for applying the force to the middle layer of the specimen, and the lower part is a U-section that acts as a support of the outer layers of specimens and allow the mid-layer to displace downward as illustrated in Figure 25a. As will be discussed in the next section, specimens for this test are composed of three printed layers, where the middle layer is loaded as shown in Figure 25b until failure, that is illustrated in Figure 25c. The force that causes separation at one of the interfaces of mid-layer is recorded by the machine, and is divided by the effective area of that interface to obtain the bond shear strength in MPa.

**3.4.7 Shape retention.** It is very important to take into account variations in the actual geometry of printed layers from design geometry (nozzle geometry) in order to predict the actual print geometry from a given design geometry. Figure 26 illustrates how settlements occur while additional layers are being printed. In this study, specimens that were casted for flexural test (two stacking layers) and bond shear test (three stacking layers) are used to trigger variations in the geometry in comparison to the design nozzle size. After size reductions occurred in printed specimens, the width and depth of each specimen is recorded so that an index for shape stability/retention (SRI) is represented by width variation similar to the conducted approach in [56]. Additionally, another index is created for height retention (HRI). SRI is calculated by



**Figure 25: (a) Load Mechanism on the Fixture, (b) Unloaded Specimen, and (c) Loaded Specimen.**

dividing the nozzle width (40 mm) by the actual filament width, whereas HRI is calculated the other way around (total height of printed part divided by the product of nozzle height and number of printed layers.) The difference in way of calculating width and height indices is considered for the purpose of maintaining the ratio below or equal to 1, by keeping the potentially larger term in the denominator (refer Figure 26: nozzle height  $\geq$  actual height, and nozzle width  $\leq$  actual width.)

### 3.5 Test Specimens

Three tests were implemented in this study to target three major mechanical properties of 3D printed concrete that are compressive strength, flexural strength, and bond shear strength. Furthermore, every test was implemented on both molded specimens that are control in this study, and printed specimens with a geometry that matches the molded specimens as far as possible. Exact matching of molded and printed specimens was not possible due to that the latter were extruded through a nozzle with a fixed size (20 mm high x 40 mm wide.) Furthermore, geometry of printed specimens is not only controlled by the size of the nozzle, but also by the settlements that occur after printing and variation of printing speed due to the nature of manual extrusion. This is the reason behind small variations in geometry and size of specimens for each test. Those variations will be demonstrated when shape retention results are discussed.

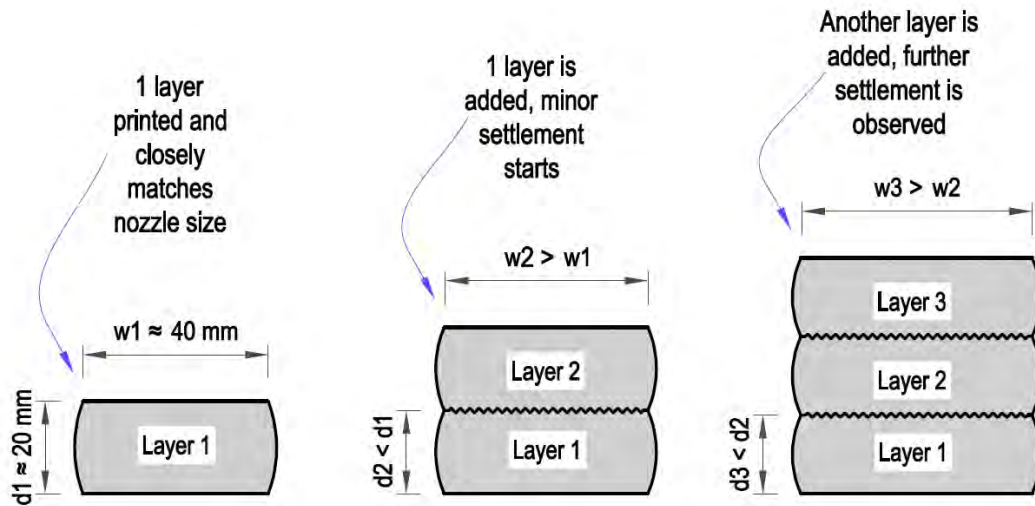


Figure 26: Settlement of Concrete Layers while Additional Layers are Added.

**3.5.1 Compressive strength specimens.** Control specimens for compressive strength test are cubes that are 50 mm on each side as per the ASTM C109 standards [53]. However, printed specimens are composed of two stacking layers where each layer is 20 mm high, 40 mm wide, and 50 mm long. This was the closest geometry to the control specimen as can be seen in Figure 27.

**3.5.2 Flexural strength specimens.** Standard size for mortar prisms as per ASTM C348 standards (200 mm long and 50 mm in height and width [55]) were used as the control specimens for flexural strength test as shown in Figure 28. Printed specimens were composed of two stacking filaments where each of the layers was 20 mm high, 40 mm wide, and 160-200 mm long as illustrated in Figure 29a. However,

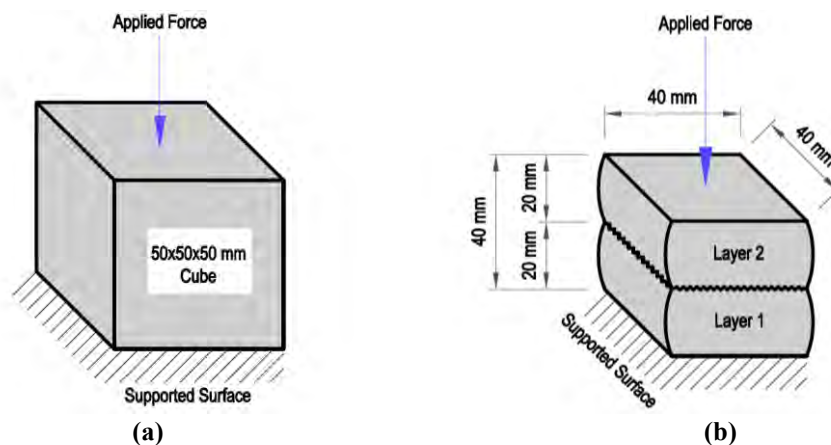


Figure 27: Specimens for Compressive Strength (a) Molded and (b) Printed.



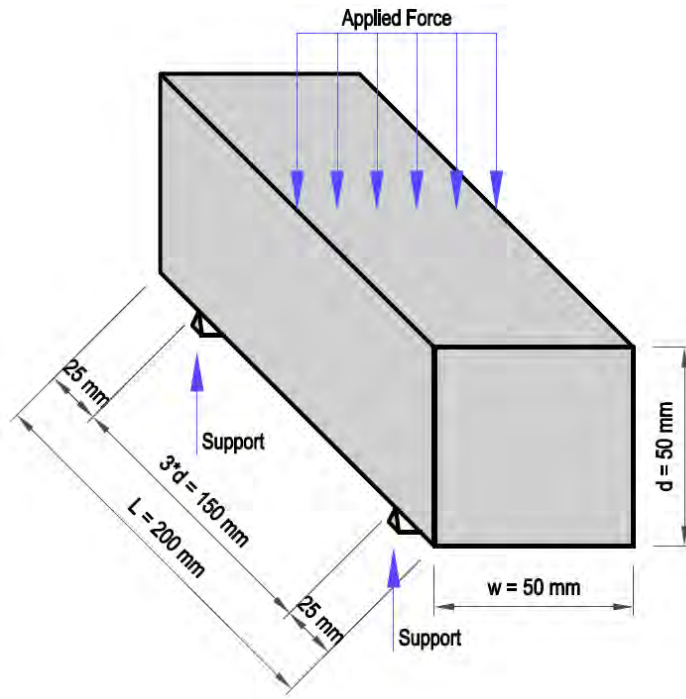


Figure 28: Molded Concrete Prism for Flexural Strength Test.

printed specimens do not attain the exact designed geometry, and this is due to settlements happening after printing. Accordingly, to comply with the test standards in

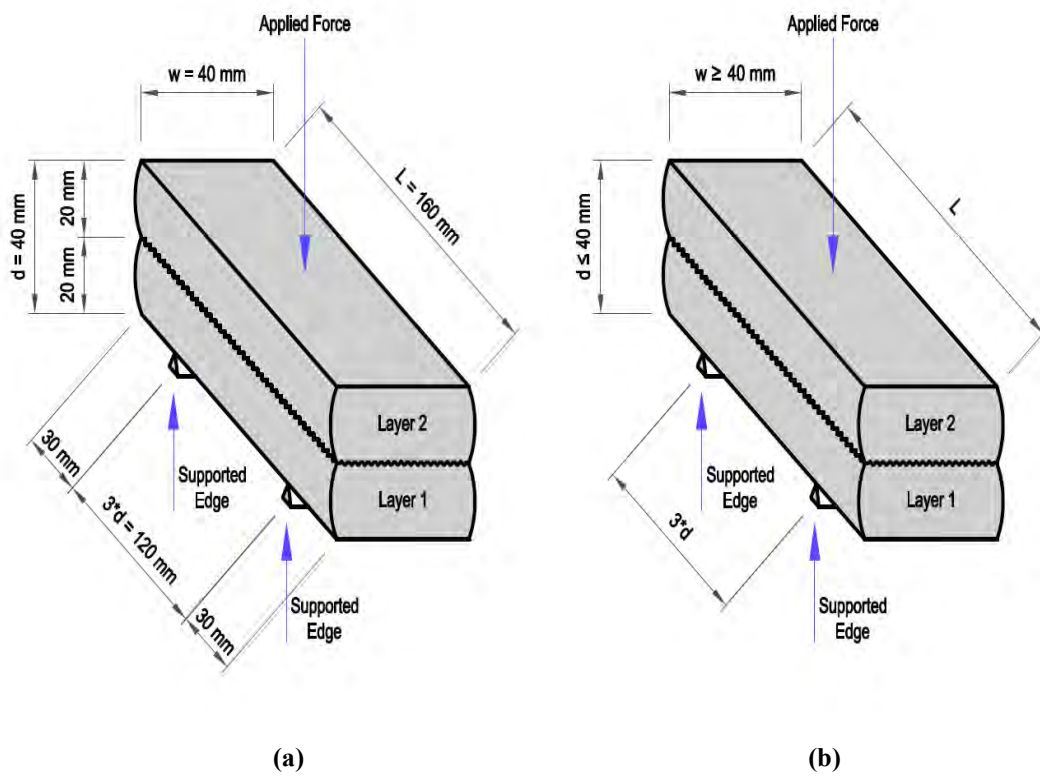
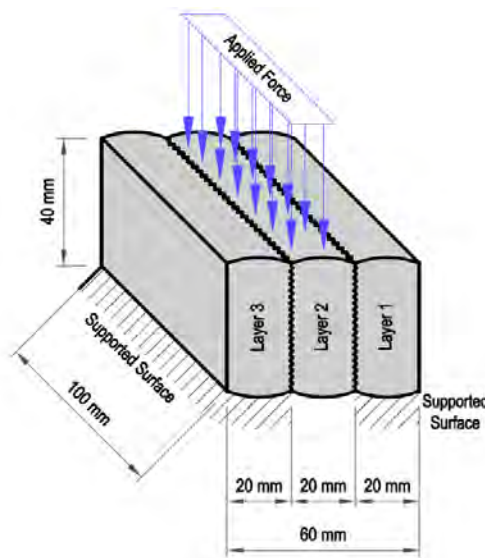


Figure 29: Printed Specimen for Flexural Strength Test (a) Designed and (b) Actual.

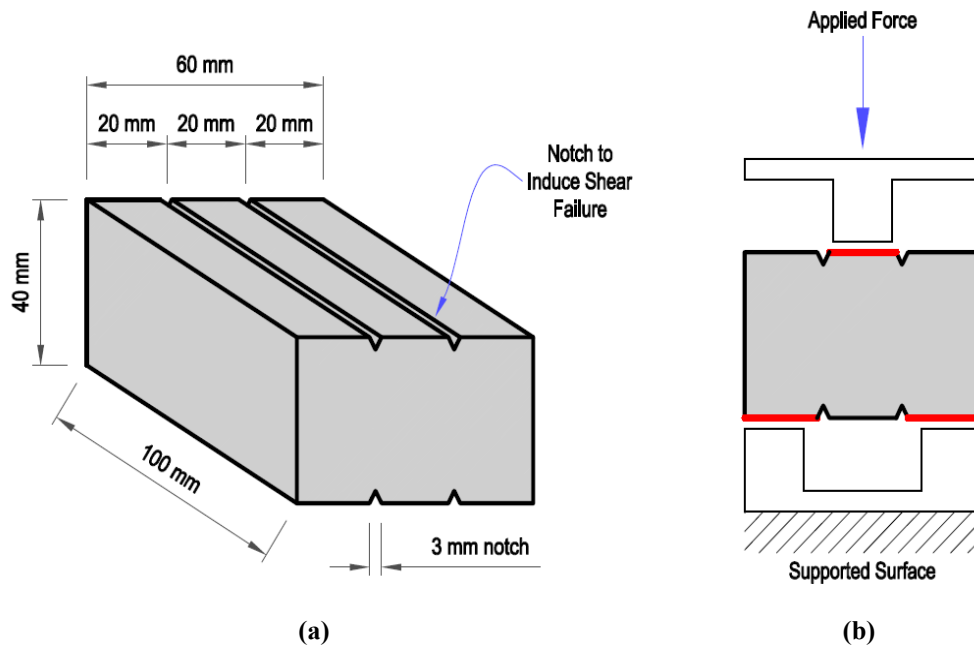
[55], the span between supports was considered to be three times the overall effective depth of the specimen as shown in Figure 29b.

**3.5.3 Bond shear strength specimens.** Since the bond shear test is developed in this study for evaluation of 3D printed concrete, control specimens were also designed through the study to match the printed concrete specimens. Bond shear test printed specimens consisted of 3 stacking layers where each layer is 20 mm high, 40 mm wide, and 100 mm long. Printed specimens are tested in a 90° orientation with respect to the printing direction as shown in Figure 30. In correspondence to the discussed print geometry, timber molds were designed to be 100 mm in length, 60 mm in height, and 40 mm in width to match the printed concrete specimens for the same test. In order to induce shear failure, notches that are 3 mm in depth and width were made at 20 mm height intervals along the specimen length. An example of bond shear molded specimen and its load configuration are better illustrated in Figure 31.



**Figure 30: Printed Specimen for Bond Shear Test.**

Additionally, time interval of printing process between each layer and the stacking one is essential in effect on bond shear strength at interfacial regions. Hence, three different time intervals ( $t$ ) were considered in the study that are 30 seconds, 2.5 hours, and 4 hours. Those values were chosen as they related to initial and final setting times of cement. As shown previously, specimens for bond shear test consist of three stacking layers. The first and second layers will be printed with a constant time interval



**Figure 31: Control Specimen for Bond Shear Test (a) Geometry and (b) Load Configuration.**

of 30 seconds, while the third layer will have different time intervals. Thereby, three categories (one category for each time interval) are considered in the study. The first category represents printing the third layer at 30 seconds after the second layer is printed, the second category is for a 2.5 hours interval, and the last category is for a 4 hours interval. Those categories are better illustrated in Table 2.

**Table 2: Bond Shear Test Categories.**

Category	Time of Printing Layer 2 after Layer 1 is Printed	Time of Printing Layer 3 after Layer 2 is Printed
1	30 s	30 s
2	30 s	2.5 hrs.
3	30 s	4 hrs.

### 3.6 Materials

A conventional concrete mixture is basically a combination of a binding material, water, aggregate fillers, and chemical admixtures. There are plenty of materials that belong to each category, and represents large number of options that can be chosen for the mixture of this study. In the following subsections, materials that were

used in all mixes of this research, whether at the trial mixing stage or at the later evaluation stage, are briefly discussed and identified.

**3.6.1 Aggregates.** Aggregates are “a mass of crushed stone” that is used to lower the cement content and provide a better-quality material since it has a higher stability than cement in terms of volume [57]. The targeted mixture in this study will contain local aggregates of maximum size equal to 4.75 mm for the purpose of consistency with the intended use i.e. extrusion.

**3.6.2 Portland cement type 1.** Portland Cement is a combination of lime, silica, alumina, and carbon oxide. This combination ends up in tricalcium and dicalcium silicate after specific heating processes, which are the compounds that provide strength to concrete after being hydrated by water [57]. Type I is the most commonly used and available cement type that satisfy the usual needs and requirements. In this study, ordinary Portland cement (type 1) will be used for mixing, that is provided by local industries.

**3.6.3 Mineral fillers.** Mineral Fillers are basically replacements for cement usage and considered environmentally friendly materials when compared to cement that has a high carbon footprint caused by production processes. Different types of mineral fillers can be used in the design of a concrete material, and these types are illustrated in the following paragraphs.

**3.6.3.1 Ground granulated blast furnace slag (GGBS).** It is a mineral filler that results from the processes of metal manufacturing. It is used as a cement replacement in concrete mixtures due to its relatively low cost compared to Portland cement [4].

**3.6.3.2 Fly ash.** It is another type of mineral fillers that forms as a remainder of burning coal. Similar to GGBS, it is involved in concrete production to reduce cement amount needed to achieve the desired properties in a specific mixture. It is not only a replacement material, but also helpful in enhancing strength and durability of the final product [4].

**3.6.3.3 Silica fume.** It is an important mineral filler that takes place in almost all high-strength concrete mixtures, and it is a by-product resulting from the

manufacturing of silicon material. It enhances the strength of concrete, provides better rheology, densifies the concrete, and makes it more homogeneous [4].

**3.6.4 Water reducing admixtures.** The most common water reducing admixtures are superplasticizers, which are used mainly to lower the water content in a concrete mixture, thereby, increasing early and long-term strength. It is also beneficial for having a good-quality concrete material that is able to be pumped and flowable [57]. The superplasticizer used in this research is MasterGlenium ACE 456, which is a product of Master Builders BASF chemicals and available locally. This product is based on polycarboxylate ether polymers, and it has a major role in the rheology and rapid strength gain when it is used. It is primarily designed for use in precast concrete production to achieve robustness and high-quality in the final product. It was preferred among other superplasticizer due to its combined effect of flowability enhancement and early-age strength development, thus, those are considered essential and advantageous for extrusion easiness and shape retention [58]. However, older version of superplasticizers (MasterRheobuild 857) can be used to reverse the action of Master Glenium ACE 456 if dosage seemed excessive. Such reverse action takes place due to the incompatibility between the two products.

**3.6.5 Set retarders.** Retarders are admixtures that cause delay in the initial setting time of concrete, and although it maintains the mixture workable for a longer period of time, it could reduce the time between setting stages of concrete. However, it can be helpful in the consideration of 3D printing mixtures as it increases open time, but the use of such admixture shall be carefully investigated and properly proportioned to provide the desired results [57]. This admixture may be appropriate when delayed action of superplasticizer is desired i.e. extended open time. MasterSet R 107 is a popular set retarder that is also available locally by BASF chemicals.

**3.6.6 Accelerators.** Accelerators are used to speed up strength gain in concrete without really affecting long-term strength of the material [57]. It can help in assuring enough strength in a printed concrete layer before the subsequent layer is extruded. MasterRoc SA 430 is widely known as a good accelerating admixture in the region.

**3.6.7 Micro fibers** The purpose of using micro fibers is mainly the brittle nature of concrete. Short or micro fibers (lengths not exceeding 12 mm) are key factors in

enhancing the ductility and strength of concrete, especially tensile and flexural strengths. It acts by arresting cracks and allowing strain hardening behavior [4], [57]. In this study, ultra-high modulus polyethylene fibers are used in some of the concrete mixtures. In addition, the use of fibers is expected to enhance the cohesion of the mix at its fresh state and help in having better shape quality of final product. The properties of fibers used in this study are shown in Table 3. Their aspect ratio is equal to length of each fiber divided by its diameter, which is  $12/0.038 \approx 316$ .

**Table 3: Properties of Polyethylene Fibers Used in the Study.**

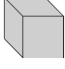
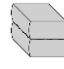
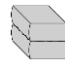
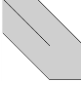

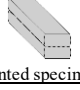
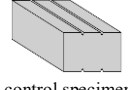
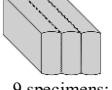
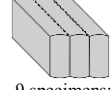
Type	Tensile Strength	Modulus of Elasticity	Fiber Length	Fiber Diameter	Specific Gravity
Ultra-High Modulus Polyethylene Fiber	2500 MPa	70 GPa	12 mm	38 $\mu\text{m}$	0.96

**3.6.8 Viscosity modifying admixtures (VMA)** The use of pumping in the 3D printing techniques could cause concrete to lose homogeneity at certain points. The main purpose behind using viscosity modifiers is to prevent concrete from internal bleeding and increase its cohesiveness while maintaining flowability parameters unaffected [57]. MasterMatrix 110 will be used as a viscosity modifying agent, that is a product of BASF chemicals like other admixtures used in the study.

### 3.7 Experimental Program

Since this study will consider achieving a proper concrete mixture for the application of 3D printing, it will start by mixing trial batches of concrete. Trial mixtures will be composed of local materials, and will differ by varying the proportions of those materials until reaching optimum outcomes. It will be based on observing flowability and shape quality of the outcome. Observation will take place on trial batches that are each of 1-litre volume. Selection of materials will be based on the properties they provide to the concrete. After reaching the optimum mixture, experiments that were discussed in the methodology will be applied to that mixture in two scenarios. As shown in Table 4, the first scenario considers the use of cool water for concrete preparation, where extrusion and the subsequent storage are inside the laboratory under cool environmental conditions. The second scenario (exposure scenario) accounts for the use of heated water for concrete preparation, where the

**Table 4. Experimental Matrix of the Study.**

Description	Parameter	Experimental Scenarios		
		Scenario 1	Scenario 2	
General details for testing scenarios	Mixing water condition	Cool water from the laboratory's faucet		
	Curing	7 days for control (molded) specimens only		
		No curing for all printed specimens		
	Storage prior to testing	Molded specimens are stored in the curing tank inside the laboratory for 7 day	Molded specimens are stored in the curing tank outside the laboratory for 7 day	
Printed specimens are stored without curing inside the laboratory for 7 days		Printed specimens are stored without curing outside the laboratory for 7 days		
Tests for fresh concrete properties	Flow table	3 repetitions		
	Open time	3 repetitions		
	Extrudability	3 repetitions		
Tests for hardened concrete properties	Compressive strength	 <u>3 control specimens:</u> CONTROL-CT-01 CONTROL-CT-02 CONTROL-CT-03	 <u>6 printed specimens:</u> AK-01-CT-01 AK-01-CT-02 AK-01-CT-03 AK-01-CT-04 AK-01-CT-05 AK-01-CT-06	 <u>6 printed specimens:</u> AK-02-CT-01 AK-02-CT-02 AK-02-CT-03 AK-02-CT-04 AK-02-CT-05 AK-02-CT-06
	Flexural strength	 <u>3 control specimens:</u> CONTROL-FT-01 CONTROL-FT-02 CONTROL-FT-03	 <u>4 printed specimens:</u> AK-01-FT-01 AK-01-FT-02 AK-01-FT-03 AK-01-FT-04	 <u>4 printed specimens:</u> AK-02-FT-01 AK-02-FT-02 AK-02-FT-03 AK-02-FT-04
	Bond shear strength	 <u>9 control specimens:</u> 1. Time interval = 30 s CONTROL-BT-30S-01 CONTROL-BT-30S-02 CONTROL-BT-30S-03 2. Time interval = 2.5 hours CONTROL-BT-2.5H-01 CONTROL-BT-2.5H-02 CONTROL-BT-2.5H-03 3. Time interval = 4 hours CONTROL-BT-4H-01 CONTROL-BT-4H-02 CONTROL-BT-4H-03	 <u>9 specimens:</u> 1. Time interval = 30 s AK-01-BT-30S-01 AK-01-BT-30S-02 AK-01-BT-30S-03 2. Time interval = 2.5 hours AK-01-BT-2.5H-01 AK-01-BT-2.5H-02 AK-01-BT-2.5H-03 3. Time interval = 4 hours AK-01-BT-4H-01 AK-01-BT-4H-02 AK-01-BT-4H-03	 <u>9 specimens:</u> 1. Time interval = 30 s AK-02-BT-30S-01 AK-02-BT-30S-02 AK-02-BT-30S-03 2. Time interval = 2.5 hours AK-02-BT-2.5H-01 AK-02-BT-2.5H-02 AK-02-BT-2.5H-03 3. Time interval = 4 hours AK-02-BT-4H-01 AK-02-BT-4H-02 AK-02-BT-4H-03
Shape Stability	Printed specimens for flexural and bond shear tests will be used for shape stability evaluation		Printed specimens for flexural and bond shear tests will be used for shape stability evaluation	

temperature of water is 50° C. The intent of using hot water is to simulate the mixing process that occurs outside under the harsh environmental conditions of the United Arab Emirates. Extrusion (Printing) of specimens for the second scenario is inside the laboratory, but the specimens are directly moved outside after printing to get exposed to the high temperature and sun radiation. Curing was applied only to molded (control)

specimens for complete seven days, whereas all printed specimens were not cured. This is because disregarding curing was thought out to be advantageous for the easiness of a large-scale printing process, hence, it was not considered for printed specimens in this study. However, all tests were performed seven days after preparation for both molded and printed specimens. Tests for fresh concrete properties (flow table, open time, and extrudability) differ only in water temperature between the two scenarios, where extrusion and storage are not applicable to such tests. As a summary, Table 4 shows the experimental matrix of this study using only the optimum concrete mix proportions.



## Chapter 4. Results and Discussions

In this chapter, experimental outcomes of total tests performed throughout this study are presented and discussed. Test results concerning fresh concrete properties are demonstrated first, then hardened concrete properties are presented afterward.

### 4.1 Trial Batches

This study intends to reach out an optimum concrete mix for extrusion purposes starting from a zero-slump mix proportions as shown in Table 1, and this mix is called mix 0. The first step in modifying proportions of mix 0 is omitting coarse aggregates in order to account for printability i.e. ability to extrude the material through a printing nozzle. The eliminated volume of coarse aggregates was compensated in sand and fine aggregates (maximum aggregate size = 5 mm) using Eq. 1, where  $V_{\text{fine(new)}}$  represents the modified volume of fine aggregates,  $V_{\text{fine(mix 0)}}$  is the volume of fine aggregates in mix 0,  $V_{\text{coarse(mix 0)}}$  is the volume of coarse aggregates in mix 0, and  $V_{\text{sand(mix 0)}}$  represents the sand volume in the original mix (mix 0). The modified volume of sand can be calculated similarly by replacing all volume parameters for fine aggregates with sand volume parameters. The denominator of the second term represents the sum of sand and fine aggregate old volumes, and is remained unchanged.

$$V_{\text{fine (new)}} = V_{\text{fine (mix 0)}} + \frac{V_{\text{coarse (mix 0)}} * V_{\text{fine (mix 0)}}}{(V_{\text{fine (mix 0)}} + V_{\text{sand (mix 0)}})} \quad (1)$$

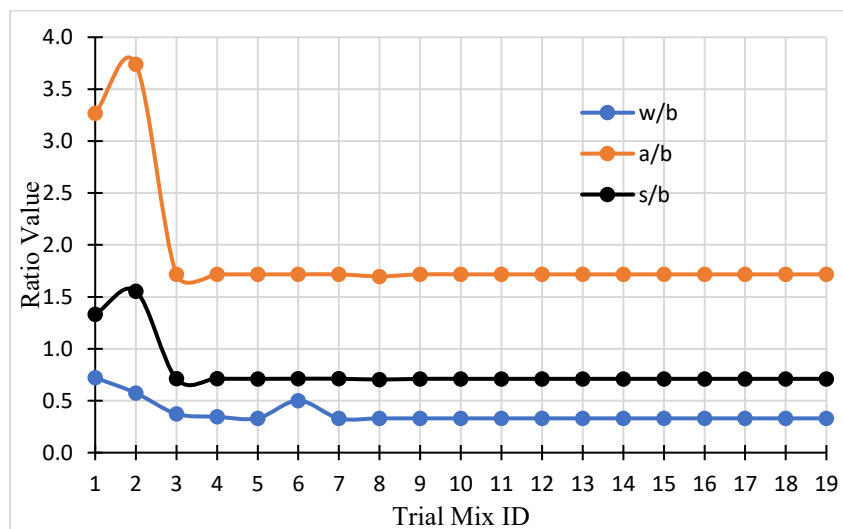
It is worth noting that water absorption of coarse aggregate is way less than that for fine aggregate and sand, hence, the water content of the mixture was adjusted to account for the higher overall absorption of the modified mix. The modified mixture was labeled mix 1, and it represents the actual starting mix where print process is experimented.

A total number of 19 trial mixes were carried out, extrusion of each mix was performed for observation. Three distinct parameters of each mix are discussed and compared to the corresponding evaluation of those mixes, where these parameters are water to binder ratio (w/b,) sand to binder ratio (s/b,) and aggregate to binder ratio (a/b.) a/b and s/b ratios were calculated by volume of the corresponding constituent, where the w/b ratio was calculated by weight of the corresponding component. The intent of considering such parameters is to characterize trial mixes in a simple platform, and due

to their effect on concrete behavior at both fresh and hardened state. w/b ratio greatly affects the compressive strength and durability of concrete, where increasing w/b leads the compressive strength to decrease [59]. a/b ratio does the opposite, where increasing a/b leads to decreasing compressive strength and negatively impacts shrinkage [60]. s/b ratio has a similar effect as the a/b to concrete, where it decreases compressive strength when it is increased [61]. Table 5 shows the trial mixes and their corresponding w/b, a/b, and s/b ratios. Figure 32 shows w/b, a/b, and s/b for all trial mixes that were conducted in this study.

**Table 5: w/b, a/b, and s/b Ratios of Trial Mixes.**

Trial Mix ID	w/b	a/b	s/b
1	0.7216	3.2690	1.3325
2	0.5744	3.7395	1.5557
3	0.3744	1.7164	0.7117
4	0.3449	1.7164	0.7117
5	0.3316	1.7164	0.7108
6	0.5011	1.7164	0.7117
7	0.3301	1.7164	0.7117
8	0.3301	1.6975	0.7039
9	0.3301	1.7164	0.7108
10	0.3301	1.7164	0.7108
11	0.3301	1.7164	0.7108
12	0.3301	1.7164	0.7108
13	0.3301	1.7164	0.7108
14	0.3301	1.7164	0.7108
15	0.3301	1.7164	0.7108
16	0.3301	1.7164	0.7108
17	0.3301	1.7164	0.7108
18	0.3301	1.7164	0.7108
19	0.3301	1.7164	0.7108



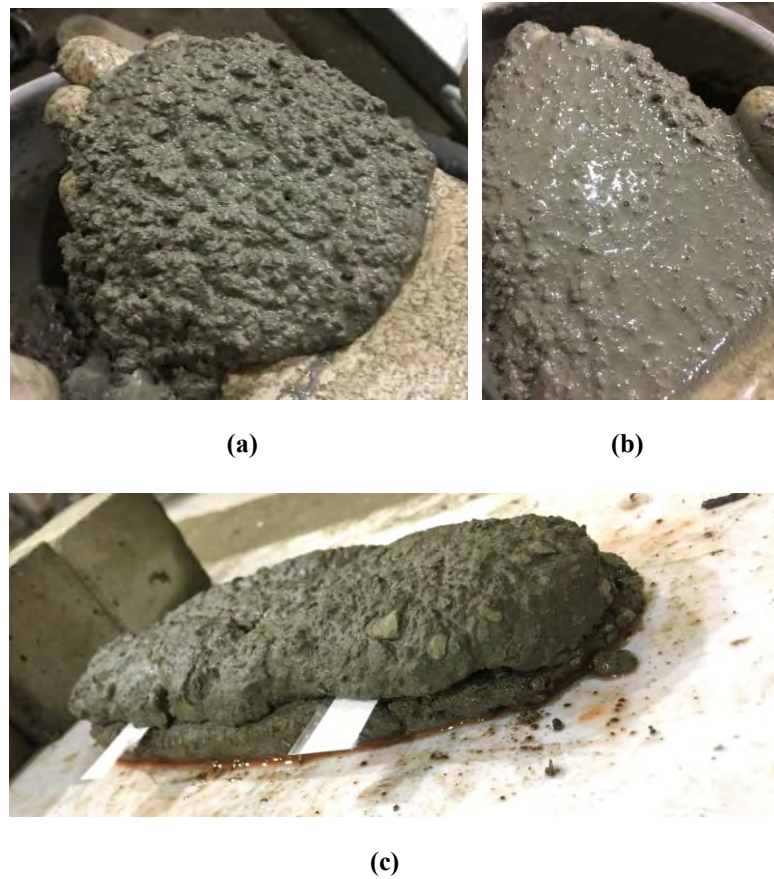
**Figure 32: w/b, a/b, and s/b Variations Among Trial Mixes.**

The starting mix (mix 1) was observed to be very dry for the designed proportions. Therefore, modification was extremely required to water and superplasticizer content due to that coarse aggregate replacement by dune sand and fine aggregate has led to a major alteration of the total surface area of mix ingredients. This basically increases the overall water absorption of the mix. Water amount was almost tripled. When one layer was printed, it maintained thickness for a while. After adding another layer, they merged together and the interface almost disappeared. Additionally, a distinct observation of mix 1 is that the surface quality was extremely poor. Nevertheless, tripling water amount is high enough to cause bleeding and large deformability of printed layers under its own weight. A sample that was extruded using mix 1 is shown in Figure 33.



**Figure 33: Printed Sample (Mix 1).**

Mix 2 started to be slightly fluid after all of the water was placed without admixtures as shown in Figure 34a, and then a large amount of MasterGlenium ACE 456 Superplasticizer was added where the mix started to be thixotropic and homogenous as seen in Figure 34b. Increasing superplasticizer in this mix has led to excessive workability and bleeding, thus, reverse action was achieved by adding MasterRheobuild 857 superplasticizer which is incompatible with ACE 456 type. This made the mix sticky, less workable, and caused segregation. Lastly, a minor amount of accelerating admixture was added to the mix in order to help laying the first filament, and it settled only 5 mm after putting the second filament with a time interval of 10 minutes. Figure 34c shows the printed specimen using mix 2.



**Figure 34: Mix 2 (a) Only Water is Added, (b) Admixtures are Added, and (c) Printed Specimen.**

In order to adjust the behavior of the previous mix, the overall binder content of mix 3 was increased while sand and aggregate contents were reduced to maintain volume. Water reducing admixture ACE 456 was increased, and led to a very good cohesion and homogeneity between aggregate and binder particles as observed while mixing. After adding MasterRheobuild 857 and accelerating admixture, the mix was seen to have a good thixotropy and an outstanding surface quality as illustrated in Figure 35a. However, excessive flowability was encountered such that shape retention cannot be possible if used for printing. After 7 minutes from adding the accelerator, it started sticking to surfaces and a printed layer took a good shape as shown in Figure 35b. Nevertheless, the print process could not be continued for a second layer placement due to that mix hardened quickly.

Water content was considered large in the previously performed trial mixes such that the compressive strength of those mixes is expected to be small. By this means, water content is reduced gradually in mixes 4 and 5 with varying admixture dosage to



(a)

(b)

**Figure 35: Mix 3 (a) Surface Quality and (b) Printed Specimen.**

try reaching an optimum w/b for the purpose of the study. High viscosity was observed in mixes 4 and 5 and no enough flowability was achieved. In mix 6, a replacement occurred by using fly ash instead of GGBS where the behavior of the mix at early age has remarkably changed, showing poor surface quality.

In all mixes following mix 6 (from mix 7 to mix 19,) fly ash was not used and water content was brought back to almost the same as mix 5. At mix 7 onward, all of the ingredients were fixed except the fiber content and admixture dosages. Mix 7, mix 8, and mix 9 did not include fibers where only superplasticizer dosage varied. Those mixes were not appropriate enough due to highly rough surface or bleeding problems. In mix 10, viscosity modifying agent (VMA) was included along with accelerator that caused a significant loss in workability as shown in Figure 36a. Figure 36b represents



(a)

(b)

**Figure 36: (a) Mix 10 Surface Quality and (b) Mix 11 Bleeding.**

mix 11. Fiber is added while VMA and accelerator were excluded. The dosage of superplasticizer remained high such that bleeding was encountered when the mix is left un-stirred.

Fiber content was increased and only ACE 456 superplasticizer (SP) was used, with a reduced dosage compared to previous mixes, in mixes 12, 13, 14, and 15. Slight increase in SP dosage was done in mixes 13 and 14 to observe its effect and avoid bleeding. Mix 15 was similar to mix 14 except that VMA was added. Mix 12 exhibited very good shape retention, satisfying flowability, acceptable stickiness, and tolerable surface quality. As shown in Figure 37a, two layers were extruded manually from the nozzle, and one discontinuity was observed on surface of the upper layer. Mix 13 was very similar to mix 12, yet flowability is enhanced, and shape retention is slightly reduced. Figure 37b shows a printed specimen out of mix 13. Mix 19 is exactly the same as mix 13 but without fibers. It was observed from the latter mix that better flowability can be achieved, and 3 layers were extruded successfully. However, the exclusion of fibers costs sacrificing shape retention and surface quality. This is better seen in Figure 38.



(a) (b)  
**Figure 37: Printed Specimen of (a) Mix 12 and (b) Mix 13.**

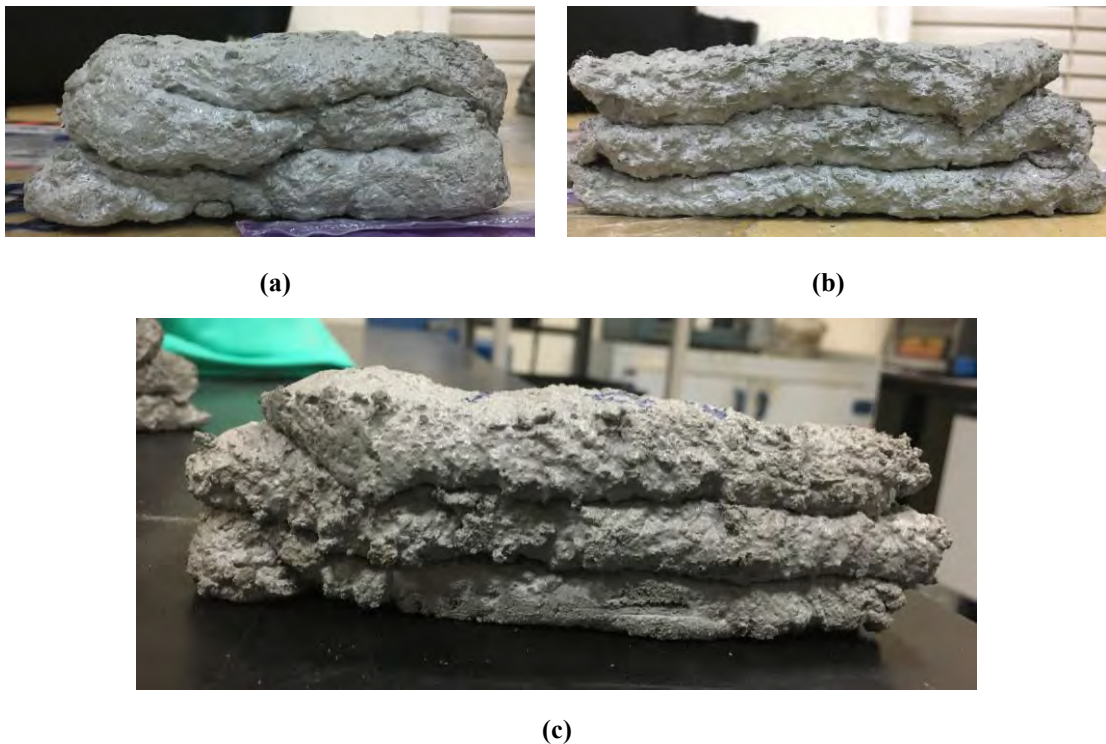


**Figure 38: Printed Specimen of Mix 19.**

Mix 14 is taken out of record due to error in proportioning. SP dosage was slightly increased again in mix 15 compared to mix 13. It was recognized that mix 15 lost the required shape stability, and layers are not taking shape due to excessive flowability. It is worth noting that the bottom layer of mix 15 specimen settled by 10 mm, which is half of the nozzle depth and is considered unacceptable. Therefore, SP dosage of mix 15 was considered exceeding the desired limit, when ACE 456 is solely used as an admixture.

Mixes 16 and 17 experimented the effect of adding VMA with the same SP dosage used in mix 15, while fiber content is reduced. Mix 18 included a reduced VMA content compared to the preceding mix, and zero fiber content. Mixes 16-18 exhibited a very good flowability, but it reduces quickly during extrusion. Those mixes need to be continuously activated by motion to maintain good flowability, and this behavior is known as thixotropy. However, mixes 16-18 were found unacceptable due to poor surface quality and shape stability of their printed specimens, as shown in Figure 39.

According to the observation-based evaluation of all trial mixes, mix 13 was chosen as the optimum mix for this study due to its relatively outstanding shape stability, acceptable surface quality, and fair extrudability.

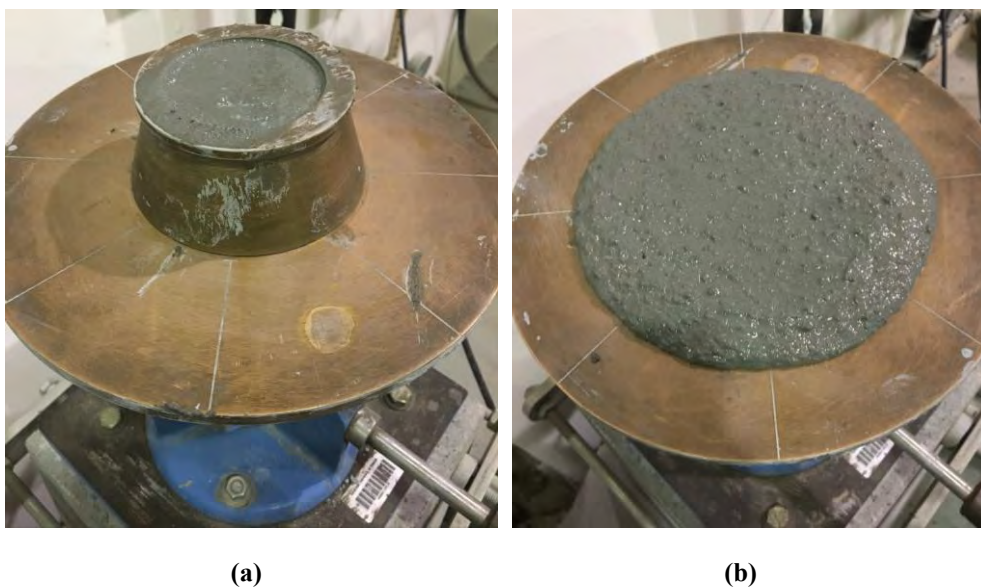


**Figure 39: Printed Specimen of (a) Mix 16, (b) Mix 17, and (c) Mix 18.**

## 4.2 Flow Table

The flow of 3D printing materials is a very important parameter to be considered for classifying how satisfying a concrete mixture is for printing. However, as mentioned before, characterization of such parameters is not standardized till date. Therefore, flow table test was conducted to identify the optimum mix. Figure 40 illustrates the operation of this test.

It can be observed through Figure 41 that the percentage increase in flow table diameter for runs of scenario 1 reached out 86% whereas runs done for scenario 2 attained only 78% increase in flow table diameter. The drop in flow between both scenarios is 9%, and it can be attributed to the highly sensitive time-dependent rheological behavior of concrete mixes for 3D printing. In other words, the use hot water in scenario 2 largely influences the setting for small time intervals leading to quick setting, which is evident by the drop in flow diameter. Furthermore, the viscosity of the mixture was decreased for the second scenario. Those results are similar to the work done by Kazemian, Yuan, Cochran, and Khoshnevis in [20], as their flow results range between 113% and 119%. However, they found out that increasing content of fine fillers in a mix reduces the flow and increases viscosity of that mix. Nevertheless, flowability measure of concrete mixes through flow table test cannot be judged by its own. There is an essential correlation with other process parameters such as nozzle size, flow rate, and print speed. It was found by Hongkyu, Bukkapatnam, Khoshnevis, and



**Figure 40: Flow Table Test Configuration (a) Before Flow and (b) After Flow.**



Saito that nozzle shape also affects flow properties of 3D printing cementitious materials [19]. Additionally, slump values were found to increase when mixing water temperature increases, along with occurrence of bleeding and segregation. The optimum mix temperature was found to be 14-18° C as per the work in [62]. Values of 86% and 78% that were obtained in this study may represent a good measure for the given nozzle size of 20x40 mm<sup>2</sup> and the manual extrusion characteristics (speed and flow rate.) Additionally, they are within the range reported by Tan, Qian, and Tay. They have observed that flow values of 30-90% are acceptable for printing and pumping, and demonstrated that higher s/b and lower w/b ratios reduce flowability [63].

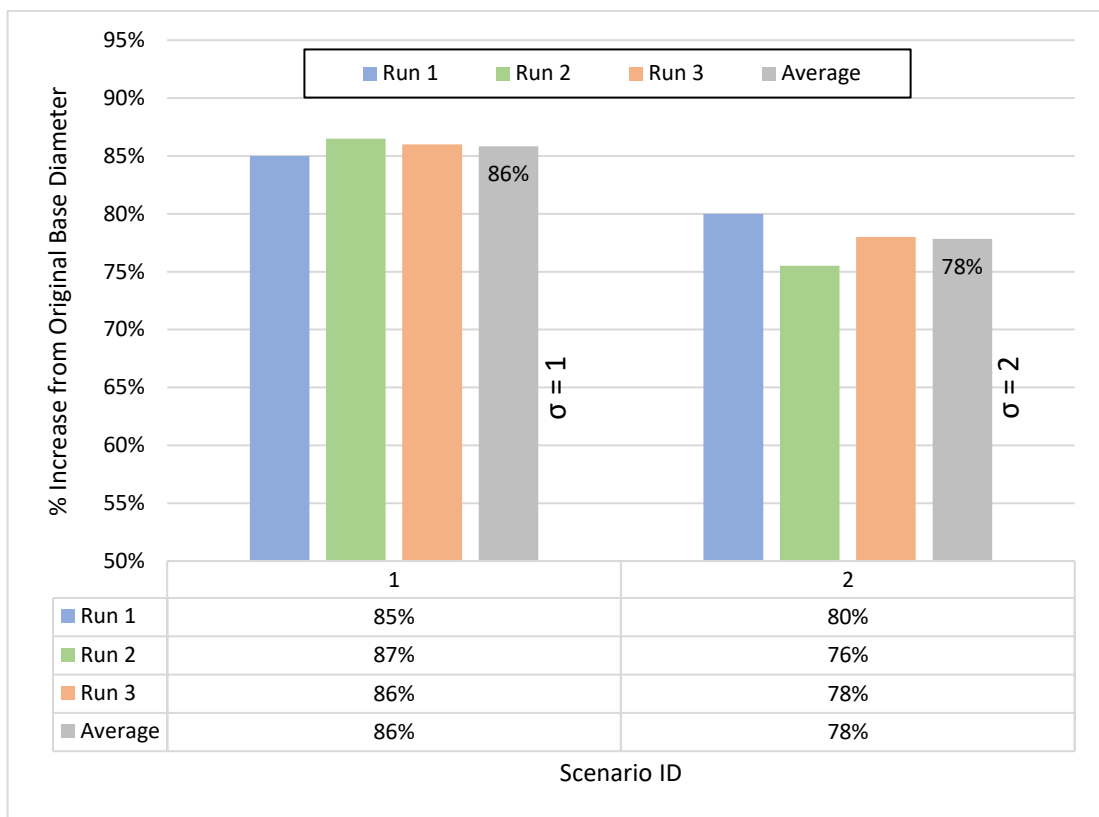


Figure 41: Flow Table Test Results for Both Scenarios.

### 4.3 Open Time

Open time is defined as the time range that a fresh concrete material maintains the ability to be printed. In this study, it was measured starting from the time mix is ready for printing until when extrusion process starts experiencing stoppage, shape quality issues, and relatively high material stiffness against extrusion e.g. higher pressure is required to print. Table 6 shows open time results of three runs that were

performed for each scenario. The average open time values for scenario 1 and scenario 2 were observed to be 7.2 minutes and 6 minutes respectively. This test exhibited a 16% reduction in open time between the two scenarios, which represents another indicator of the loss of workability and printability in the second scenario due to the high temperature of the mix.

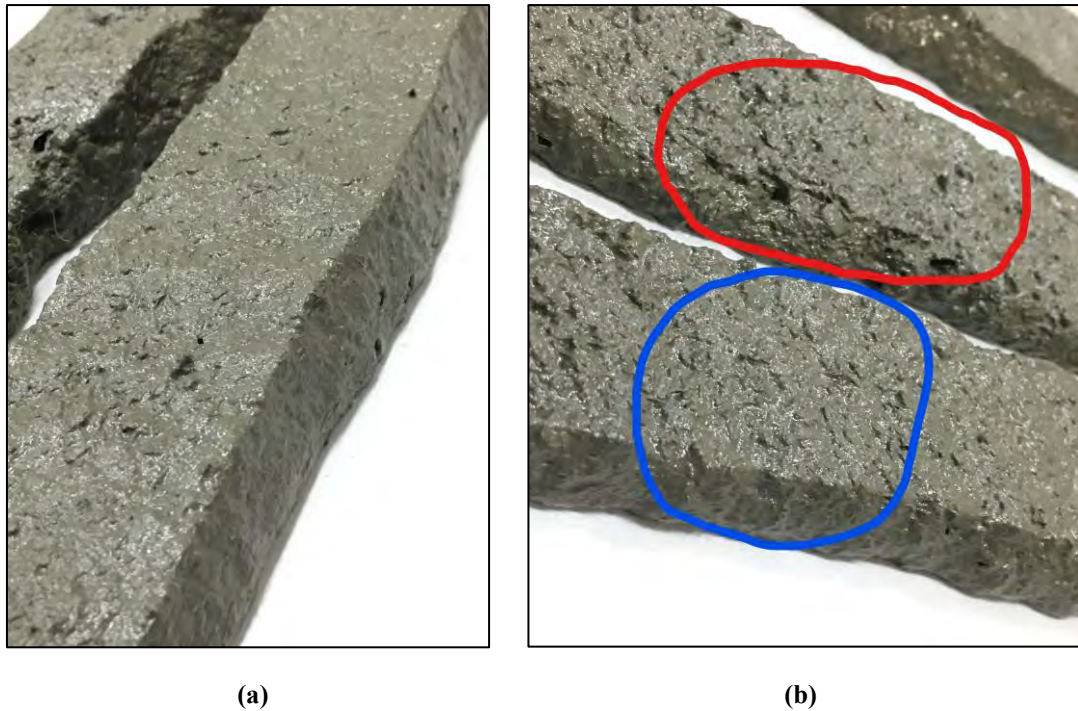
**Table 6: Open Time Results for Both Scenarios.**

Scenario ID	Open Time (minutes)			
	Run 1	Run 2	Run 3	Average
1	6	8	7.5	7.2
2	5.5	6	6.6	6.0

Stoppage of extrusion is an indicator of loss in open time, and it is shown in Figure 42 (red marker.) However, as discussed earlier, open time is not only characterized by print walkout, but can also be identified through the loss of shape or surface quality. Figure 43a shows that surface quality is well improved under cool temperature extrusion conditions (scenario 1,) where design geometry (nozzle size) is maintained and edge of filament is well-defined. On the other hand, Figure 43b demonstrates the surface of printed samples at different times within open time range under scenario 2 conditions. The blue marker indicates surface quality when extrusion occurred at the middle of open time interval, whereas the red marker signposts the



**Figure 42: Stoppage in Extrusion Process.**



**Figure 43: Surface Quality of Open Time Specimens (a) Scenario 1 and (b) Scenario 2.**

surface quality at nearly the end of that range. It can be clearly observed how surface quality reduces while extrusion is performed at the end of open time interval, and the quality of surface for scenario 1 specimens (Figure 43a) is much enhanced compared to those of scenario 2. However, open time values obtained in this study can suit only concrete printing that utilizes sequential batching of the material. This means that the print process shall combine many parameters together (print speed, flow rate, nozzle size, and path length of delivery hose) to specify the amount needed from the material for each batch. In such printing techniques, powdered admixtures are used instead of liquid ones to make the process of mixing dependent only on water addition, which facilitates the control of operation. However, higher values of open time were achieved by other researches with mixtures that are suitable for print processes relying on bulk batching of materials. Ma, Li, and Wang achieved open time values up to 80 minutes with their mix that used rapid hardening cement type [22], and values 30-60 minutes were reported by Paul, Tay, Panda, and Tan in [34]. Mixtures in this study were not agitated while extrusion is being performed, thereby, open time values shown in Table 6 are very close to values achieved by Le et al. [24] for non-agitated mixes, that is equal to 8 minutes on average for the same superplasticizer dosage in this study (1.2% by weight of binder.) Surprisingly, agitation of the same mix in their research exhibited a

375% increase in open time, which is a proper indicator of the thixotropic behavior of printing concrete mixes. This was also concluded by Panda and Tan with their GGBS-based mix that had open time values of 10-15 minutes, where they reported the need for batch mixing to suit such thixotropic behavior [33]. They also remarked the ability to adjust mix design for assuring compatibility with total time of the process and printed object geometry [33].

#### 4.4 Extrudability

In a simple form, extrudability represents the pass-ability of a cementitious material through a nozzle with a specific size. This property can be described subjectively (as in this study) by telling whether the material is able to pass the nozzle or not. It was demonstrated that the optimum mix of this study was extrudable during its corresponding open time for both scenarios. Figure 44 shows samples that were extruded on the printing bed within the open time with a nearly constant speed and pressure. It was observed that extrudability of a concrete mix highly depends on nozzle size and applied pressure. In this line, the same optimum mix of study was not extrudable through a smaller nozzle (10 mm deep and 40 mm wide) for both scenarios. Additionally, extrusion was still possible at times beyond open time intervals of the mix



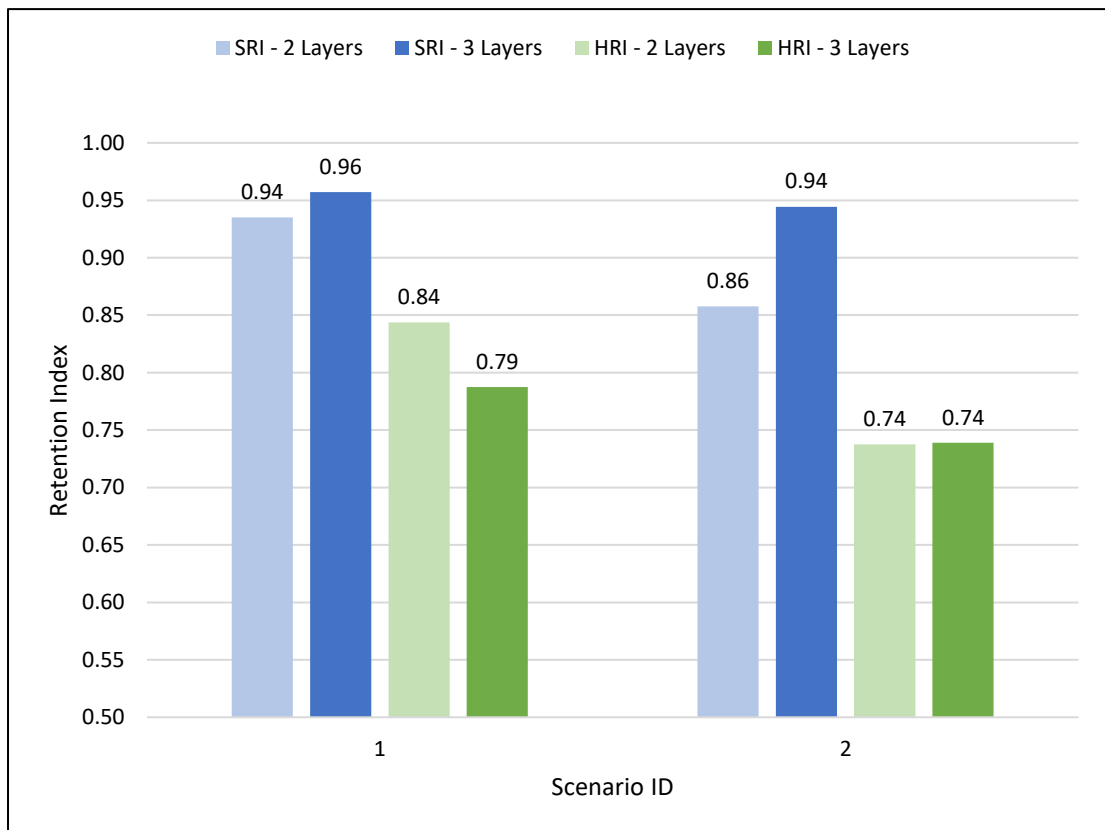
Figure 44: Continuously Printed Filaments for Extrudability Evaluation.

in each scenario using the normal nozzle (20 x 40 mm<sup>2</sup>,) but with a noticeably increased pressure requirement. This was clearly observed despite that extrusion was done manually in this study. However, extrudability can be evaluated objectively also by printing a pre-specified length of filament such as 2 m in [22] and 4.5 m in [24]. It was observed by Ma, Li, and Wang that the rate of extrusion shall be higher than the hydraulic conductivity of the mix for the extrusion to be successful, and the dependency of extrudability on nozzle size is evident [22]. This is because using smaller nozzles sacrifices effectiveness of construction and extrudability, but gives room for more complex geometry to be printed [22]. The first two trial batches in this study contained a high amount of sand (high sand-to-binder ratio,) and it was observed that extrudability of these mixes is certainly more difficult than the optimum mix (lower sand-to-binder ratio) through the same nozzle. By this means, it can be remarked that the higher the sand content in a mix, the more difficulty in extrusion is experienced because of tendency to segregation and blockage. This is similar to the conclusions reported by Le et al. [24] and Panda and Tan in [33]. Nevertheless, extrudability was also evaluated indirectly through other material parameters in some research works. Herewith, Zareiyan and Khoshnevis utilized a stability index that expresses the percentage difference in width of filament compared to nozzle width, and found out that values below 20 % represent a good extrudability measure [32]. Additionally, Soltan and Li reported that flowability factors, that are obtained via flow table test, between 1.2 and 1.4 (120% and 140% as percentages) are adequate for a good extrusion and shape preservation [64]. It is worth noting that flowability factors in this study were out of the range that is recommended by Soltan and Li in [64], but the mix was still exhibiting a good level of extrudability for short open time intervals. This signposts that extrudability is interrelated to other print process parameters, which are but not limited to nozzle size, print speed, flow pressure or rate, and material composition (sand, admixture, and binder content.)

#### **4.5 Shape Retention**

As discussed earlier, shape stability or retention is an important parameter to investigate for 3DCP mixes. It allows for sufficient prediction of the geometric variation between design and reality. In this study, specimens that are casted for flexural and bond shear tests were used to trigger geometric variations through shape retention

indices. Flexural test specimens are composed of two stacking layers (almost 200 mm long,) whereas specimens for bond test are shorter (100 mm long) and composed of three layers. Additionally, bond test specimens are subdivided into three categories as shown in Table 2 (based on time interval to print third layer.) The time intervals of printing last layer in 3-layers specimens are realized to have effect on the overall shape stability. This is because the longer the time interval is, the more time bottom layers have to harden before it is loaded by the third layer. Figure 45 shows the SRI and HRI results using the optimum mix for both 2-layers and 3-layers specimens, and both scenarios of the study. It can be observed that there is a drop in the values of both SRI and HRI in the second scenario when compared to the first one. These drop values are 8.5% for 2-layers SRI, 2% for 3-layers SRI, 12% for 2-layers HRI, and 6% for 3-layers HRI. Furthermore, SRI of 3-layers specimens were higher than those for specimens composed of 2 layers, and the drop values between both scenarios were larger for 2-layers specimens than those for 3-layers specimens for both SRI and HRI. This was attributed to that 2-layers specimens are longer (200 mm) than 3-layers specimens (100 mm,) despite having a smaller number of stacking layers. This gives room for further



**Figure 45: Shape Retention Index for Both Scenarios (SRI and HRI).**

settlements to take place and reduces the ability of layers to pertain its designed geometry. The portion of specimen close to the nozzle maintain better stability than far portions. In other words, printing 100 mm long specimens does not keep a large portion of the filament away from nozzle, but 200 mm long ones leave longer portions far from the nozzle. However, in scenario 1, HRI value of 3-layers specimens is decreased compared to 2-layers specimens by 6%, and this contradicts the earlier conclusion. This is where further investigation is required, for example by printing more stacking layers and trigger the height variations. It is worth noting that height of filaments was not considered explicitly for shape stability evaluation in previous research works unlike the width of filaments. Width of printed layers was seen more influential and critical to shape retention of printed parts. The common trend of all parameters in Figure 45 is that shape retention indices drop in the second scenario compared to the first one, and this can be attributed to the higher early age flowability when using hot water, that is accelerating chemical reactions between components of the mix and leading to excessive flowability at the first few minutes of its age. Nevertheless, shape retention index is a time-dependent parameter, especially for mixes with short open time. In other words, shape stability of such mixes can be enhanced by avoiding printing directly after the mix is being ready, but not after its open time interval. The shape retention results obtained in this study are within the recommended ranges by other researches. Zareiyan and Khoshnevis evaluated shape retention using a ratio of the variation between width of part and width of nozzle to the width of nozzle. They concluded that values less than or equal to 20% are considered appropriate for shape stability [32]. The same ratios were calculated and fell in the recommended range, which are 7% and 18% for 2-layers specimens in scenario 1 and 2 respectively, as well as 5% and 7% for 3-layers specimens in scenario 1 and 2 respectively. The higher the ratio, the less shape is preserved. However, SRI values of the study were very similar to those achieved in [56]. Shape stability measures are not the same among all research works, since no standard test was developed for that purpose. By this means, some studies created a solidity ratio to evaluate shape stability by using cross sectional area of nozzle and printed filament, in correlation with yield strength of the fresh mix (proportional relationship) [33]. Some studies have shown that it was linked to print speed and pressure in [65]. Additionally, flow table factors were used to evaluate shape retention by Soltan and Li and concluded that factors of 1.2-1.4 can be a good measure to preserve

shape of printed parts [64], where Nematollahi et al. [38] used flow table spread diameter for that evaluation. Ma, Li, and Wang investigated shape retention through slump test, and found out that values of 3-8.5 cm are appropriate for that purpose.

The inclusion of polyethylene fibers (1.4% volume fraction of binder) in the optimum mix of the study (Mix 13) has significantly enhanced the shape quality, where the same mix was carried out without adding fibers (Mix 19.) Printed parts from those mixes can be seen in Figure 46, where it is evident that surface quality and shape preservation is well improved when fibers are added. This can be due to fiber action in concrete material that prevents large deformations at both hardened and fluid states. The same was reported, but using polypropylene fibers instead, by Ma, Li, and Wang in [22] and by Nematollahi et al. [56]. It is important to note that shape stability continues to improve as long as more fibers are added to a 3D printing cementitious material [56], but this will indeed negatively influence the extrudability of the mix. Moreover, the contribution of fiber addition in preventing plastic shrinkage cracks was



(a)



(b)

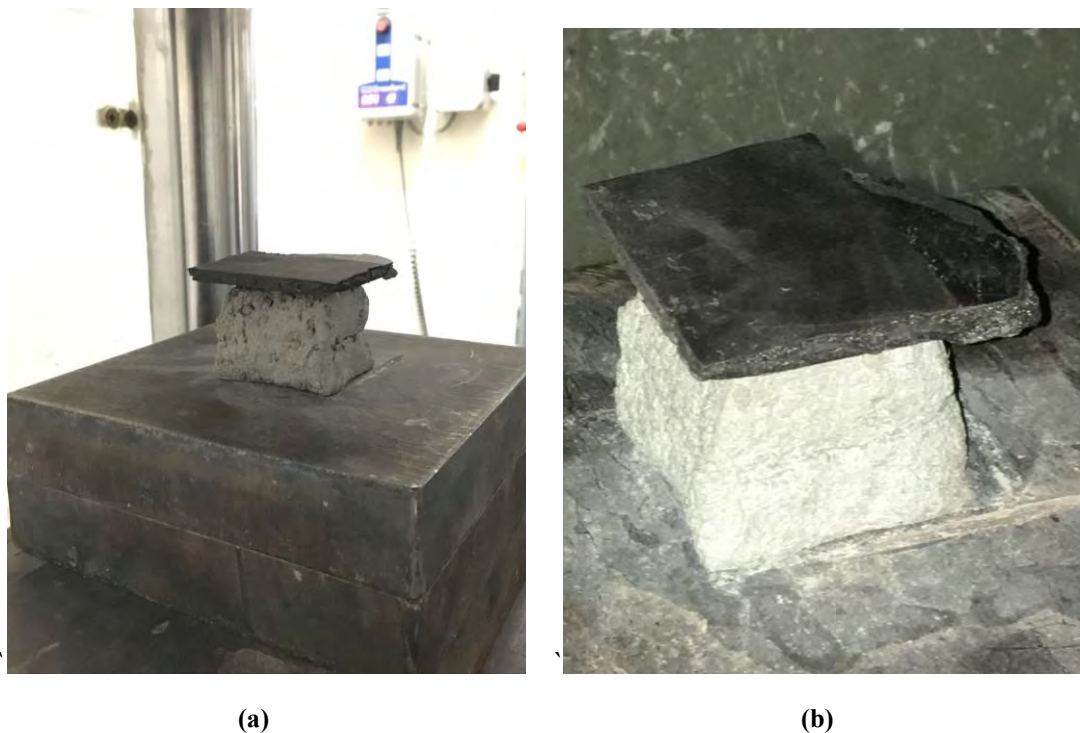
**Figure 46: Shape Retention and Surface Quality of Printed Parts (a) Mix with Fibers (b) Mix Without Fibers.**



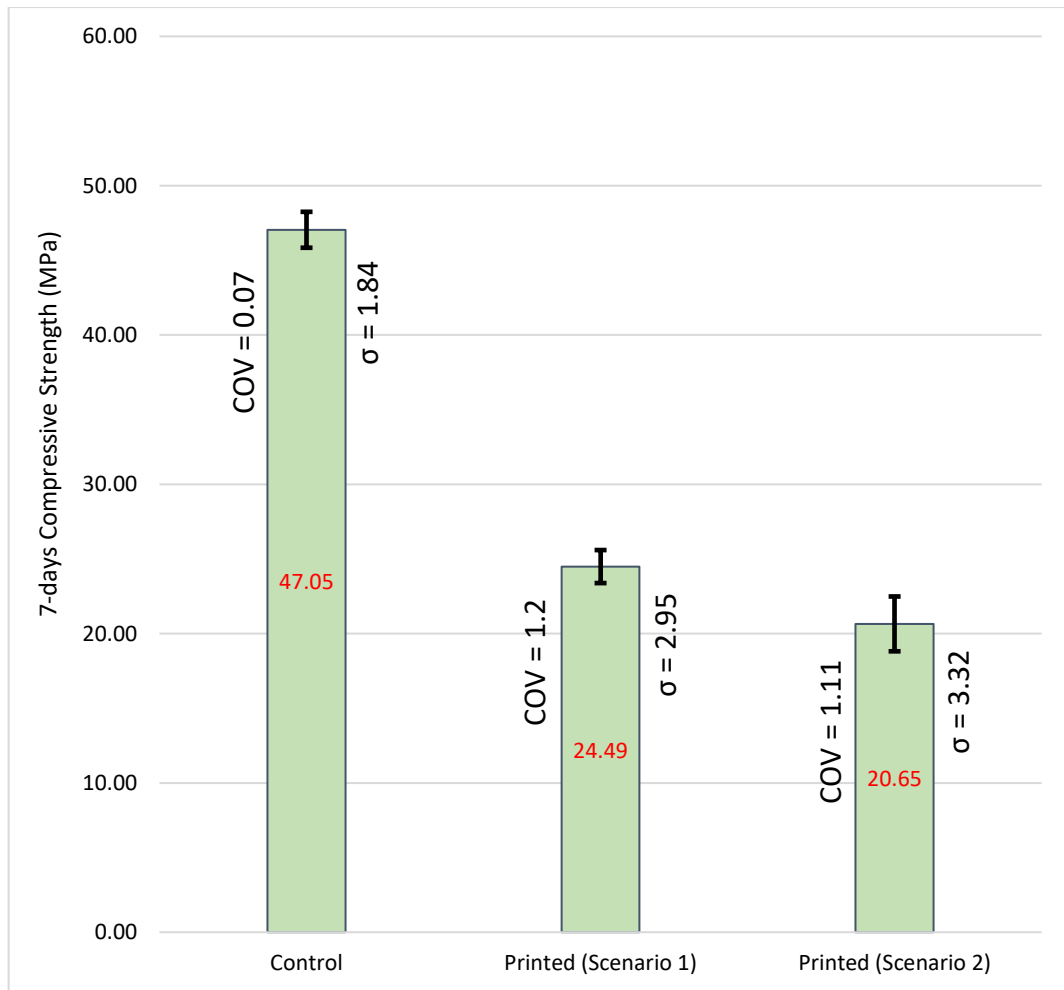
seemingly obvious especially in scenario 2 specimens, where the exposure to sun and the use of hot water did not impose shrinkage on concrete. This was attributed to the fiber's bridging effect, where crack propagation and widening are controlled [66], [67].

#### 4.6 Compressive Strength

In this study, conduction of compressive strength test for 3D printed cubes is done as it is the most definitive mechanical property of any concrete material. Evaluation of compressive strength took place on printed specimens from both scenarios, and on control molded specimens as per the standard ASTM C109 guidelines (50 mm x 50 mm cubes) [53]. Printed specimens were tested in exactly the same manner as control cubes using cardboard pads for load distribution on printed surfaces due to its irregularity, as shown in Figure 47. Strength evaluation of printed specimens was based on their actual top surface area measured before conducting the test. Figure 48 demonstrates the 7-days compressive strength of printed cubes in both scenarios and control cubes. Control cubes exhibited 47 MPa 7-days compressive strength on average, whereas printed specimens showed only 24.5 MPa and 20.65 MPa in scenario 1 and scenario 2 respectively. It can be noted that there is a significant drop in compressive strength between the control cubes and scenario 1 printed cubes, and it is



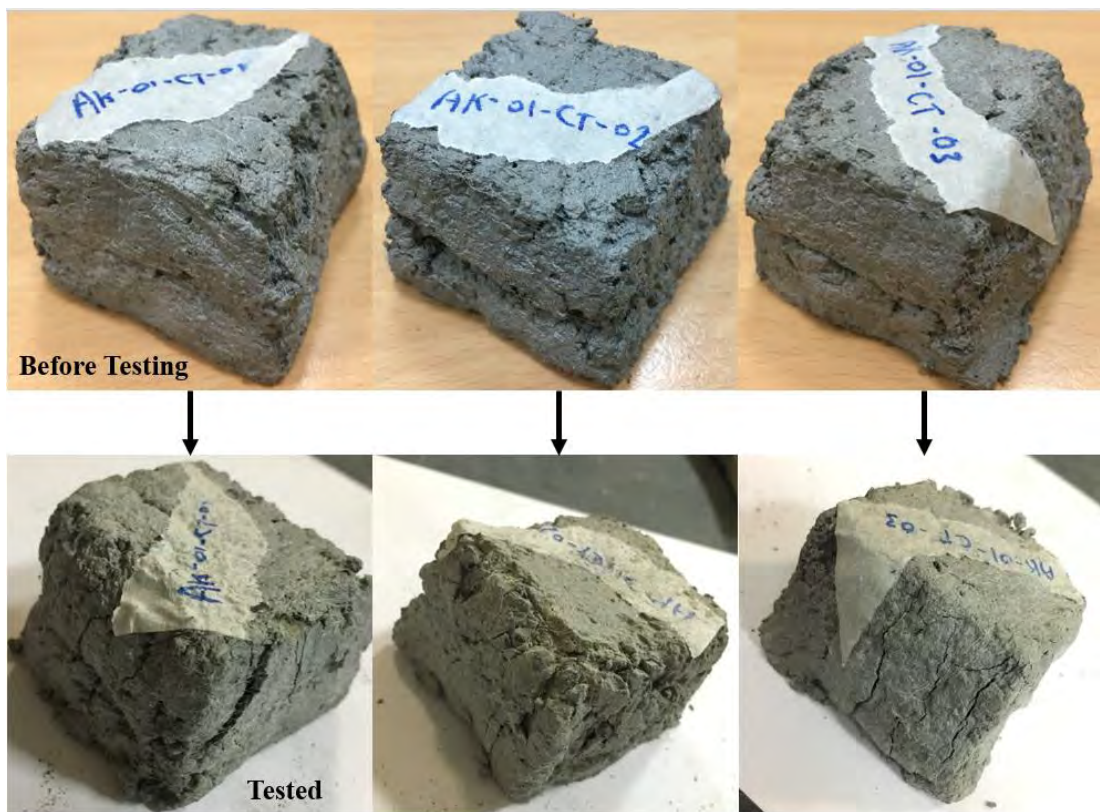
**Figure 47: Compression Test Setup for Printed Specimens (a) Configuration and (b) Cardboard Pad for Load Distribution.**



**Figure 48: Summary of Compressive Strength Results of Control Cubes and Printed Cubes in both Scenarios.**

calculated to be 48%. This drop can be due to the loss of homogeneity in the presence of joints (layer interface) in printed cubes. This conforms in principle to many previous research works, but compressive strength reduction between molded and printed specimens were less than that obtained by this study. Rahul, Santhanam, Meena, and Ghani reported a maximum reduction of 20% that was attributed to the porosity effect at interface between layers [49], and similar reduction in strength was reported also in [68]. Wolfs, Bos, and Salet stated that casted cubes exhibited a 31% higher compressive strength compared to printed cubes (with no directional dependency) [48]. Nevertheless, some research works reported no significant difference in the compressive strength between molded and casted samples as in [64] and [34]. That was expected to be due to the higher surface area as a result to extrusion process which provides more confinement while resisting compression.

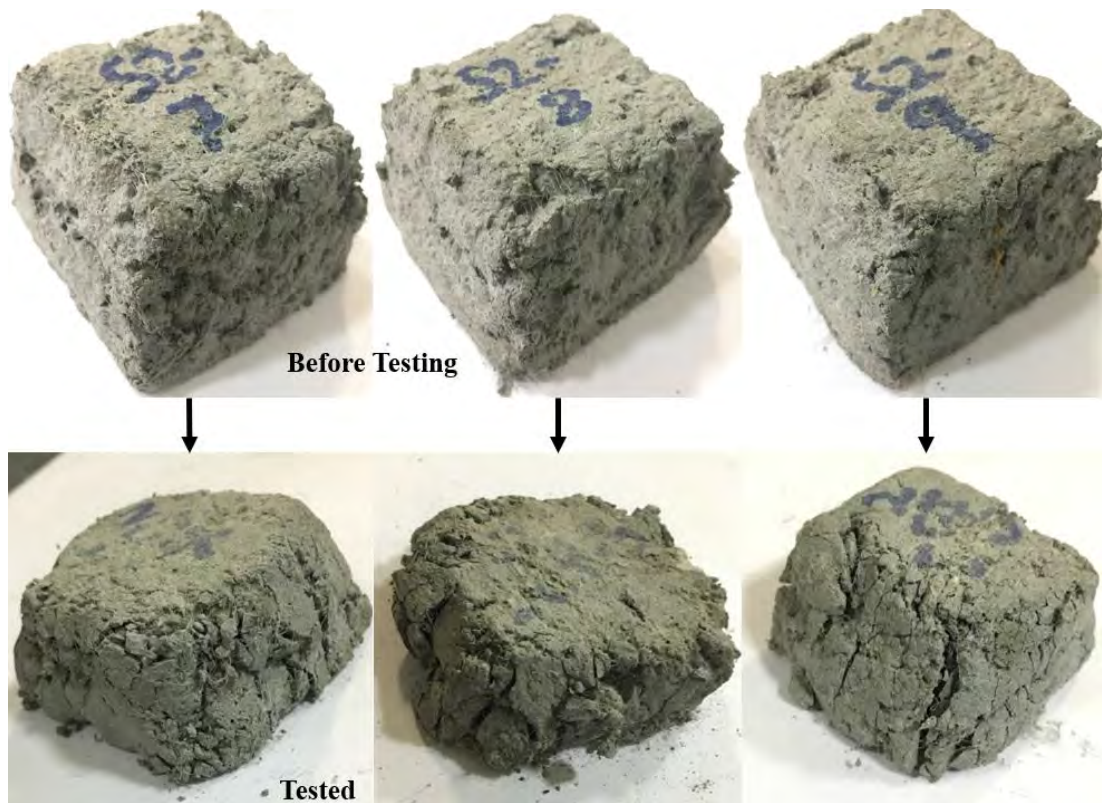
It is important to note that geometry of printed specimens is not exactly cubic. This is because minor settlements or flattening occur due to imperfect shape retention of the optimum concrete mix in this study. Seemingly, this effect is not only reducing the compressive strength of the specimens, but also changing the cracking patterns from the norm with standard cubes. Thereby, a correlation between shape stability, compressive strength, and failure modes of printed parts could be true, but is still not investigated yet. Figure 49 and Figure 50 shows printed samples from scenario 1 and



**Figure 49: Printed Cube Specimens before and after Compression Test (Scenario 1).**

scenario 2 respectively, prior to testing and after fracture. It can be noted that cracking patterns of fractured printed cubes are similar in both scenarios. Most of the cracks propagate vertically, and the overall behavior of printed cubes is seemingly a flattening behavior. This is more obvious in specimens of scenario 2.

Around 16% reduction in compressive strength on average was encountered while observing scenario 2 specimens compared to scenario 1. This can be attributed to the use of hot water in scenario 2 (simulation of hot weather conditions) mixes that



**Figure 50: Printed Cube Specimens before and after Compression Test (Scenario 2).**

expedite strength development up to a certain limit. After that, the grow of strength with time slows down so that compressive strength in scenario 1 becomes higher at the age of 7 days. This is similar to the conclusion of [69]. Moreover, the higher temperature of mix in scenario 2 increases the rate of water evaporation. Thereby, cement hydration process is negatively affected due to having less water for chemical reactions compared to scenario 1 (less evaporation.) This in return reduces the compressive strength of printed cubes in scenario 2.

The compressive strength of the optimum mix is considered good for 7-days curing only, that is 47 MPa. It is important to note that aggregate content was relatively high compared to binder, whereas the overall binder content was quite lower than that used in other studies. This provides the mix an economic value since binder content is controlled not to be very high. Hence, the presence of polyethylene fibers has a major contribution to the compressive strength of the optimum mix. This is mainly attributed to the prevention of crack spread and ceasing deformations of stressed concrete [22]. This study considered loading concrete specimens in the vertical direction only, but

other studies took into account the directional dependency of mechanical properties of printed concrete. Panda, Paul, and Tan reported that compressive strength is maximized when printed parts are loaded in the same direction of printing, that is due to material densification caused by extrusion action as a result of higher pressure [70]. However, it was also found that fiber contribution to strength characteristics of concrete is highly dependent on the material ability to accommodate fibers, and its direction within the mix matrix after extrusion. Fibers that are parallel to the load direction act as voids on the surface of concrete specimens, which is a reason for the resulting reductions in compressive strength when fiber dosage exceeds a specific limit [38], [70]. Nevertheless, some authors stated that no dependency in printed concrete to direction of loading [48], which implies the need for further investigations in that regard.

#### 4.7 Flexural Strength

Flexural strength test is performed on both molded and printed specimens. Test setup on printed specimens is shown in Figure 51, where the same test configuration of molded specimens is used. It is important to note that span between supports was

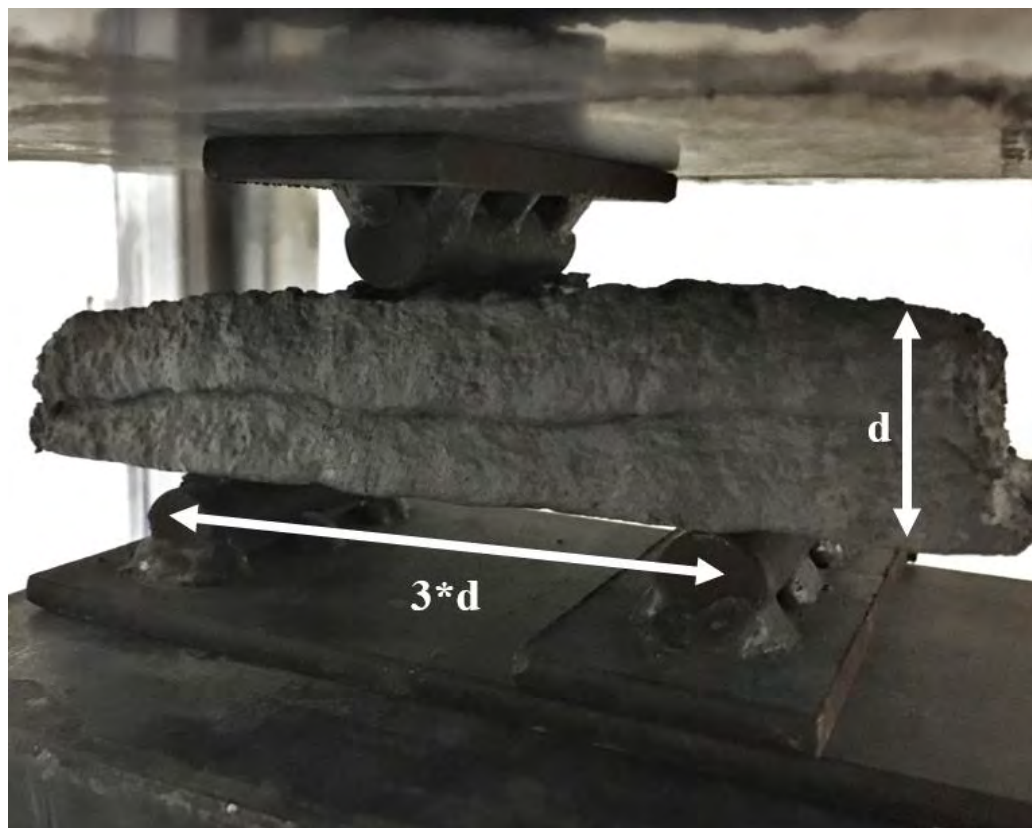
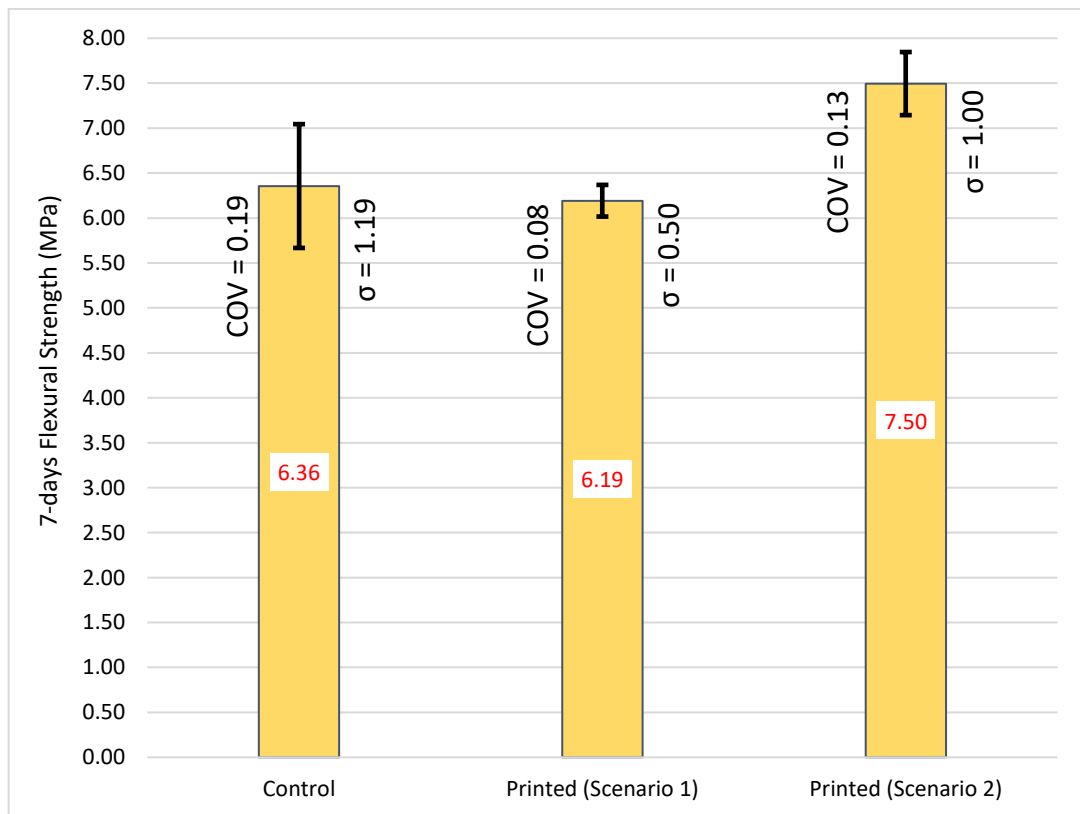


Figure 51: Flexural Test Setup for Printed Prisms.

considered triple the actual depth ( $3*d$ ) of printed prisms, which is not 40 mm always due to process settlements. The average flexural strength results for molded and printed (scenario 1 and 2) were evaluated from the force causing the first midspan crack at the bottom of prisms, and are shown in Figure 52. Note that a total number of 8 printed specimens were tested for flexure in each scenario rather than 4 (test matrix showed 4 specimens for each scenario) to further validate the trend of variation between test categories. At age of 7 days, control prisms exhibited a flexural strength of 6.36 MPa



**Figure 52: Flexural Strength Results of Molded and Printed Prisms.**

and printed prisms (scenario 1) showed 6.19 MPa, which is approximately equal to the control strength (3% less.) This does not follow the reduction trend seen in compressive strength evaluation, and may be attributed to the presence of fibers and its orientation in specimens with respect to loading direction. It is important to note that fiber has a major contribution to the flexural strength of concrete. This is due to its bridging action between tensile cracks formulated when bending is applied. For the bridging action to take place, fibers have to be oriented perpendicular to the load direction [70]. It was observed that casting control specimens do not assure a proper orientation of fibers, but

extrusion seemingly does. As shown in Figure 53, it was evident from fractured printed prisms that a good amount of fibers in extruded specimens are oriented parallel to the printing direction (normal to loading direction in flexure case,) This can be attributed



(a)



(b)

**Figure 53: Fractured Printed Prisms and Fiber Orientation (a) Side View and (b) Bottom View.**

to that exerted pressure during extrusion help orienting fibers in that direction. Additionally, the pressure used to extrude mortar is possibly densifying concrete filaments and leading to improved bending resistance in printed parts. These conclusions were similarly reported in other researches [49], [70]. Nevertheless, it is important to consider that fiber content must be large enough and of high strength to be able to contribute in the flexural resistance. On the other hand, the presence of fibers in concrete mortars results in higher porosity, and low fiber contents make that porosity

dominant in effect rather than crack bridging. This was demonstrated by Nematollahi et al. [38] using 0.25-0.75% polypropylene fibers.

The failure mode of flexural prisms is important because it can be induced by interfacial weaknesses between stacking filaments. Such interfacial regions can be considered cold joints. It was observed in the study that all printed prisms failed by tensile stresses rather than interface shear fracture. This can be explored in Figure 54, showing a fractured prism side view and cross section, where the interface between layers is not visible. This proves that 3D printed concrete using the optimum mix of the study attain a good level of homogeneity when undergoing in-plane bending. Bong, Nematollahi, Nazari, Xia, and Sanjayan have reported a similar conclusion when testing 3D printed prisms for flexure. They obtained 5.8 MPa flexural strength associated with a tensile failure mode, using geopolymer-based printing material [56].



(a)



(b)

**Figure 54: Cross Section of a Fractured Printed Prism (a) Cross Section and (b) Side View.**



Figure 52 shows that printed prisms in scenario 2 achieved a flexural strength higher than scenario 1 specimens by 21% (7.5 MPa) on average. This can be attributed to enhanced fiber orientation as a result of higher water temperature in the mix. Flexural prisms of the second scenario were extruded during the open time interval of the mix. This phenomenon is expected to be induced by the higher early age flowability and less viscosity of the mix with hot water at early age (scenario 2,) which is relevant to the conclusions drawn by Eskandarsefat, as he reported higher slump for higher temperature concrete mixes [62]. By this means, more fibers may be allowed to respond to pressure exerted by extrusion, and orient parallel to the printing direction. Additionally, better compaction might be achieved due to the extrusion pressure. It is important to note that same pressure is almost used for both scenarios, and the higher early age flowability (due to quicker reactions of the hot mix) of scenario 2 mixes makes it more responsive to extrusion pressure. Hence, mix compaction is relatively enhanced. However, this might also be due to that specimens were casted at age of 7 days rather than 28 days, and flexural strength values are relatively small compared to compressive strength ones. As a result, flexural strength could require more than 7 days to provide a trend for its incrementation with respect to age. Compressive strength relationships with age of specimens were conducted for different mixes by Burg [69] and Nasir, Al-Amoudi, Al-Gahtani, and Maslehuddin [71]. Nevertheless, both of the mentioned research works have in common the absence of fibers within their mixes. 24% rise in 7-days compressive strength was encountered when casting temperature is increased from 10° C to 32° C [69], whereas 20-28% increase in 7-days compressive strength for was explored when temperature rises from 25° C to 45° C, for mixes incorporating Silica Fume and GGBS [71]. At ages longer than 7 days, the trend of flexural strength can follow the compressive strength variation with respect to the printing scenario, but this needs to be addressed in future research by triggering the flexural strength variation between both scenarios at age of 28 days.

Flexural-to-compressive (F/C) strength ratio represents an important classification parameter for a concrete material. The absence of reinforcement steel in 3D printed concrete parts makes F/C ratio significant. In this study, F/C ratios of 14%, 25%, and 36% were modestly achieved for control, printed (scenario 1,) and printed (scenario 2) specimens, respectively. In absence of steel reinforcement, these values

can be considered high enough to resemble a good level of in-plane bending (flexural) resistance of parts printed using the optimum mix of the study. This is in line with other researches on 3D concrete printing materials. Close F/C ratio (30%) for printed specimens was achieved by Paul, Tay, Panda, and Tan in [34]. However, lower F/C ratios were more encounterable in other researches. Considering print samples, Wolfs, Bos, and Salet have reported 15% F/C ratio with a mix incorporating polypropylene fibers [48], and similar ratio was achieved in [22]. Moreover, 10% F/C ratio was reported by Le et al. [68] considering mold-cast specimens rather than printed specimens, given that polypropylene micro fibers were incorporated in their mix.

The latter discussion indicates that a comparative flexural strength is achieved in the optimum mix of this study. It is worth noting that F/C ratio is an essential mechanical parameter for consideration in 3D printing applications, especially in absence of steel reinforcement to avoid construction complexity. Recall that fiber inclusion has a major contribution to the enhancement of flexural strength, but it is worth noting that selection of fiber type and amount is critical to achieve that enhancement [36], [38].

#### 4.8 Bond Shear Strength

In this study, bond shear strength (BSS) of 3DCP specimens was targeted through a simple novel test setup as illustrated in Figure 55. Three major categories were considered, that are control specimens (molded,) printed specimens in scenario 1

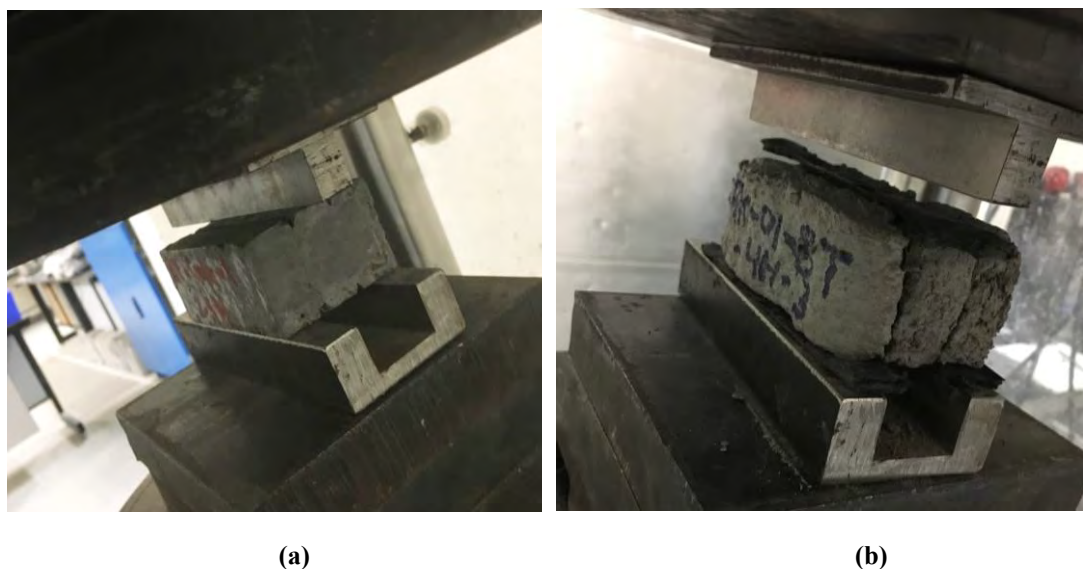


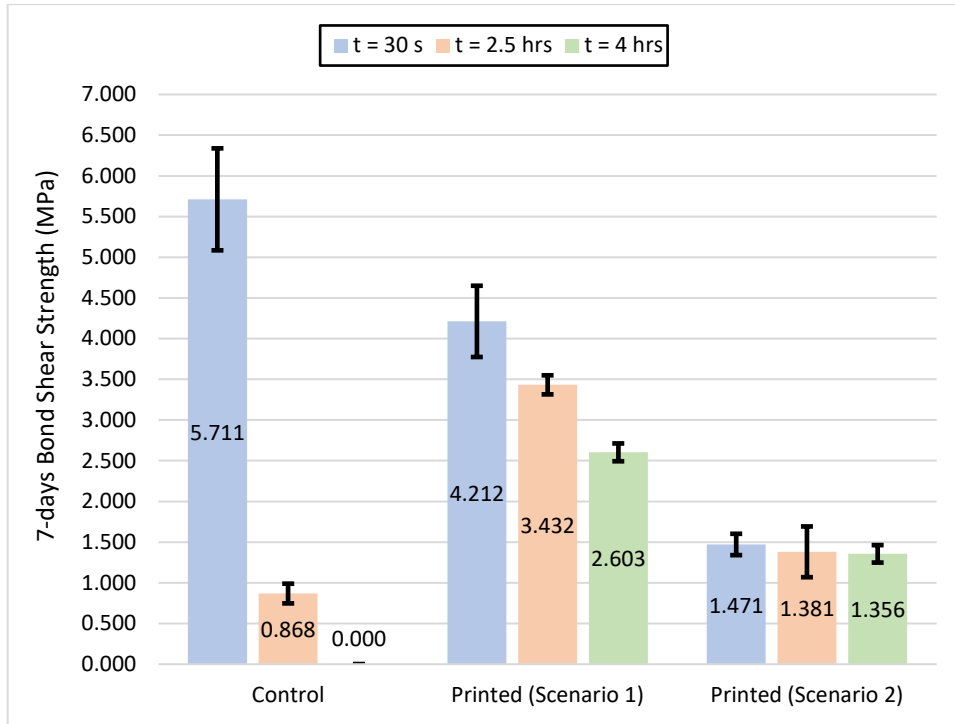
Figure 55: Bond Shear Test Setup for (a) Control and (b) Printed Specimens.

(S1,) and printed specimens in scenario 2 (S2.) Each category was subdivided into three parts where 3 specimens were considered for each part. Those parts were classified based on the time interval ( $t$ ) or time gap between the last printed layer and the preceding one. Figure 56 shows timber molds used to cast control specimens, having notches to induce shear failure.



(a) (b)  
Figure 56: Bond Shear Test Control Specimen (a) Mold and (b) Blow Up.

**4.8.1 Bond assessment.** The average 7-days bond shear strength results are summarized in Figure 57. Control specimens that have been monolithically casted (represented by  $t = 30$  s in Figure 57) exhibited an average bond shear strength (BSS) of 5.71 MPa. Specimens that correspond to 2.5 hrs and 4 hrs time intervals had BSS values of 0.868 MPa and 0 MPa respectively, and were casted at two stages. 2/3 of the mold was casted at once, and the remaining 1/3 was filled with concrete after the corresponding time interval has passed. At 2.5 and 4 hrs time intervals, the control BSS expectedly experienced a large reduction of 85% and 100% respectively. For the first scenario (S1) printed specimens, 7-days BSS was evaluated to be 4.212 MPa, 3.432 MPa, and 2.603 MPa for 30 s, 2.5 hrs, and 4 hrs time intervals respectively. on the other hand, printed specimens of S2 exhibited BSS values of 1.471 MPa, 1.381 MPa, 1.356 MPa for 30 s, 2.5 hrs, and 4 hrs time intervals respectively. Despite the scatter of the results, it can still lead to a decreasing trend in BSS, more importantly in printed



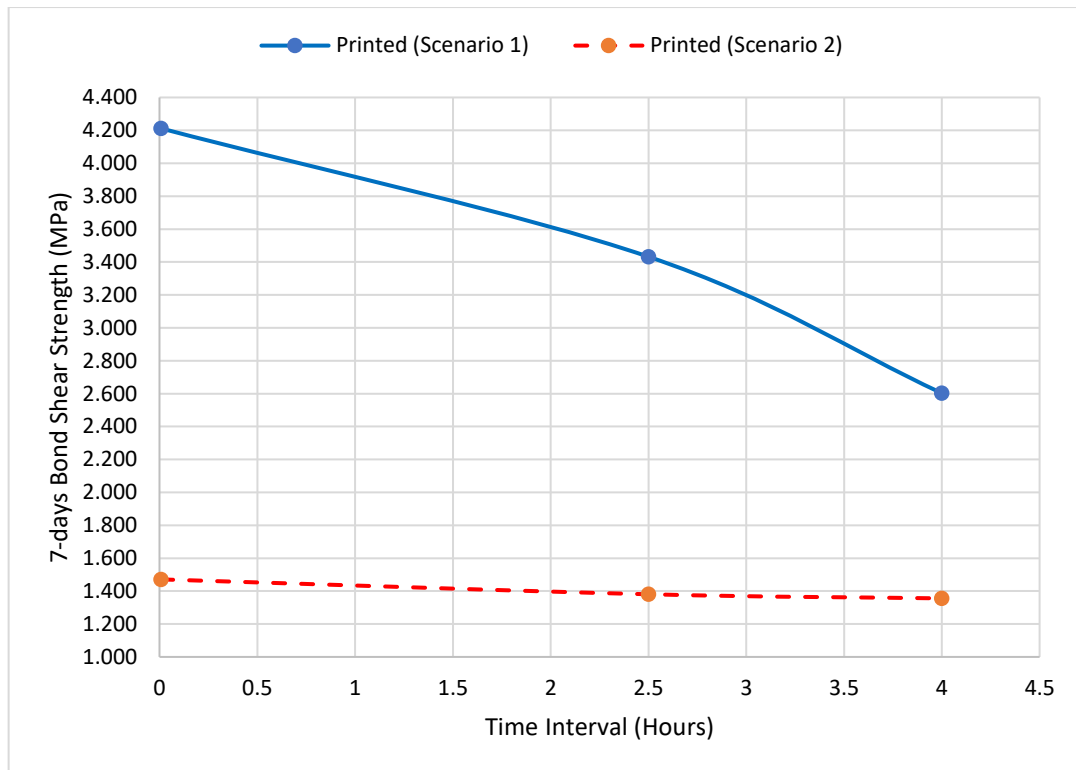
**Figure 57: Summary of Bond Shear Strength Results in the Study.**

specimens, when time interval is increased. This can be further clarified in Figure 58 showing the bond shear strength of printed specimens versus time interval. For further illustration, Table 7 shows the % reduction in BSS in both scenarios for 2.5 hrs and 4 hrs time intervals, while 30 s is considered the reference time interval. Regardless of how large the reduction is between different time intervals; it can be clearly observed that there is a strong correlation between BSS and “t”.

**Table 7: Percentage Reduction in BSS in Both Scenarios for Different Time Intervals.**

Scenario ID	Reduction in BSS with respect to value at t = 30 s	
	t = 2.5 hrs	t = 4 hrs
1	18.5 %	38 %
2	6 %	8 %

The reduction of BSS in control specimens with respect to “t” was expected, since surface roughness and compaction level differ when mortar is poured in molds rather than freely printed. Hence, this ends up in majorly changing interfacial cohesion and dramatically reducing shear resistance at the interface. On the other hand, such substantial drop in BSS when t is increased was not encountered in printed specimens at both scenarios. This makes it evident that the nature of print process and its



**Figure 58: Bond Shear Strength of Printed Specimens versus Time Interval.**

parameters such as printing speed, nozzle height, and printing pressure are influential on the bond shear strength between filaments. Higher nozzle speeds do not give enough time for subsequent layers to develop good contact. Additionally, higher nozzle position and lower pressure reduce the amount of merging force applied on the preceding layer when a new layer is being printed. In other words, squeezing effect at the interface is reduced, which in return impacts the development of good bond strength at interfaces of concrete filaments. This was pointed out by other researches in the literature as well, but considering tensile bond strength or indirect shear strength [20], [27]. Nevertheless, printed specimens still exhibited reduced BSS when time interval is increased, more considerably in S1 specimens. Two major things to discuss in here, which are the potential cause of the common reduction in BSS among all specimen categories with respect to time interval, and the reason behind less reduction encountered in S2 when compared to S1. The latter will be discussed in the next paragraph when BSS variation between categories is addressed. Aside from the dependency of any mechanical property on the material composition, other parameters are of considerable significance in 3DCP application. As discussed before, the open time of the optimum mix in this study was low when compared to other developed

materials in the literature, which allow for classifying it as a rapid hardening mix. It is important to note that quicker hardening leads to faster surface dehydration and loss of moisture. Surface moisture in 3DCP is considered essential for the development of good bond between layers, because it is a layering-based application. In other words, the less hardened the material is, the more capable of merging with the subsequent layers and forming better bond strength at the interface. Such parameters were also targeted and found influential by the authors in [24], [66]. Rahul, Santhanam, Meena, and Ghani have extracted specimens from 3DCP objects, and tested for direct bond shear strength. Results in their study were better than the obtained in this study (8 MPa for molded, and 5.6 MPa for printed [49],) but it can still be due to testing at older age of specimens compared to 7-days age considered for testing in this study. Furthermore, they found out that reductions of bond shear strength with respect to time gap is in line with reduced material porosity with time [49]. Wolfs, Bos, and Salet evaluated bond strength indirectly using split tensile test with different time intervals. They reported that covered specimens had double the bond strength of uncovered specimens for a time interval of 4 hrs [48], which is attributed to the influence of surface dehydration on bond strength. Many other authors have addressed the drop in bond strength between nearly zero-time gap and 4 hrs, either using tensile bond test or splitting test. For the same specified time range, 34% reduction in tensile bond strength was stated in [27], and was attributed to the increased water absorption of a printed layer with time. In other words, when a new layer is placed, moisture exchange takes place leading air in the bottom layer to move up as water is being absorbed by the that layer. By this means, air gets entrapped in the interface. This is in line with surface dehydration issues that were discussed earlier. However, Le et al. [68] reported 43% reduction in tensile bond strength, and concluded that void formation occur at interfaces of printed filaments as a result of the nature of printing process. However, BSS of the reference printed specimens (S1) in this study can represent a good measure, mainly by having a tensile failure pattern (no interface separation) when in-plane bending is applied. This was discussed earlier when flexural strength was addressed. Furthermore, reductions in BSS with time intervals of 2.5 hrs and 4 hrs were relatively low (18.5% and 38%) compared to some researches in the literature. Such reductions can be further avoided if the upper edge of printing nozzle is rough enough. This would result in enhanced bond strength with longer time gaps, and can be very helpful to rapid hardening concrete mixes.

However, extrudability might be negatively affected due to edge roughness of nozzle. On the material level, the optimum mix of the study contained 10% silica fume replacement by weight of binder. In this perspective, the good bond shear strength of 4.212 MPa can be attributed to the presence of silica fume. Silica fume, as a filler, improves packing of the layered material, which helps developing an satisfactory bond at the contact area between layers [72]. This corresponds to findings in other research where 3DCP specimens were tested for bond assessment using split tensile test, and authors reported that as micro silica content is increased, bond strength increases accordingly [40].

Specimens of S2 at the reference time ( $t = 30$  s) exhibited a low BSS (1.471 MPa) when compared to S1 (4.212 MPa.) The fact that very low BSS can be achieved with S2 conditions makes it possibly less vulnerable to change with varying time interval, where the major contribution in BSS for that case seems to be from surface roughness. By this means, slight reductions in BSS for S2 specimens with respect to time interval were encountered and are 6% and 8% for 2.5 hrs and 4 hrs time gaps respectively. Table 8 shows the percentage reduction in BSS first between the control and S1 for 30 s time interval, then between S1 and S2 for all time intervals. 26% reduction in BSS between control specimens and S1 printed specimens ( $t=30$  s) was encountered, whereas reductions in BSS between S1 and S2 were 65%, 60%, and 48% for 30 s, 2.5 hrs, and 4 hrs respectively.

**Table 8: Percentage Reduction between Bond Strength Categories (Control, S1, and S2).**

Categories of Comparison (Category 1 $\searrow$ Category 2)	Time Interval	% Reduction
Control $\searrow$ S1	30 s	26 %
S1 $\searrow$ S2	30 s	65 %
	2.5 hrs	60 %
	4 hrs	48 %

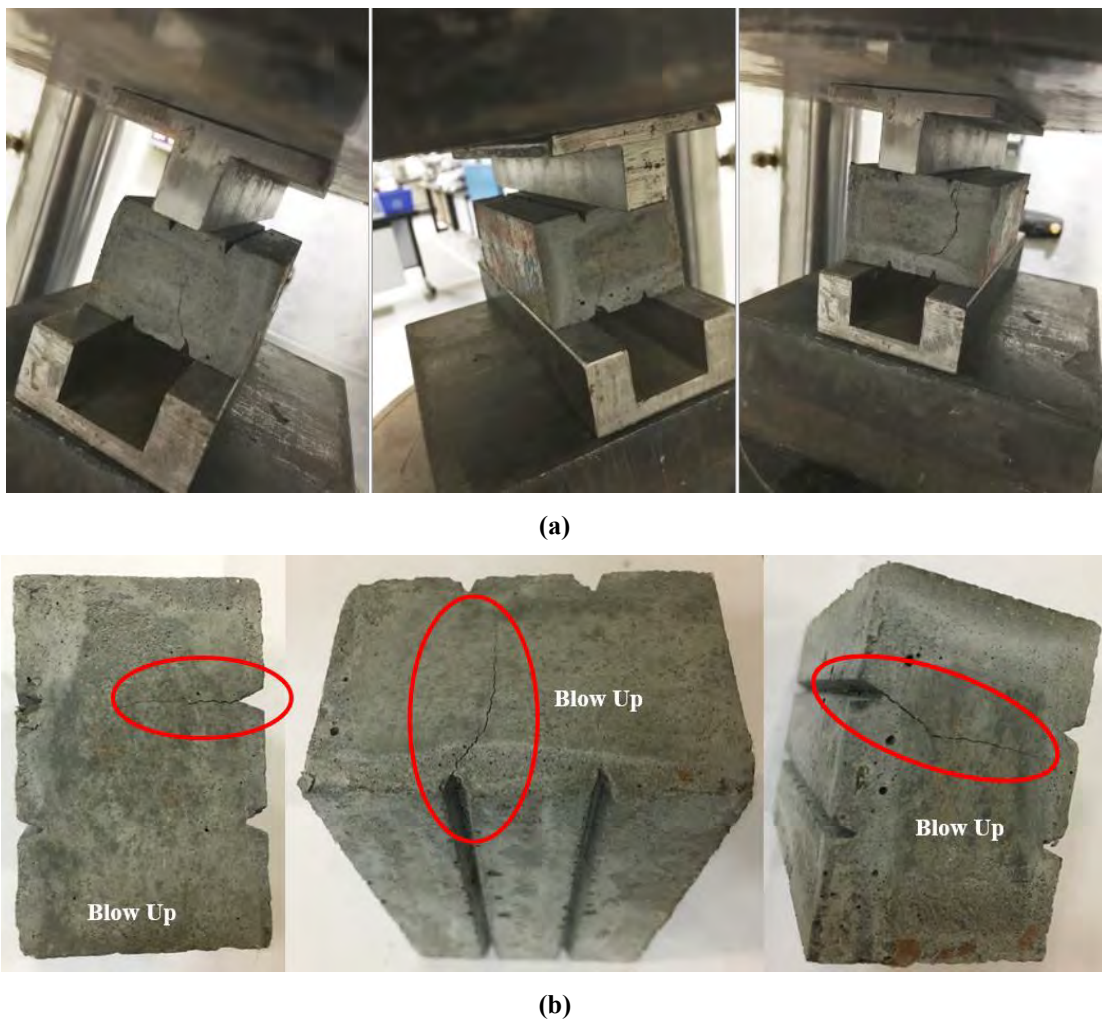
The % reduction in BSS from control specimens to printed (S1) specimens is not dramatic, being only 26%, particularly when compared to compressive strength results (48% reduction between control and printed.) Therefore, it can be considered a good indicator for classifying the optimum mix of the study in terms of bond

development at contact regions between layers. This is slightly less than results shown in [49] which demonstrated 30% reduction in BSS between molded specimens and extracted ones. The presence of fibers can contribute to bond shear strength of molded specimens that were cast monolithically. It is important to note that this contribution in printed specimens is nearly negligible, possibly due to the very low chance of having fibers shared between two stacking filaments. It is thought out that fiber role in bond shear strength development can only take place when subsequent layers are squeezed enough on the lower ones. Moreover, the presence of fibers oriented parallel to the printing direction at interfacial regions can increase the porosity of the contact area, thus, leading to weaker joint in resistance to both shear and tension. This is in line with conclusions drawn in other researches on 3D printed fiber-reinforced concrete [38]. However, other researchers concluded that fibers may increase bond strength, but when higher cohesion between layers is maintained, that is when loss of workability is not quick in the printed material [40]. On the other hand, it is worth noting that % reduction between S1 and S2 for all time intervals did not quietly vary, that are 65%, 60%, and 48% for 30 s, 2.5 hrs, and 4 hrs respectively. However, the general trend is that BSS is reduced between both scenarios. This simply emphasizes the fact that accelerated hydration reactions are taking place while hot water is used, which is basically more rapid hardening of the material. Additionally, it is important to note that surface is exposed before the subsequent layer is placed for all time intervals in both scenarios. In case of S2, specimens are exposed to outside weather and sun radiations. Thereby, this can lead to accelerated loss of moisture (higher evaporation rate) and faster surface dehydration for interfaces of S2 specimens, even for small time intervals i.e. 30 seconds. In other words, bond between filaments under S2 conditions suffer in developing a robust contact compared to S1 specimens that are printed and exposed under ambient conditions. In addition, bond in S2 is probably relying more on surface roughness of the bottom layer to develop shear resistance at the interface. This is in agreement with previous research by Sanjayan, Nematollahi, Xia, and Marchment, where they found significant impact of surface moisture on bond strength [37]. To support the reductions of BSS in S2 specimens, authors in [73] reported that when temperature of mix increases from 20° C to 30° C, drying rate increases by 80%, leading to more water being evaporated at the interface. They also stated that there is no enough time for the moisture exchange phenomenon to supply non-reacted binder in bottom



layers with water, hence, leaving lots of cement particles un-hydrated at interface region. This obviously reduces strength at the interface [73].

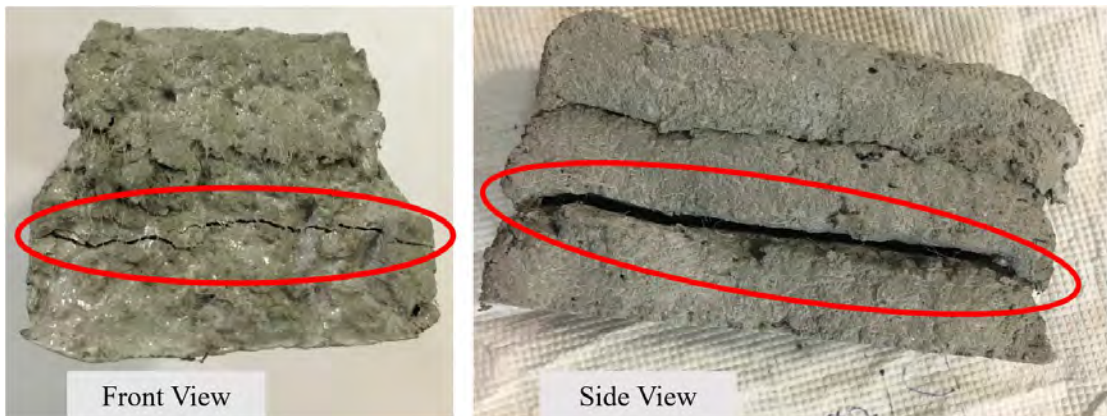
**4.8.2 Failure patterns.** In order to clarify the assessed bond shear strength of control and printed specimens, failure patterns of all specimen categories are discussed in here. Typical shear failure and crack pattern in control specimens was observed (Figure 59,) and is expectedly initiating at the notch location due to high stress concentrations. Additionally, printed specimens have exhibited layer separation at failure as illustrated in Figure 60. This inevitably supports the claim that bond specimens were ruptured in a shear failure mode. The strength values were evaluated at the time of crack formation at the interface. In some cases, it is worth noting that specimens exhibited resistance after interfacial cracks have formed, and this might be



**Figure 59: Fractured Bond Control Specimens (a) During Test and (b) Blow Up.**



(a)



(b)

**Figure 60: Fractured Bond Printed Specimens (a) During Test, (b) Crack Initiation on The Left, and Separation of Interface on The Right.**

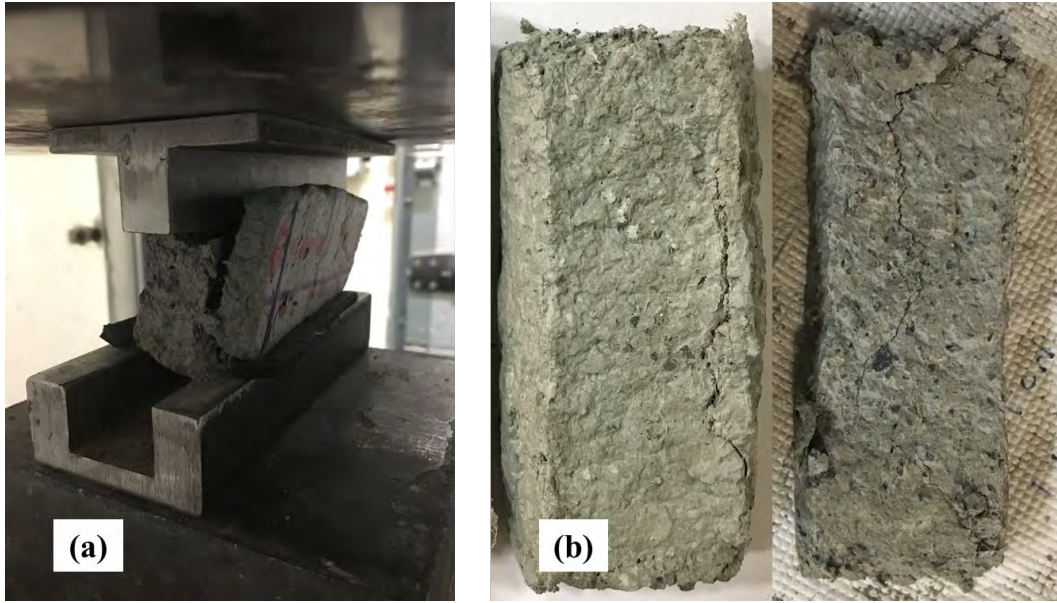
attributed to bridging action of fibers that are penetrating two layers. However, this is not true for all of the samples, where orientation of fibers at contact region between filaments is highly variable. This is because the variability in fiber orientation is dependent on printing process parameters (speed of printing, pressure, and nozzle height,) which are also inconstant as it is performed manually. Additionally, the mix used for printing in this study is batched at small volumes e.g. 1 liter, and this may cause higher material variability that can end up in different post-cracking behaviors of

the material. It was reported by Soltan and Li that for the same mix proportions, higher flowability and reduced rate of hydration can be encountered for larger batches (6.2 L) compared to smaller ones (1.2 L) [64]. It is important to consider how interfacial regions look like after separation or failure. Figure 61 shows typical interfaces of fractured bond specimen for the two different time intervals. It can be observed that void content at the interface is not the same among all specimens, regardless of the time interval. Such varying interfacial porosities can be attributed to the relatively low control (compared to robotic control) on print process parameters since extrusion is performed manually. Process parameters were found to have effect on interface conditions as reported by previous researches as in [49]. In addition, it was visually assessed that roughness of interfacial regions is higher for lower time intervals, which indicates better cohesion between layers. This is in line with conclusions of a previous research [27]. Furthermore, the higher surface roughness at lower “t” values is relevant, as greater bond shear strength values were evaluated for such lower time intervals.



**Figure 61: Typical Fractured Interface of Printed Specimens (Left)  $t = 2.5$  hrs and (Right)  $t = 4$  hrs.**

Other crack patterns were experienced at interfaces of bond specimens of the study, as shown in Figure 62b. In this case, cracks are penetrating individual layers rather than occurring only along edges of interfaces as in the norm. This was possibly attributed to eccentricity caused by alignment errors of the test setup, as illustrated in Figure 62a. However, it is important to note that such specimens were disregarded of



**Figure 62: Fractured Interface of Printed Specimens due to Setup Errors (a) During Test and (b) Blow Up at Interface.**

the record. Additionally, few specimens exhibited crack initiation along its three layers before being formed at edge of interface (Figure 63,) when undergoing bond shear test. This is most likely due to irregularity in printing path (manual printing error) by not being straight enough. Despite the use of cardboard pads, a very slight curvature in path



**Figure 63: Vertical Crack Along Layers of a Printed Specimen in Bond Test.**

is seemingly leading the specimen to have tensile stress concentrations at mid-span of the bottom side. This can be thought out as if the specimen is cambered, as illustrated in Figure 64. In this manner, cracks find its way easier to form vertically through layers (similar to crack formation in flexural test) under such stress conditions. When the specimen undergoes enough deflection, its sides become aligned with the steel support fixture. Thereby, crack at interface is formed, and propagates until intersecting the preceding vertical one. In such a case, no layer separation is experienced as interfacial crack is interlocked by the tensile one. This emphasizes the conclusions of the study about bond and flexural strengths, that bond is strong enough not to allow layer separation when tensile stress concentrations take place. However, specimens having such mode of failure were disregarded.

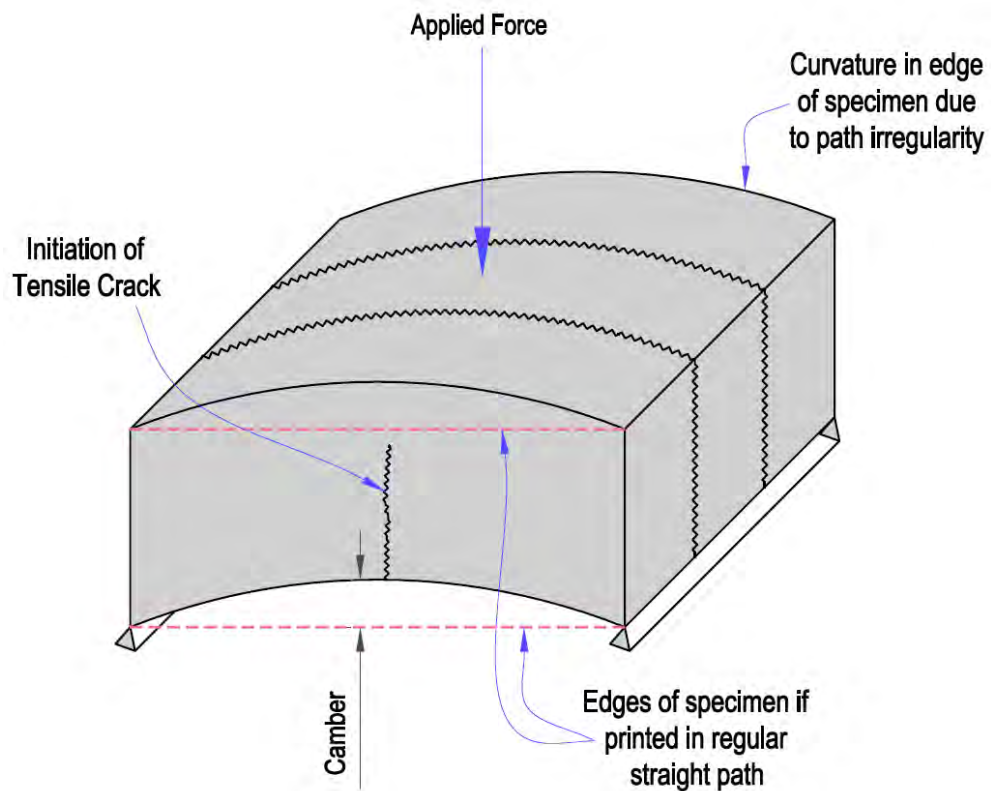


Figure 64: Curvature in Specimen Due to Irregularity in Printing Path Under Bond Test.

## Chapter 5. Conclusions and Recommendations

### 5.1 Conclusions

This study investigated the development of a concrete mix for 3D printing application by a trial and error procedure. For that, a total number of 19 trial mixes were performed. An optimum concrete mix was chosen based on visual observation of shape quality, stability, and ease of extrusion. The developed mix has shown ability to perform in both ambient (lab) and hot (site) weather conditions. Fresh state properties of the optimum mix were evaluated using flow table, open time, extrudability, and shape stability. Hardened state properties (mechanical properties) were addressed as well, using compressive strength test, 3-point flexural strength test, and bond shear test. A simplified novel setup was developed in this study for performing bond shear test. Two casting and exposure scenarios were considered in this study to examine the effects of harsh environmental conditions in UAE. The first scenario is when specimens are printed using cool water, and stored in the lab until being tested. The second scenario represents using hot water (50° C) for mixing, and exposing specimens outside the lab to hot weather conditions until being tested. Three specimen categories were considered for assessment of mechanical properties, which are molded specimens (control,) printed specimens of scenario 1, and printed specimens of scenario 2. The following conclusions can be drawn from this research:

- The use of 1.4% polyethylene fibers in the optimum mix has enhanced surface appearance and shape stability of printed parts. Yet, larger dosage of superplasticizer becomes required due to the loss of flowability caused by the presence of fibers.
- Percentage flow of scenario 1 mix was evaluated to be 86%, and was found proper for extrusion application. It dropped by 9% in scenario 2 mix, and this was attributed to the very quick loss of workability when hot water is used.
- The open time of the optimum mix was 7.2 minutes in scenario 1 conditions. This value was considered relatively low, and indicated rapid hardening of the used mix. It only suits 3DCP applications that utilize sequential batching of the material. For a complete validity and usefulness of the mix in such an application, liquid admixtures shall be replaced by powdered ones. Open time

was decreased by 16% in scenario 2 mix, and this indicates a quicker loss of flowability.

- The optimum mix of the study was extrudable in both printing scenarios using a rectangular nozzle that is 20 mm deep and 40 mm wide. The same mix was not extrudable through a smaller nozzle that is 10 mm deep, which makes extrudability dependent on nozzle size and exerted pressure. Extrudability of 3DCP mixes is strongly associated with their open time intervals.
- Shape retention index (SRI) of 3-layers (100 mm long) and 2-layers (200 mm long) specimens in scenario 1 were 0.94 and 0.96 respectively. It dropped by 2% for 3-layers specimens in scenario 2, whereas 2-layers specimens exhibited a larger decrease of 8.5%. It was observed that larger length of layers negatively affects SRI, even for a smaller number of stacking layers. Shrinkage cracks were not seen in scenario 2 specimens, owing to the presence of polypropylene fibers.
- The compressive strength of the mix was 47 MPa in control cubes. It decreased by 48% in printed cubes of scenario 1 as an effect of having a joint between layers. Compressive strength of printed cubes in scenario 2 reduced further by 56% as a result of higher water evaporation.
- The flexural strength was evaluated to be 6.36 MPa in control prisms, where it reduced by only 3% in printed prisms of the first scenario. In the second scenario, printed prisms exhibited a flexural strength larger than the control by 18%. Fiber orientation was found to be parallel to the extrusion direction in printed specimens. It is further enhanced in scenario 2 due to less viscosity of the mix, leading to more contribution in flexural strength.
- Bond shear strength was found to be 5.7 MPa in control specimens, and it decreased by 26% in printed specimens of the first scenario at  $t = 30$  s. Compared to scenario 1 printed specimens, bond shear strength has decreased in scenario 2 printed specimens by 65%, 60%, and 48% for time intervals of 30 s, 2.5 hrs, and 4 hrs respectively. Bond shear strength was observed to be reduced while time interval is increased. In scenario 2, loss of moisture due to water evaporation were reflected by the dramatic drop in bond shear strength (compared to scenario 1) at contact regions. Printed specimens had a tensile failure mode rather than layer separation, when tested for flexure. Accordingly, bond strength was considered good for the optimum mix in this study.

## 5.2 Recommendations

According to the work performed in this study and the presented results, the following recommendations can be helpful for future research in the 3D concrete printing field:

- 3DCP mixes are sensitive to batch volume. For easiness of evaluation, mix design is better performed using small batches e.g. 1 L. Extensive care on water amount and admixture dosage shall be taken when scaling a designed mix to larger volumes, in order to get an outcome similar to the smaller batch.
- Shape retention would give more practical results if performed on long specimens e.g. 500 mm long.
- The mix in this study has a low open time, and it is important to address the effect of set retarders on the overall performance of the mix and its open time interval.
- Flexural strength at 28 days of different specimen categories is interesting to address, since it had a different trend of variation in this research between the three categories, when compared to compressive and bond strength.
- Load-displacement relationships for bond between layers can represent a ductile behavior, and is important to address in future research.
- The effect of fibers at different dosages is a good perspective to be considered, since it affects both fresh and hardened state properties of 3D printed concrete.



## References

- [1] P. Stavropoulos, P. Foteinopoulos, A. Papacharalampopoulos, and H. Bikas, "Addressing the challenges for the industrial application of additive manufacturing: Towards a hybrid solution," *Int. J. Light. Mater. Manuf.*, vol. 1, no. 3, pp. 157–168, Sep. 2018.
- [2] A. Warszawski and R. Navon, "Implementation of Robotics in Building: Current Status and Future Prospects," *J. Constr. Eng. Manag.*, vol. 124, no. 1, pp. 31–41, 1998.
- [3] B. Khoshnevis, "Automated construction by contour crafting - Related robotics and information technologies," *Autom. Constr.*, vol. 13, no. 1, pp. 5–19, 2004.
- [4] S. Mindess, "Advanced concrete for use in civil engineering," in *Advanced Civil Infrastructure Materials*, 1st ed., H. C. Wu, Ed. Boca Raton: Woodhead Publishing Limited, 2006, pp. 1–29.
- [5] T. Wohlers and T. Gornet, "History of additive manufacturing," *Wohlers Rep.*, vol. 24, no. 2014, p. 118, 2014.
- [6] "Lithography – Art Term | Tate." [Online]. Available: <https://www.tate.org.uk/art/art-terms/l/lithography>. [Accessed: 20-Sep-2018].
- [7] "Stereolithography Apparatus (SLA)," *Cyant*, 2017. [Online]. Available: <https://www.cyant.co/lexicon/2017/9/2/stereolithography-apparatus-sla>. [Accessed: 22-Sep-2018].
- [8] K. R. Bakshi and A. V Mulya, "A Review on Selective Laser Sintering: A Rapid Prototyping Technology," *IOSR J. Mech. Civ. Eng.*, vol. 4, no. 4, pp. 53–57, 2016.
- [9] C. Chua, K. Leong, and C. Lim, *Rapid Prototyping: Principles and Applications*, 3rd ed. World Scientific Publishing Company, 2010.
- [10] E. Ebel and T. Sinnemann, "Fabrication of FDM 3D objects with ABS and PLA and determination of their mechanical properties," *RTEjournal*, vol. 2014, no. 1, 2014.
- [11] "The Working Principles of Fused Deposition Modeling (FDM) 3D Printers.," *DesignTech Systems Ltd.* [Online]. Available: <https://www.designtechsys.com/articles/working-fdm-3d-printers>. [Accessed: 25-Sep-2018].
- [12] J. Pegna, "Exploratory investigation of solid freeform construction," *Autom. Constr.*, vol. 5, no. 5, pp. 427–437, 1997.
- [13] Additive fabrication method, by B. Khoshevis. (1997, Aug. 12). *US005656230A*. Accessed on: Sep. 29, 2018. [Online]. Available: <https://patents.google.com/patent/US5656230A/en>
- [14] Kolan , K.C.R. ; Leu , M.C. ; Hilmas , G.E. ; Velez , M. Selective laser sintering of 13–93 bioactive glass . In Bourell , D.L. , Crawford , R.H. , Seepersad , C.C. , Beaman , J.J. , Marcus , H. Eds.; Proceedings of the 21st Annual International

Solid Freeform Fabrication Symposium , Austin , Texas , USA , 2010 ; pp. 504 – 512.

- [15] B. Khoshnevis, S. Bukkapatnam, H. Kwon, and J. Saito, “Experimental investigation of contour crafting using ceramics materials,” *Rapid Prototyp. J.*, vol. 7, no. 1, pp. 32–41, 2001.
- [16] “Contour Crafting Update,” *Fabbaloo*, 2014. [Online]. Available: <https://www.fabbaloo.com/blog/2014/1/2/contour-crafting-update.html>. [Accessed: 29-Sep-2018].
- [17] J. Gardiner, “Exploring the Emerging Design Territory of Construction 3D Printing – Project Led Architectural Research,” Ph.D. dissertation, School of Architecture and Design, RMIT University, Melbourne, Australia, 2011. Accessed on: Sep. 29, 2018. [Online]. Available: [https://www.researchgate.net/publication/314116498\\_Exploring\\_the\\_Emerging\\_Design\\_Territory\\_of\\_Construction\\_3D\\_Printing\\_-\\_Project\\_Led\\_Architectural\\_Research](https://www.researchgate.net/publication/314116498_Exploring_the_Emerging_Design_Territory_of_Construction_3D_Printing_-_Project_Led_Architectural_Research)
- [18] Z. Yeh and B. Khoshnevis, “Geometric conformity analysis for automated fabrication processes generating ruled surfaces: Demonstration for contour crafting,” *Rapid Prototyp. J.*, vol. 15, no. 5, pp. 361–369, 2009.
- [19] H. Kwon, S. Bukkapatnam, B. Khoshnevis, and J. Saito, “Effects of orifice shape in contour crafting of ceramic materials,” *Rapid Prototyp. J.*, vol. 8, no. 3, pp. 147–160, 2002.
- [20] A. Kazemian, X. Yuan, E. Cochran, and B. Khoshnevis, “Cementitious materials for construction-scale 3D printing: Laboratory testing of fresh printing mixture,” *Constr. Build. Mater.*, vol. 145, pp. 639–647, 2017.
- [21] N. Leach, A. Carlson, B. Khoshnevis, and M. Thangavelu, “Robotic Construction by Contour Crafting: The Case of Lunar Construction,” *Int. J. Archit. Comput.*, vol. 10, no. 3, pp. 423–438, 2012.
- [22] G. Ma, Z. Li, and L. Wang, “Printable properties of cementitious material containing copper tailings for extrusion based 3D printing,” *Constr. Build. Mater.*, vol. 162, pp. 613–627, 2018.
- [23] S. Lim, R. A. Buswell, T. T. Le, S. A. Austin, A. G. F. Gibb, and T. Thorpe, “Developments in construction-scale additive manufacturing processes,” *Autom. Constr.*, vol. 21, no. 1, pp. 262–268, 2012.
- [24] T. T. Le, S. A. Austin, S. Lim, R. A. Buswell, A. G. F. Gibb, and T. Thorpe, “Mix design and fresh properties for high-performance printing concrete,” *Mater. Struct. Constr.*, vol. 45, no. 8, pp. 1221–1232, 2012.
- [25] B. Panda, J. H. Lim, and M. J. Tan, “Mechanical properties and deformation behaviour of early age concrete in the context of digital construction,” *Compos. Part B Eng.*, vol. 165, no. December 2018, pp. 563–571, 2019.
- [26] ASTM D 2573 – 01, “Standard Test Method for Field Vane Shear Test in Cohesive Soil,” West Conshohocken, PA, 2001.

- [27] B. Panda, S. C. Paul, N. A. N. Mohamed, Y. W. D. Tay, and M. J. Tan, "Measurement of tensile bond strength of 3D printed geopolymers mortar," *Meas. J. Int. Meas. Confed.*, vol. 113, no. August 2017, pp. 108–116, 2018.
- [28] Method and Device for Building Automatically Conglomerate Structures, by E. Dini, M. Chiarugi, and R. Nannini. (2008, Jun. 26). *US20080148683A1*. Accessed on: Oct. 14, 2018. [Online]. Available: <https://patents.google.com/patent/US20080148683A1/en>
- [29] G. Cesaretti, E. Dini, X. De Kestelier, V. Colla, and L. Pambaguian, "Building components for an outpost on the Lunar soil by means of a novel 3D printing technology," *Acta Astronaut.*, vol. 93, pp. 430–450, 2014.
- [30] S. Lim, T. Le, J. Webster, R. Buswell, S. Austin, A.G.F. Gibb, T. Thorpe, "Fabricating construction components using layer manufacturing technology", *Proc. Int. Conf. Glob. Innov. Constr.*, Leicestershire, UK, 2009, pp. 512–520.
- [31] P. Wu, J. Wang, and X. Wang, "Automation in Construction A critical review of the use of 3-D printing in the construction industry material Finished," *Autom. Constr.*, vol. 68, pp. 21–31, 2016.
- [32] B. Zareiyan and B. Khoshnevis, "Effects of mixture ingredients on extrudability of concrete in Contour Crafting," *Rapid Prototyp. J.*, vol. 24, no. 4, pp. 722–730, 2018.
- [33] B. Panda and M. J. Tan, "Experimental study on mix proportion and fresh properties of fly ash based geopolymer for 3D concrete printing," *Ceram. Int.*, vol. 44, no. 9, pp. 10258–10265, 2018.
- [34] S. C. Paul, Y. W. D. Tay, B. Panda, and M. J. Tan, "Fresh and hardened properties of 3D printable cementitious materials for building and construction," *Arch. Civ. Mech. Eng.*, vol. 18, no. 1, pp. 311–319, 2018.
- [35] S. A. Austin, C. I. Goodier, and P. J. Robins, "The rheological performance of wet-process sprayed mortars," *Mag. Concr. Res.*, vol. 51, no. 5, pp. 341–352, 1999.
- [36] B. Nematollahi, M. Xia, J. Sanjayan, and P. Vijay, "Effect of type of fiber on inter-layer bond and flexural strengths of extrusion-based 3D printed geopolymer," *Mater. Sci. Forum*, vol. 939, pp. 155–162, 2018.
- [37] J. G. Sanjayan, B. Nematollahi, M. Xia, and T. Marchment, "Effect of surface moisture on inter-layer strength of 3D printed concrete," *Constr. Build. Mater.*, vol. 172, pp. 468–475, 2018.
- [38] B. Nematollahi *et al.*, "Effect of polypropylene fibre addition on properties of geopolymers made by 3D printing for digital construction," *Materials (Basel)*, vol. 11, no. 12, 2018.
- [39] A. Mather, R. Cipra, and T. Siegmund, "Structural integrity during remanufacture of a topologically interlocked material," *Int. J. Struct. Integr.*, vol. 3, no. 1, pp. 61–78, 2012.
- [40] B. Zareiyan and B. Khoshnevis, "Effects of mixture ingredients on interlayer

- adhesion of concrete in Contour Crafting,” *Rapid Prototyp. J.*, vol. 24, no. 3, pp. 584–592, 2018.
- [41] B. Zareiyan and B. Khoshnevis, “Effects of interlocking on interlayer adhesion and strength of structures in 3D printing of concrete,” *Autom. Constr.*, vol. 83, no. August, pp. 212–221, 2017.
- [42] T. Marchment, J. Sanjayan, and M. Xia, “Method of enhancing interlayer bond strength in construction scale 3D printing with mortar by effective bond area amplification,” *Mater. Des.*, vol. 169, p. 107684, 2019.
- [43] “Dubai 3D printing Strategy - Dubai Future Foundation.” [Online]. Available: <https://www.dubaifuture.gov.ae/our-initiatives/dubai-3d-printing-strategy/>. [Accessed: 22-Nov-2018].
- [44] Dubai Future Foundation, “The World’s First 3D Printed Office.” [Online]. Available: <http://www.officeofthefuture.ae/#>. [Accessed: 23-Dec-2019].
- [45] TheNational, “Dubai unveils world’s largest 3D printed two-storey building,” 2019. [Online]. Available: <https://www.thenational.ae/uae/government/dubai-unveils-world-s-largest-3d-printed-two-storey-building-1.927590#1>. [Accessed: 23-Dec-2019].
- [46] J. Saundalkar, “Construction at Sharjah’s first 3D printed house in full swing,” 2019. [Online]. Available: <https://meconstructionnews.com/37140/construction-at-sharjahs-first-3d-printed-house-in-full-swing>. [Accessed: 23-Dec-2019].
- [47] E. Hosseini, M. Zakertabrizi, A. H. Korayem, and G. Xu, “A novel method to enhance the interlayer bonding of 3D printing concrete: An experimental and computational investigation,” *Cem. Concr. Compos.*, vol. 99, no. October 2018, pp. 112–119, 2019.
- [48] R. J. M. Wolfs, F. P. Bos, and T. A. M. Salet, “Hardened properties of 3D printed concrete: The influence of process parameters on interlayer adhesion,” *Cem. Concr. Res.*, vol. 119, no. September 2018, pp. 132–140, 2019.
- [49] A. V. Rahul, M. Santhanam, H. Meena, and Z. Ghani, “Mechanical characterization of 3D printable concrete,” *Constr. Build. Mater.*, vol. 227, p. 116710, 2019.
- [50] *PCI Manual for the Design of Hollow Core Slabs and Walls*, MNL-126-15E, 2015.
- [51] I. Abuzayed, H. Alajmani, and A. Al-tamimi, “EVALUATION OF MECHANICAL PROPERTIES AND SERVICE LIFE OF HIGH PERFORMANCE CONCRETE,” *NED Univ. J. Res. - Struct. Mech.*, vol. XIII, no. 3, pp. 53–60, 2018.
- [52] ASTM C 230/C 230M – 08, “Standard Specification for Flow Table for Use in Tests of Hydraulic Cement,” West Conshohocken, PA, 2010.
- [53] ASTM C 109/C 109M – 07, “Standard Test Method for Compressive Strength of Hydraulic Cement Mortars (Using 2-in. or [50-mm] Cube Specimens),” West Conshohocken, PA, 2007.

- [54] Control-Groups, “Flexural test devices for mortar beams ASTM c348.” [Online]. Available: <https://www.controls-group.com/eng/cement-testing-equipment/flexural-test-devices-for-mortar-beams.php>. [Accessed: 09-Sep-2019].
- [55] ASTM C 348/C 348M – 18, “Standard Test Method for Flexural Strength of Hydraulic-Cement Mortars,” West Conshohocken, PA, 2018.
- [56] S. H. Bong, B. Nematollahi, A. Nazari, M. Xia, and J. Sanjayan, “Method of Optimisation for Ambient Temperature Cured Sustainable Geopolymers for 3D Printing,” *Materials (Basel)*, vol. 902, no. 12, 2019.
- [57] M. S. Mamlouk and J. P. Zaniewski, *Materials for Civil and Construction Engineers*, 3rd ed. Prentice Hall, 2011.
- [58] BASF Construction Chemicals UAE, “MasterGlenium ® ACE 456,” 2014.
- [59] P. Aïtcin, "The importance of the water–cement and water–binder ratios," in *Science and Technology of Concrete Admixtures*, Cambridge, UK: Woodhead Publishing, 2016, ch.1, sec.1, pp. 3-13. Accessed on: Dec. 13, 2019. [Online]. Available: <https://www.sciencedirect.com/science/article/pii/B9780081006931000011>
- [60] T. Al-Attar, “Effect of Aggregate to Binder Ratio on Shrinkage and Creep of High Performance Lightweight Concrete.,” *Int. J. Civ. Environ. Eng.*, vol. 11, pp. 54–58, Dec. 2011.
- [61] S. Chen, H. Wang, J. Zhang, H. Xing, and H. Wang, “Experimental Study on Low-Strength Similar-Material Proportioning and Properties for Coal Mining,” *Adv. Mater. Sci. Eng.*, vol. 2015, pp. 1–6, Mar. 2015.
- [62] S. Eskandarsefat, “Investigation on the effects of mix water temperature on High-Early strength cement concrete properties – An experimental work and a case study,” *J. Build. Eng.*, vol. 20, no. June, pp. 208–212, 2018.
- [63] Y. W. D. Tay, Y. Qian, and M. J. Tan, “Printability region for 3D concrete printing using slump and slump flow test,” *Compos. Part B Eng.*, vol. 174, no. May, p. 106968, 2019.
- [64] D. G. Soltan and V. C. Li, “A self-reinforced cementitious composite for building-scale 3D printing,” *Cem. Concr. Compos.*, vol. 90, pp. 1–13, 2018.
- [65] Y. W. D. Tay, M. Y. Li, and M. J. Tan, “Effect of printing parameters in 3D concrete printing: Printing region and support structures,” *J. Mater. Process. Technol.*, vol. 271, no. December 2018, pp. 261–270, 2019.
- [66] F. Pelisser, A. B. D. S. S. Neto, H. L. La Rovere, and R. C. D. A. Pinto, “Effect of the addition of synthetic fibers to concrete thin slabs on plastic shrinkage cracking,” *Constr. Build. Mater.*, vol. 24, no. 11, pp. 2171–2176, 2010.
- [67] N. Yousefieh, A. Joshaghani, E. Hajibandeh, and M. Shekarchi, “Influence of fibers on drying shrinkage in restrained concrete,” *Constr. Build. Mater.*, vol. 148, pp. 833–845, 2017.
- [68] T. T. Le *et al.*, “Hardened properties of high-performance printing concrete,”

*Cem. Concr. Res.*, vol. 42, no. 3, pp. 558–566, 2012.

- [69] R. G. Burg, *The Influence of Casting and Curing Temperature on the Properties of Fresh and Hardened Concrete*. Skokie, Illinois, U.S.A.: Research and Development Bulletin RD113, Portland Cement Association, 1996.
- [70] B. Panda, S. Chandra Paul, and M. Jen Tan, “Anisotropic mechanical performance of 3D printed fiber reinforced sustainable construction material,” *Mater. Lett.*, vol. 209, pp. 146–149, 2017.
- [71] M. Nasir, O. S. B. Al-amoudi, H. J. Al-gahtani, and M. Maslehuddin, “Effect of casting temperature on strength and density of plain and blended cement concretes prepared and cured under hot weather conditions,” *Constr. Build. Mater.*, vol. 112, pp. 529–537, 2016.
- [72] P. Fidjestøl and R. Lewis, “Microsilica as an Addition,” *Lea’s Chem. Cem. Concr.*, pp. 679–712, Jan. 1998.
- [73] E. Keita, H. Bessaies-Bey, W. Zuo, P. Belin, and N. Roussel, “Weak bond strength between successive layers in extrusion-based additive manufacturing: measurement and physical origin,” *Cem. Concr. Res.*, vol. 123, no. November 2018, p. 105787, 2019.

## **Vita**

Aktham Alchaar was born in 1996, in As-Suwayda, in the Syrian Arab Republic. He earned his high school degree from Al Basel secondary school for superior students. In 2013, he moved to Ras Al Khaimah, United Arab Emirates. He graduated summa cum laude from the American University of Ras Al Khaimah in 2017. His degree was a bachelor of Science in Civil and Infrastructure Engineering. In that period, he worked as Mathematics tutor, research assistant, and lab assistant in the American University of Ras Al Khaimah. Since then, he is a structural engineer specialized in precast concrete design. He joined the American University of Sharjah in 2018 to earn a Master of Science degree in Civil Engineering. He worked as a graduate teaching assistant and as a research assistant, while being at the American University of Sharjah. His research interests include mechanical behavior and bond assessment of 3D-printed concrete, construction-scale 3D printing materials, and finite element modeling.